Cape Peninsula University of Technology

Correlation of liquefaction and settlement in windblown sands using the Flat Plate Dilatometer

Patrick M Neal

196067219

A thesis submitted to the Faculty of Engineering, Cape Peninsula University of Technology, Cape Town, in partial fulfilment of the requirements for the M-Tech Degree in Civil Engineering"

Cape Town

16 MAY 2011

Declaration

I declare that this research thesis is my own unaided work. It is being submitted for the M-Tech Degree at Cape Peninsula University of Technology, Cape Town. It has not been submitted before for any degree or examination in any other University.

_____

(Signature)

Signed in Cape Town this _____ day of _____ 2010

Abstract

Dwellings in impoverished and upper class urban areas of the Western Cape have undergone serious structural failure due to problematic underlying sand deposits, generally known as Cape Flats windblown found in areas such as Delft, Blue Downs and the Atlantic Beach Golf Estate. The problem is compounded further when moisture penetrates below the footings and reaches saturation in the winter months. When poorly graded sand with a high fines content is coupled with vibration (through earth tremors), liquefaction may occur and without proper precautions, this can lead to inadequate foundation design, more than expected settlement and eventual structural failure. Some sand deposits are highly contaminated with organic debris, leading to compressible and collapsible conditions. Little knowledge is locally available of liquefiable conditions in windblown dune sand and what long-term settlement can be expected. The Western Cape is not known as an area exposed to serious seismic activity, but an updated (and more locally applicable set of data) is needed to eliminate possible erroneous foundation design.

Samples have been extracted from typical sandy sites in the Western Cape where windblown dune sand is evident. Laboratory tests have been carried out on representative samples for closer examination and have been placed inside a purpose built calibration chamber that facilitates easy densification and probe testing. A DMT (flat blade dilatometer) was used to hydraulically penetrate the chamber sand sample to varying depths (up to 800 mm). The device can measure (with reduction formula) horizontal stress, angle of friction, bearing capacity and settlement. An accelerometer was attached to the chamber wall and vibration measured with the sand in varying states of moisture.

The DMT is an unexplored in-situ soil testing device in South Africa and so far the outcome indicates favourably compared to other devices such as the Dynamic Cone Penetrometer (DCP. The DMT has the ability to measure the in-situ stiffness, strength and stress history parameters of soil for better site characterisation. Settlement within the chamber is easily measured. The DMT has, for example, indicated that sand from the Philippi area are a problematic founding soil and should be treated with special care at shallow founding levels. The horizontal stress index is low and according to the available knowledge on soil stress history, these sand, coupled with low densities, can liquefy easily and result in structural damage. The West Coast dune sand, being coarser and easily consolidated, poses less of a problem under liquefiable conditions. A suitable terrain device for easy on-site manoeuvrability is required to assist the DMT in further testing.

Acknowledgements

I wish to acknowledge all the assistance and guidance I received from my internal and external supervisors, Professor R. Haldenwang (CPUT) and Dr Silvano Marchetti (L'Aquila University, Faculty of Engineering in Italy), respectively. I also extend gratitude to Professor Hannes Grabë from the University of Pretoria and Dr Gerald Rosenthal for their editorial comments and technical advice. My gratitude also goes out to my fellow staff and undergraduate students, who provided useful research test data and encouragement in the compilation of this work.

As iron sharpens iron,
so a friend sharpens a friend. Proverbs 27:17

Table of Contents

Page

List of Figures

Page

Body

Appendices

List of Tables

Page

Body

List of Symbols

Constants

ΔA	Correction determined by membrane calibration (kPa)
ΔB	Correction determined by membrane calibration (kPa)
Ar	Area ratio for sample disturbance (%)
B	Width of strip footing (mm)
C	Cohesion (kPa)
C_c	Coefficient of curvature
C_h	Horizontal coefficient of consolidation
C_u	Undrained shear strength (kPa)
D_{10}	Effective grain size (mm)
D_f	Depth influence factor
D_R	Relative density (%)
DCP_{DN}	Number of blows with DCP (mm/blow)
D_o	Outside diameter (mm)
D_i	Inside diameter (mm)
E	Modulus of soil elasticity (MPa)
E_s	Young's Modulus (MPa)
E_D	The dilatometer equivalent to oedometer modulus (MPa)
E_{PLT}	E-modulus, plate test (MPa)
g_s	Projected ground acceleration, PGA (m/s²)
G_s	Relative density of soil particle
G_w	Relative density of soil suspension medium
Hz	Hertz frequency (cycles per second)
H_o	Existing horizontal stress
$I\sigma_Z$	Stress influence factor based on sand depth layering
I	Boussinesq's stress influence factor
I_D	The material index, empirical factor
I_z	Depth factor used in Terzaghi and Peck formula
K_0	In-situ coefficient of lateral earth pressure (kPa)
K_D	The horizontal stress index by DMT
k	Stiffness for Geogauge (MN/m)

K	Coefficient of permeability
L	Distance travelled in suspension medium by soil particle (cm)
$M_{CBR\text{-}RL}$	E-modulus from CBR reload test (MPa)
mc	Moisture content (%)
M_N	Stiffness reading for Geogauge (MN/m)
M_R	Modulus of resistance (MPa)
$M1$	Original mass of soil fines (grams)
$M2$	Remaining mass of soil fines (grams)
M_r	Vibration sensitivity (mV per m/s²)
$M_{7.5}$	Magnitude 7.5 earthquake on the Richter scale
M_R	Modulus reaction (MPa)
M_{DMT}	DMT constrained Modulus determined (MPa)
n	Viscosity of suspending medium (Pa.s)
ND	DMT bearing capacity factor
P_0	Correction for membrane stiffness (kPa)
P_1	Correction for membrane stiffness (kPa)
pH	measure of the acidity or basicity of an aqueous solution (log scale)
Q_c	CPT cone resistance (MPa)
Q_u	Ultimate bearing pressure (kPa)
R_D	Stress reduction coefficient for depth Type equation here.
r	Radius of Geogauge footing (mm)
S	Settlement for DMT (mm)
SPT_N	Number of blows with SPT (blows/305 mm)
S_{DMT}	Settlement by DMT method (mm)
Sf	Soil fines passing 0.425 mm sieve (%)
T	Time period for sedimentation (minutes)
U_0	In-situ pore pressure (kPa)
UCS	Unconfined Compressive Strength (kPa)
V_0	Vertical effective stress (kPa)
Z_M	Gauge zero offset (m)
Z	Depth below ground level
ΔZ	Depth increment (m)
$\Delta_{\sigma v}$	change in stress as calculated with Boussinesq formula (kPa)

Greek letters

γ	Unit weight (kN/m^3)
δ	Settlement for related to plate bearing test (mm)
ρ_d	Dry density of soil (kg/m^3)
θ	Angle of repose
ρ_w	Wet density of soil (kg/m^3)
ρ	Density of soil (kg/m^3)
σ'_{vo}	Effective overburden stress (kPa)
σ	Normal stress *(kPa)*
τ	Shear stress (k*Pa*)
τ_{av}	Average cyclic shear stress (kPa)
υ	Poisson's ratio
$\varphi_{safe(DMT)}$	Phi angle of friction by DMT method (degrees)
φ	Phi angle of friction by shear box (degrees)

Subscripts/superscripts

N_c; N_γ and N_q	Classic bearing capacity factors

Terms and concepts

AASHTO	American Association of State Highway and Transportation Officials
AGIS	Agricultural Geo-Referenced Information Systems
ASTM	American Society of Test Methods
CBD	Compacted bulk density
BBF	Below bottom of footing
CBR_{RL}	CBR (Californian Bearing Ratio) reload test
CBR	Californian Bearing Ratio
CPT	Cone penetrometer test
CRR	Cyclic resistance ratio
CSIR	Council for Scientific and Industrial Research
CSR	Cyclic stress ratio
DCP	Dynamic cone penetration test (8 kg model)
DMT	Flat blade dilatometer
DMT-ELAB	Software program for parameter calculation
e	Void ratio
FM	Fineness modulus
ISS	Ionic soil stabiliser
NC	Normally consolidated soils
NBRI	National Building Research Institute of the CSIR
NGL	Natural ground level
NHBRC	National Homebuilders Registration Council
OC	Over-consolidation
OCR	Over-consolidation ratio
PGA	Peak ground acceleration
PLT	Plate load test
PMT	Pressure meter test
SAICE	South African Institute of Civil Engineers
TMH1	Technical Methods for Highways 1
USCS	United Soils Classification System
UCS	Unconfined Compressive Strength
V_S	Shear wave velocity

Chapter 1 Introduction

This chapter introduces the investigation of windblown (Aeolian) sand in a study area close to Melkbos Strand which includes selected areas that have similar characteristics and properties. Some structures built using shallow foundations in these sands have shown a growing trend of failure due to uncontrolled settlement. The following sections introduce the reasons why this study was initiated and then discusses the possible methods to evaluate why these sands can become problematic. The windblown sand of the study area in Melkbos Strand will be referred to as “drift sand”; a term synonymous with the upper sand deposit that was recently (geologically) laid down by the predominant South Easterly winds of the Western Cape, and containing a high percentage of organic contamination.

1.1 Background and Motivation

Predicting long-term settlement in problematic soils such as saturated clays has been problematic but can be overcome by proper investigative geotechnical work. Settlement in sands has been less of a problem to geotechnical engineers, because the sand loses its pore water pressures easily due to the drainable conditions. Yet, unpredicted disasters have been recorded in the study area where movement has occurred through either punching of the foundations (with added mass to the superstructure) or via building activities close by causing vibration. In windblown (Aeolian sand) found along the coast in the Western Cape, this can become problematic if not examined properly for composition and effective depth. Coupled to this is the nature of the in-situ sand itself, and the geological properties associated with it. With a number of in-situ test methods available to geotechnical engineers, the gathering of important information is essential to ascertain before these structures can be built.

The aforementioned soils are known to develop a tendency to collapse and subside under unequal loading. Some useful instrumentation for in-situ measurement has been available for some time, but many (that can yield trustworthy results) are expensive and take long to set up and calibrate. The prediction of settlement below shallow foundations is crucial for the long-term stability of any light structure. Housing development in the Western Cape has suffered in part from structural failure due to poor settlement prediction and site classification (Rosenthal, 2002). The situation may become more critical when vibration takes place via light earth tremors or more seriously, earthquakes. The seismic event triggers the process commonly known as liquefaction, when the loosely compacted granules undergo further consolidation in saturated conditions and so, massive settlement causes the substructure to move unevenly.

The potential damage to man-made structures associated with earthquake-induced liquefaction has been demonstrated in catastrophic fashion over the past forty to fifty years. The phenomenon of liquefaction of relatively clean, poorly graded sand is well-understood. However, the same cannot be said for cases where fine-grained materials are present within the sand matrix. The nature of the fines itself may have a measurable effect on the matrix behaviour (Sadek & Saleh, 2004). The soft, finer texture of the sands within the area known as the Cape Flats can be fairly dangerous to build structures upon, especially when the structure is close to the leeward side of any dune formation, as has been observed personally within the confines of Atlantic Beach Golf Estate in 2005. A useful in-situ device such as the DCP has proven to be invaluable but does have limitations. Another instrument which can assess such conditions is the Flat Blade Dilatometer, which is one focal aspect of this study.

1.2 Research problem

Some residential homes built in windblown sand conditions have suffered structural failure to varying degrees. Severe settlement has been blamed for the damage. A proper investigation must be done in Aeolian sand within a study area, to establish the in-situ geological conditions. To evaluate the properties of the sand it should be evaluated in a laboratory calibration chamber under controlled conditions. To assess the strength parameters and other influential properties, the chamber must be vibrated at varying time based frequencies to assess its relative density. To do this successfully, a suitable instrument must be calibrated and used in the chamber to assess its performance. The DMT must be able to predict unfavourable internal stress conditions. The instrument must also be able to predict settlement comparable to other easy to use in-situ devices such as the Dynamic Cone Penetrometer (DCP).

1.3 Research Question

- Why are some of the Aeolian sands problematic to build on in the Western Cape? Can the open top calibration chamber, with its ability to densify windblown sand to varying degrees, enable the DMT device to predict lateral stresses and settlement?
- Can settlement be predicted with comparable in-situ devices such as the Dynamic Cone Penetrometer?
- Can the DMT device become a useful in-situ instrument for in-situ geotechnical investigations?

1.4 Objectives and outcomes

The objectives of this research are as follows:

- To investigate problematic windblown (Aeolian) sands in a study area along the West Coast of the Cape Peninsula.
- To design and construct an open top calibration chamber to evaluate the characteristics of Aeolian sand.
- To investigate the possibility of liquefaction and correlate this to settlement in the chamber.
- To compare the DMT device to other in-situ test instruments such as the DCP.

1.5 Significance

The significance of the research is to aid geotechnical investigators in their search for trustworthy data resulting from test work in windblown sand that simulates on-site conditions for shallow foundations. The research will aid construction work in similar Aeolian sands in identifying potentially poor subsoil and conditions and steps to avoid it. No significant literature on the usefulness of the DMT device is available in South Africa. A test methodology into how windblown sand behaves under poor site conditions is required, which should include liquefiable conditions. The important aspect of this work is to provide more useful information to the geotechnical database by using a relatively unknown device such as the DMT. This will allow geotechnical engineers to correlate data with other standard test apparatus such as the Standard Penetration Test (SPT) and DCP. Although the aforementioned apparatus has its own role to play in predicting soil conditions below ground, the DMT device may produce more conclusive results that can highlight a possible problem much sooner than other in-situ tests, for example predicting the pre-stress history of the soils and layer based settlement. This, and along with other important criteria is required to assess possible liquefiable conditions.

The data will be useful to geotechnical technicians who need more information regarding the potential loss of stability in windblown sand when it is exposed to potential collapse. This will lead to better designed foundations and more solid superstructures, thereby limiting the amount of possible cracking and structural failure.

1.6 Delineation

The windblown sand will not be tested inside the chamber with the SPT device as this is impractical and too large to manoeuvre inside the planned test location. Only four sites for sampling sand were chosen,

namely inside the Atlantic Beach Golf Estate close to Melkbos Strand; the Big Bay dune formation on the West Coast close to Blaauwberg Strand; the West Coast beach sand in Blaauwberg and the Macassar (Philippi) filling sand from the Cape Flats area. Two of these sands were tested in the calibration chamber; namely the West Coast beach sand from Blaauwberg Strand and the Macassar (Philippi) filling sand. The test depths within the calibration chamber were limited to 800 mm.

1.7 Assumptions

Tests done in the calibration chamber with the DMT device will be affected by a degree of boundary effect. This is acknowledged but will be ignored due to the chamber design (no instrumentation was in place to measure the boundary effect). Nitrogen gas flowing through system is assumed to be constant and that no moisture effect (condensation) has taken place. The sand in the chamber is not assumed to be consistently dense at all depth intervals, whether it be vibrated or not, under saturation or in a dry state. All laboratory apparatus is assumed to be within the SABS tolerances for quality control purposes. The operation of all in-situ devices such as the DCP and DMT is assumed to be within the manufacturer guidelines for accurate measurement.

1.8 Methodology

- Field work

Field investigations were carried out in the study area which centralised in the confines of the Atlantic Beach Golf Estate, Melkbos Strand. Trial holes were dug next to homes whose owners have reported damage to a local housing authority, the NHBRC (the National Home Builders Registration Council). Dunes outside the Estate were examined to gain a perspective of its geological characteristics. Samples were removed to a local laboratory for geotechnical analysis. An independent laboratory was appointed to assist in shear tests and particle size distribution on recovered dune sand.

In-situ probe tests were conducted in the form of the Dynamic Cone Penetrometer. Shelby tubes were inserted to extract non-disturbed samples for density and void calculation.

Some laboratory experimental work for this project was conducted in a modified calibration chamber apparatus rig at the Cape Peninsula University of Technology. The DMT device required a small modification to allow the blade of the DMT device to be fitted into a loading frame. The loading frame (with load cells) controls the penetration and depth process.

- Laboratory work

The scope of the research work is to assess windblown sand from two identified areas in the Western Cape at shallow depths, as the chamber will only allow test depths to 800 mm. Field samples were taken from inside trial holes (positioning via GPS was recorded) and removed to a laboratory for geotechnical analysis. Tests performed were particle size distribution, shear box analysis, void ratio, angle of friction, grading modulus, simulated angle of repose, and dry density.

The calibration chamber was built using similar specifications to the one constructed at TU Delft in the Netherlands. The chamber used at Cape Peninsula University of Technology (CPUT) is open-ended above and completely exposed to atmospheric pressure. The test protocol is to set up the chamber above ground on air actuators (to restrict movement and absorb vibration), fill the chamber with the test dune sand, vibrate the sand in its dry state, take measurements with the DMT. Thereafter the sand is saturated and the tests are repeated with the DMT. Alongside the DMT, the DCP was used under the same conditions. This is to compare the two devices and see whether the results can be correlated or not. The rest of the test regime will include settlement, vibration frequency and modulus reaction (soil stiffness).

1.9 Organisation of dissertation

Chapter 1 Introduction

In this chapter the current deficiency of geotechnical test data is discussed as far as liquefiable conditions in windblown sand are concerned. The need for more reproducible results can be seen from the need for a calibration chamber suitable for shallow test work.

Chapter 2 Literature Review

The history of the DMT device is discussed with reference to its uniqueness in identifying unstable soil conditions that are conducive to liquefaction and early settlement. The manner in which the DMT device calculates settlement is shown.

Chapter 3 Research Methodology

The work plan of the design process for the calibration chamber and how the test devices were operated, are discussed. The DCP is also discussed as a reference tool to settlement prediction.

Chapter 4 Results and discussion

The results of the two sand samples are discussed and the DMT device is evaluated. Evidence is presented to show how the results point to the possibilities of liquefaction prediction and what soil properties are crucial to be aware of.

Chapter 5 Conclusions and recommendations

Conclusions resulting from the outcome of the test work are discussed and recommendations for ground improvement are made based on the test evidence derived from the calibration chamber.

References and Bibliography

This section of the work contains references from research in the study of the behaviour of sandy soils. The emphasis is on test work done using the Dilatometer and other in-situ test devices. Test methods and methodology is included.

Appendices

Recorded data and apparatus specifications in this research work are shown here. Images of structural damage to homes undergoing light to severe settlement are displayed here.

Chapter 2 Literature review

2.1 Introduction

This thesis discusses the associated problems of founding shallow foundations within the drift zone of Aeolian (windblown) sands in the Melkbos Strand area. The drift may be associated with the recent deposit of windblown sand, interspersed with organic vegetation and shattered shale fragments from the Malmesbury group. Recent development in areas within the confines of the Atlantic Beach Golf Estate (see Appendices Figure B.7) have resulted in a number of quality built homes with clear evidence of serious tension cracks because of foundation failure. Upon own investigation it has been found that many of these homes have foundations resting within the drift. Drift contains a huge amount of contamination such as compressible organic vegetative matter that results in volume loss and eventual uneven sagging of the foundations.

The term “drift” is occasionally referred to by local geotechnical consultants when discussing the upper zone of the soil stratum, containing organic debris that may have been transported and deposited by dynamic forces. The sands are wind-borne and moved by wind rather than water or by decomposition of local rock. Most Aeolian sand is of marine origin, although some rivers may provide sand (such as the Berg or Diep Rivers) for wind dispersal. The transport mechanisms can include, but are not limited to, glacial and fluvial (e.g. by glaciers or rivers), and mass movement including landslides. In the deposition process, accepted as having taken place during the Quaternary Age (Harnady et al, 1989), organic matter accumulated alongside. Trial holes can reveal how this happened, and how the movement of the windblown dunes were shaped into its current form.

Homes that were unfortunately built along dunes containing organic contamination in the drift are exposed to uncontrolled settlement. In these cases, not many home builders are aware of the dangers that lay below. In the study area of Melkbos Strand and inside the Atlantic Beach Golf Estate, the drift can vary from 0.9 m to 1.5 m in thickness as being showed measured in Figure 2-1. Assessing these depths can be either via trial holes (preferred) or a hand auger of at least 1.5 m in length. It would appear that not many contractors are privy to the concept of establishing how deep the drift is on any applicable site along with its associated problems for founding shallow foundations therein.

Sufficient documentation exists on how to identify and treat problematic soils (CSIR, 1997; Paige-Green et al, 2008). Although available research provides general identification and treatment of some soils, what would be more useful is to be area specific and to document it in a database. Some good research

has already been done in the Aeolian sands of Parklands, Table View (Laubscher, 2009) using the DCP (Dynamic Cone Penetrometer), and focuses on the characterisation of these sands in the design of shallow foundations with this instrument. No specific geotechnical engineering data for shallow foundations exists in Melkbos Strand/ Duynefontein area. This investigation looks at the geotechnical parameters and characteristics of Aeolian sands within the drift zone of the study area and attempts to highlight why these sands respond poorly under loading in the way it does.

Figure 2-1 Measurement of drift zone at Atlantic Beach Golf Estate

The literature research highlights the need to assess the ground conditions adequately before the construction work of foundations begin. The importance of accurate settlement prediction and the pitfalls associated with this process, such as layer influence, tremors leading to liquefaction and inadequate compaction, are discussed. A device known as a flat blade dilatometer (DMT) is discussed as a tool to be used in a laboratory as well as on site to assess the predicted settlement and when liquefaction may occur in the presence of a high water table and vibration due to earth tremors.

Settlement analysis is one of the more important geotechnical engineering problems. A construction site without adequate founding conditions could be improved by placing fill material above. The fill will inadvertently increase the load on the lower lying soil strata according to Terzaghi and Peck (1967). For

instance, if there is soft clay lying under a layer of sand, the increased load will force water out of the clay, creating a new equilibrium void ratio. The settlement in clay due to the water being forced out by the applied load is called consolidation. The settlement that is caused by this volume change in the clay will also appear on the surface. The ratio of change in volume of the soil multiplied by the initial thickness of the clay layer gives the predicted settlement.

2.2 Aeolian sand origins and locality

Superficial deposits such as drift are produced by fairly young sedimentary deposits at the Earth's surface and are rarely adequately cemented or consolidated to be considered as rock for excavation purposes. Academic geologists, geographers and soil scientists use the term "drift" as subsoil or as a connection with superficial deposits underlying the upper zone of the soil profile. Quaternary deposits have been found up to 70 m thick, consisting of alluvial, Aeolian and marine origin, and generally known locally as the Cape Flats Formation. These deposits consist of fine to medium sand, although coarser deposits are found and contain silty clays and "foul smelling" organic matter (Mountain, 1989). The total volume of Aeolian sand between Koeberg Beach and Saldanha Bay, based on average thicknesses of 7-10 meters, is estimated to be between 1000 and 1200 million m^3 (Franceschini et al, 2003).

The area of the Western Cape, known as the Cape Flats, covers a surface area of 630 km^2. The geographical location of this Aeolian sand-covered coastal plain is shown in Figure 2-3. On this map the Cape Flats is assumed to be the area bounded by the Cape Town – Muizenberg, Cape Town– Bellville – Kraaifontein and Bellville – Eerste River – Strand railway lines and the False Bay coast, with a narrow strip of sand along the western coast, extending northwards from Cape Town through Bloubergstrand and Melkbos. Geologically placed within the Witzand formation (Rogers, 1980; Theron et al, 1992), the sand may be described as fine, siliceous, and weakly cemented sand which probably originated from a marine source. In places a high percentage of sea shells are present (Hill et al, 1981).

The sands are derived from 3 sources:

- Weathering followed by deposition, under marine conditions. It quite possibly was transported on the wind from beaches in close proximity to the now existing southern coastal area.
- The beaches along the coast, from where Aeolian sand was deposited as dunes on the top of the marine sands via the dominant south easterly winds.
- River deposition which is responsible for the coarser grained particles, washed from river beds, into the sea and transported along the coast (Figure 2-4).

Almost 50% of the Cape Flats area is blanketed by these sands, ranging in thickness from 5 to 35 meters. Further north, in the area of the Duynefontein and Melkbos surrounds, the sand profile varies considerably in thickness inland, to almost 60 meters thick within the dune area of Atlantis, also known as the Atlantic plume (Cole, 2005). The thickest deposits of the Springfontyn Formation occupy basement depressions north of Melkbosstrand (Council of Geoscience, 2001). Figure 2-2 Strand below illustrates the depth of the sand dunes close to the Koeberg Power Station, outside Melkbos Strand.

Figure 2-2 Koeberg dunes outside Melkbos Strand

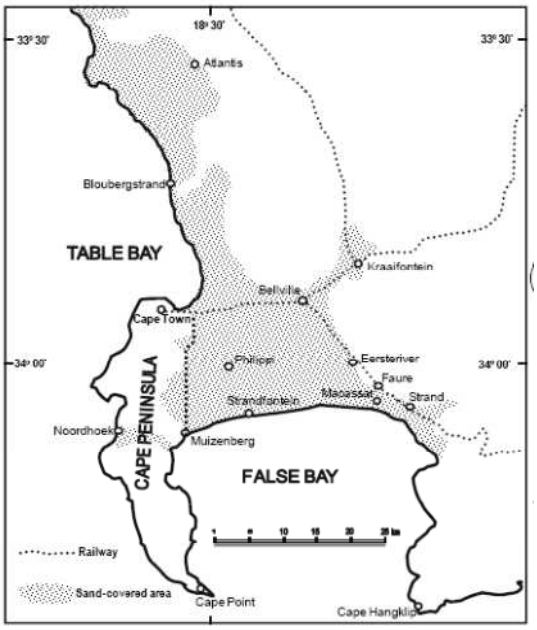

Figure 2-3 Distribution of Aeolian sands

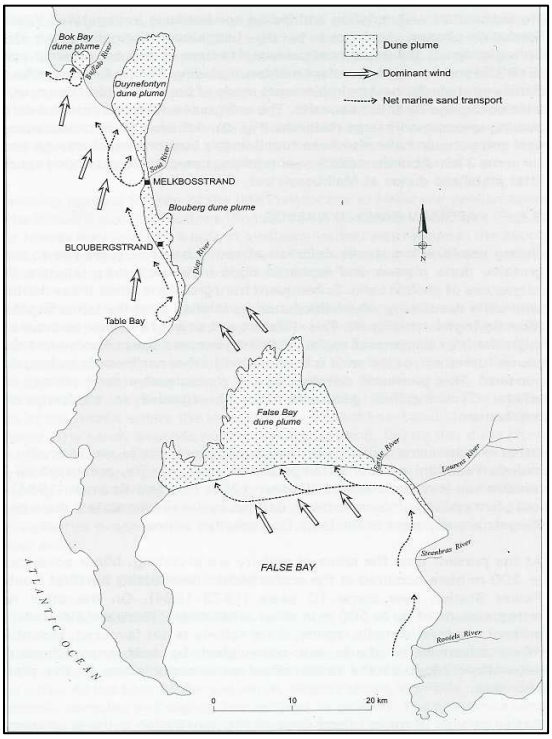

Figure 2-4 Movement of transported sand

2.2.1 **Aeolian sand contaminants**

The Cape Flats sand is today more susceptible to pollution as a result of industrialization, urbanisation and intense overuse of the land area for waste disposal and agricultural purposes. Calcareous materials, industrial wastes, organic materials and illegal dumping of human waste have contaminated large parts of the Cape Flats sand. Deeper down the sand yields a strong smell of H_2S, indicating decaying organic matter (Amdurer, 1956). Iron enrichment zones also occur. The sand in the Melkbos area is slightly acidic, ranging from pH =5.9 – 6.7 (Council for Geoscience, 2005). Many dunes have undulated zones of decaying vegetative matter (including charcoaled branches and roots) that straddle the footprint below homes in the Atlantic Beach Golf Estate of reasonable size (>250 m²) for example.

2.2.2 **Industrial usefulness**

Glass silica sand has been exploited on the Cape for almost 80 years. Sources for building sand are also mined for foundry purposes on the farm Brakkefontyn 32, near Atlantis.

Building sand is found in the vicinity of most major towns in the Western Cape (Theron et al, 1992). In the Greater Cape Town area, it is predominantly restricted to Aeolian dune sand near Philippi and Macassar, and to hill wash sand south of Malmesbury. The sands in the Klipheuwel district are good for concrete works and bituminous road slurry surfacing (known as the Cape Seal). Dune sand is generally too fine grained, rounded and well sorted to be used as fine aggregate in concrete (SABS 1976). It tends to bleed to the surface after vibration. Although these sands are suitable as plaster and mortar sand, care should be exercised when used in reinforced concrete, as corrosion of steel may occur. It may be blended with other coarser sands to provide sands for other building purposes (concrete sand, micro-slurry for road surfaces). Clean Aeolian sands make good filter beds for water purification as well as backfill for trenches, floor slabs and minor concrete works of low strength.

2.3 Known geotechnical properties

The windblown sand 5 km further North of the study area up to Atlantis is comprised of well-sorted, clean, fine to medium grained quartzitic Aeolian sand. Generally the sand can be described as uniform, singular sized fine sand, grey to dirty white in colour. The classification is a SP (USCS) or A.3 (AASHTO). Fineness Modulus values range from 0.7 – 2.56. Aeolian sands have low heave potential and possible collapse potential, dependant on its dry density, organic contamination and stress history (Council for Geoscience, 2005).

The geotechnical properties of windblown sand, for example, around the Koeberg Power Station site are consistent over vast areas (Lunderstedt, 2007). This Impact Assessment Report describes the sand within the Koeberg confines as having a bearing capacity of between 100 – 250 kPa, depending on contamination of buried humus and vegetative debris. Internal angle of frictional shear varies from 29° - 34°. DCP values in the upper region may vary from 55 – 100 mm/blow with the light 8 kg probe, to below 25 mm/blow, once penetration has gone past the upper drift zone. Density values can range from 1550 to 1875 kg/m².

2.3.1 **Local research in Aeolian sand**

Amdurer (1956) used an earth auger in the Cape Flats over a large area, varying his technique from auger extraction to borehole washings. His study area extended from Pinelands to Epping, and included Goodwood, Bellville and Kuilsriver. Boreholes were spaced at about 330 meters. C_c (co-efficient of conformity) values vary from 2.1 to 2.2 in the Cape Flats and are also classified as poorly sorted,

according to the Trasks sorting order, S_0. Figure 2-5 is included for comparative interest between the two sands from the Cape Flats and Koeberg. It is clear to see that the sand extracted is highly contaminated.

Figure 2-6 below is an illustration of a typical borehole profile produced in Amdurer's Ph.D thesis (Amdurer, 1956). The sand extracted by borehole washings is described as round to sub-angular particles, classified mostly as fine sand. The upper zone is rich in iron minerals. The sandy silt below the water table appears green to brown in colour. Within this layer a strong smell of H_2S yields decomposing matter. The silty sands appear often and are classified as fine to medium in size. The silty fraction contains angular particles of quartz, and when found dry is known as "koffieklip" (interstitial brown colloidal cement). Amdurer found evidence deeper down of peat, organic matter, silcrete, calcrete and ferricrete. The consolidated triaxial tests completed by Umdurer are shown below in Table 2-1. The tests were done on the silty clayey sands.

Table 2-1 Shear Strength of Cape Flats sandy silts and clays (Amdurer, 1956)

Parameter	Along bedding plane	Normal to bedding plane
Angle of internal resistance, °	12	21
Cohesion, kPa	213	55

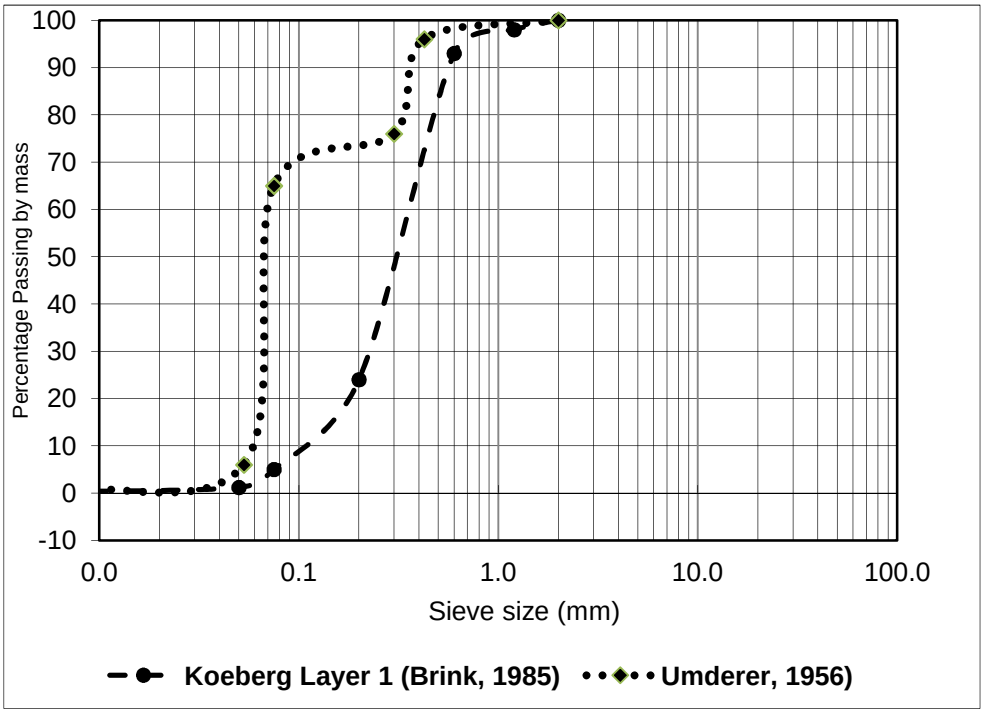

Figure 2-5 Contaminated Cape Flats and Koeberg sub-surface sand below reactor (Brink, 1985)

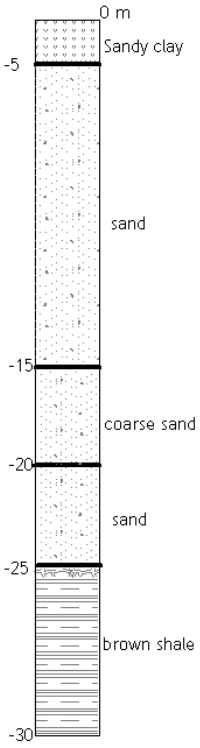

Figure 2-6 Borehole profile (Amdurer, 1956)

Recorded data for other sandy areas of the Cape Flats (location unknown) and Klipheuvel hillwash (near Malmesbury) are listed below in Table 2-2.

Table 2-2 Mechanical Properties of Western Cape sands (Kaytech, 1995)

Mechanical Property	Cape Flats sand	Klipheuvel hill wash sand
Specific Gravity, Gs	2.67	2.7
Maximum Dry Density, kg/m^3 and % OMC	1660/7.0	1915/10.8
Co-efficient of Uniformity, C_u	2.26	8.24
Internal angle of shearing resistance, °	41	54

2.4 Recent case studies

ABA Brink (Brink, 2001) reported extensively on the geological properties of the Aeolian sands below the Koeberg Power Station structure. These sands were removed to depths up to 15 meters and backfilled using 5 % sulphate - resistant cement by weight. The final layer works were compacted to a controlled

MOD.AASHTO of 97%. This densification ensured suitable durability, strength and resistance to foreseeable liquefaction. The upper layer (±6 m) deep was discovered to contain less than 1 % of organic matter. A typical borehole in the study area of the Koeberg reactor is shown below in Figure 2-7 with the corresponding expected uncorrected SPT data alongside.

The relative densities recorded through 3 layers at the Koeberg site are shown in Table 2-3; the testing frequency is shown in brackets.

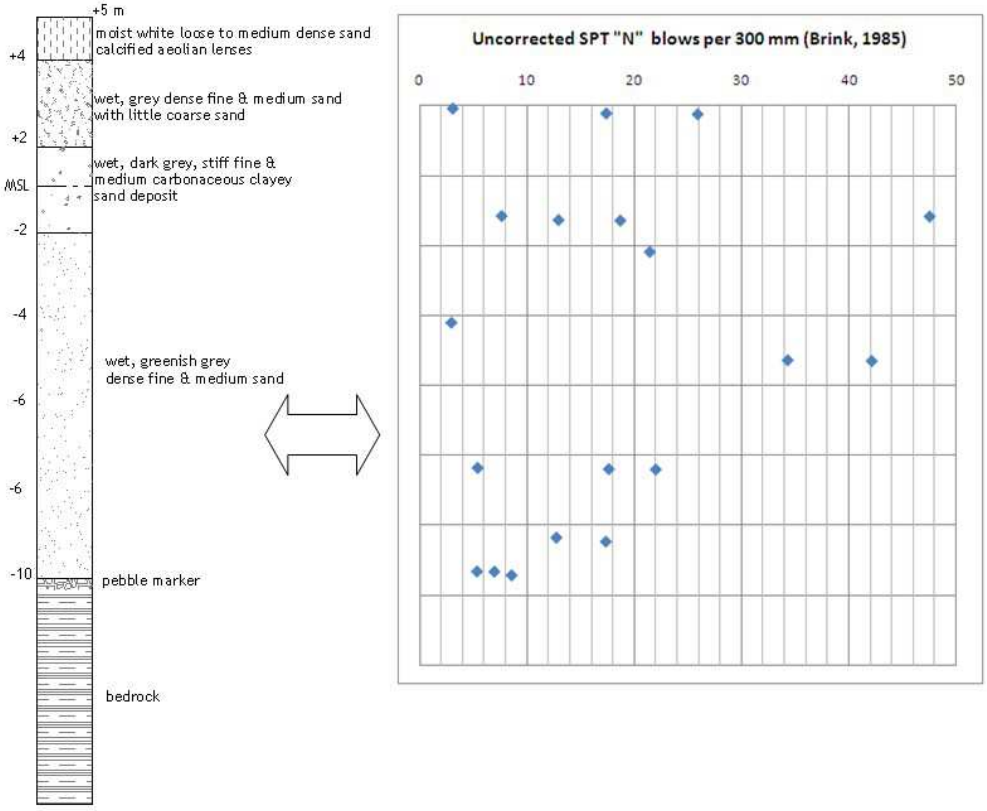

Figure 2-7 Soil profile and corresponding SPT data below Koeberg reactor (Brink, 1985)

Table 2-3 Field and relative density data recorded at Koeberg (Brink, 1985)

Layer	Average MDD (kg/m^3)	Average field density (kg/m^3)	Average relative density (%)
1	1770 (12)	1670 (24)	71 (24)
2	-	1670 (9)	-
3	1790 (2)	1650 (44)	68 (44)

Shown below in Figure 2-8 are typical particle size distributions for the sand in the upper surface below Koeberg Power Station; the grading represents the average percentage passing by mass. On this graph Brink (1985) transposed by way of comparison, the typical average grading of the sands that liquefied in the earthquake-hit regions of Niigata and that was reported by Idriss and Seed (1967).

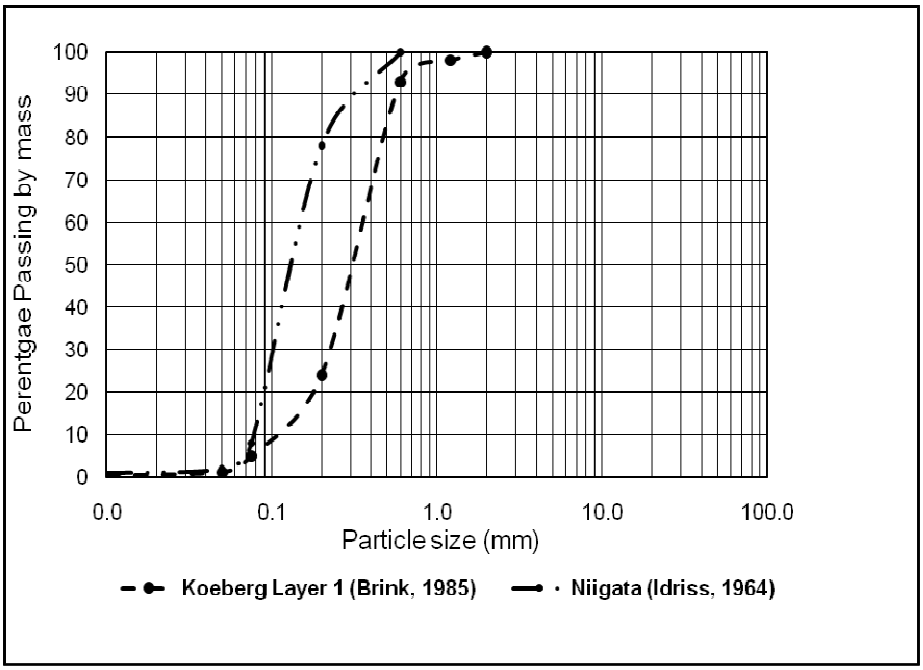

ink, 1985)

2.4.1 **Erosional deposition in the Cape Flats**

Aeolian conditions are dominated by erosional and depositional activities of the wind. Homes exposed to these conditions are susceptible to structural damage, by having sand eroded from below corners of the buildings, as has been documented in the Delft area of the Cape Flats (Goliger et al, 2008). The pictures below (Figure 2-9 and Figure 2-10) from this report highlight the damage due to dynamic forces of the seasonal South Easterly wind. The pictures are of homes close to Strandfontein and Delft in the Cape Flats.

Figure 2-9 Wind deposition (Goliger, et al, 2008)

Figure 2-10 Erosional collapse (Goliger, et al, 2008)

2.4.2 **Recent contributions to local geology**

In their study of the Engineering Geology of Cape Town (Mountain et al, 1989) it was recorded that interesting geological problems exist for the Cape Flats region. Buried beneath the Cape Flats sands are pans, alluvial features, drainage systems, some expansive clays, all of which can cause foundation design problems. Table 2-4 highlights the properties of the Aeolian sands under the report's investigation.

In this monographic report various foundation types are listed for significant structures that were built in the Western Cape. The typical footing type for small residential homes was cited as strip (spread) footings carrying light loads. Bearing capacity and settlement issues are listed as parameters not to be ignored. Coupled to this is the question of how dense these sands are?

The Stapelberg report for the Council of Geoscience (Stapelberg, 2005) examines the geotechnical properties of the Aeolian sands closer to Melkbos Strand. The study records, amongst other Formations, the Witzand Formation of the Sandveld Group, under which the study region fell. An extraction from this report is given below in Table 2-5.

Table 2-4 Geological Problems associated with soil types (Mountain, 1989)

Soil Type	Origin/Stratigraphy	Material Description	Potential problems
Transported soil	Aeolian	Loose to dense sands, cemented in places	Variable founding conditions and bearing capacity
	Marine	Loose to dense sands	Differential settlement
	Alluvial (rivers, streams, fans)	Loose to dense, soft to firm sediments, ranging from clays to boulder gravels	
	Colluvial (hill wash, talus) pediment deposits	Variable sediments, ranging from clayey silts to boulder gravels	Mass movement on slope; seepage; settlement; expansive potential

Table 2-5 Aeolian sand of the Witzand Formation (Stapelberg, 2005)

Sample Nr & depth (m)	Origin	Land -form	% Clay	Heave poten-tial	Collapse potential	pH/ Conduct. (mS/m)	Perm (cm/s	Soil classifications & grading curves			
Witzand Formation								USCS	PRA	Fm	Gm
CB9/1 1.35	Aeolian/ littoral	Stabilised dunes	34.7	Low	No	6,45/14,9	$<4x10^{-6}$	SM	A.4	2,37	1,08
CB10/1 3.5	Aeolian	Stabilised dunes	0,99	Low	No	8,34/0,05	$1.13X10^{-2}$	SP	A.3	1,27	0,99
CB14/1 0.9	Littoral	Stabilised dunes	1,0	Low	No	6,17/13,5	$2.29x10^{-2}$	SP	A.3	1,37	0,99

2.4.3 Shifting sands along the West Coast

Figure 2-11 below illustrates the areas along the West Coast (light blue shade) that has been designated as containing shifting sands. The AGIS web based facility (which allows users to extract user based geological features) has small-scale derived maps published as the National Resources Atlas (ARC-ISCW, 2004). Users can request to see potentially problematic soils. Heaving and swelling clays are also included.

A study on beach sand composition and the effect of wind deposition (Franceschini et al, 2003) highlights the important role of transportable Aeolian sand, especially as far as the terrigenous and carbonate material content are concerned. Terrigenous materials include clastic sediments and rocks, consisting of rock fragments and mineral grains that have been eroded from land areas. These may form in both bodies of salt and fresh water and on land.

Sand being transported down important rivers in the Western Cape, such as the Berg and Diep rivers seems to lack the aforementioned components. This seems to affect the dune field size in the area from Koeberg to Saldanha bay. The study pinpoints the effects of the long shore drift, which by calculation amounts to 0.2 $x10^6$ m^3 per year.

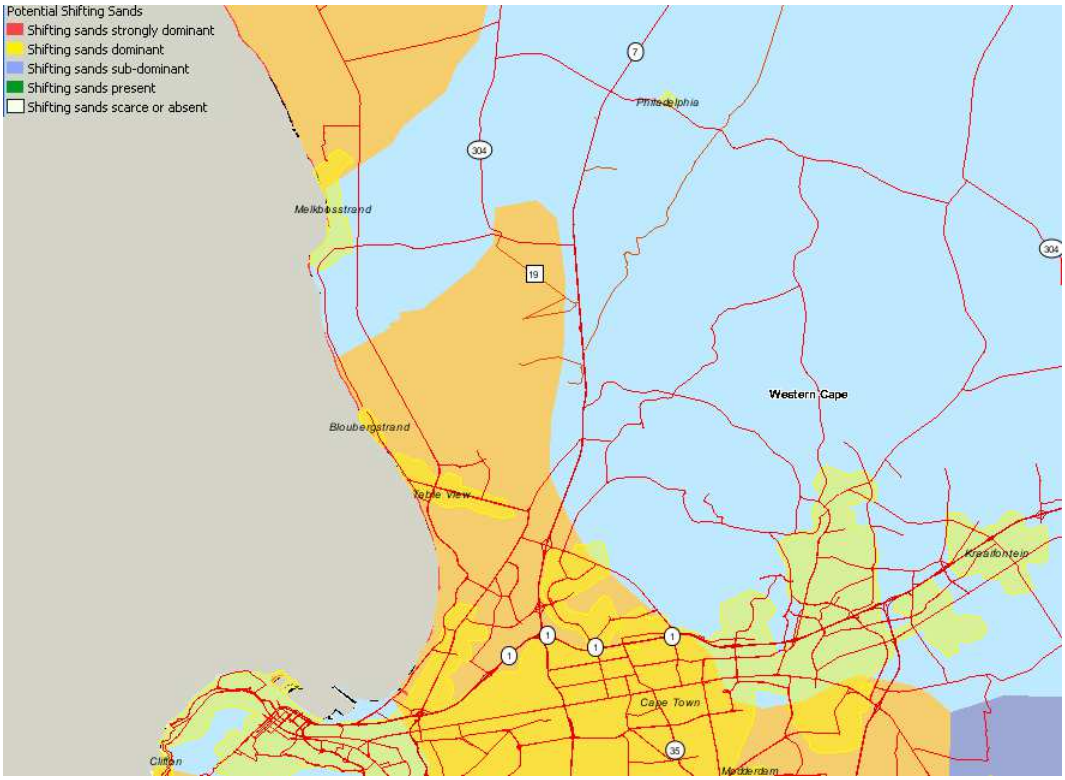

Figure 2-11Shifting sands in the West Coast region (AGIS, 2010)

2.4.4 **Relationship between the DCP and other strength parameters**

Californian Bearing Ratio (CBR) and Unconfined Compressive Strength (UCS)

Paige and Green (2009) refer to the DN of the DCP having a relationship with the CBR and UCS. Correlations are shown below in the following equations (2.1-2.4)

$$\text{If } DCP_{DN} > 2 \text{ per blow, then CBR} = 410 * {DCP_{DN}}^{-1.27} \quad (2.1)$$

$$\text{If } DCP_{DN} < 2 \text{ per blow, then CBR} = (66.66 * DCP_{DN^2}) - (330 * \text{DCP}_{\text{DN}}) + 563.33 \quad (2.2)$$

$$\text{UCS} = 15\text{x CBR}^{0.88} \quad (2.3)$$

$$\text{UCS} = 2900 \text{ x } {DCP_{DN}}^{-1.09} \quad (2.4)$$

There are more models available for converting the DCP penetration rate to the CBR. These are shown below in Table 2-6 and refer to models utilizing the 60° cone only. Table 2-6 refers to work done by Samson (1984) and Harison (1986) on the use and interpretation of the DCP.

Table 2-6 CBR Conversion models (Paige-Green et al, 2009)

Cone angle	Reference	Relationship
60°	TRL	$\log_{10}(CBR) = 2.48 - 1.057 \log_{10}(DN)$
60°	Sampson	$\log_e(CBR) = 5.8 - 0.95 \log_e(DN)$
	Plastic materials only	$\log_e(CBR) = 5.93 - 1.1 \log_e(DN)$
	PI > 6 materials	$\log_e(CBR) = 6.15 - 1.248 \log_e(DN)$
	PI < 6 materials	$\log_e(CBR) = 5.70 - 0.82 \log_e(DN)$
	PI = 0 materials	$\log_e(CBR) = 5.86 - 0.69 \log_e(DN)$
60°	Harison	$\log_{10}(CBR) = 2.81 - 1.32 \log_{10}(DN)$
	Clayey soils	$\log_{10}(CBR) = 2.56 - 1.16 \log_{10}(DN)$
	Sand S-W	$\log_{10}(CBR) = 3.03 - 1.51 \log_{10}(DN)$
	Gravel G-W	$\log_{10}(CBR) = 2.55 - 0.96 \log_{10}(DN)$
	Combined data	$\log_{10}(CBR) = 2.81 - 1.32 \log_{10}(DN)$
	Soaked samples	$\log_{10}(CBR) = 2.76 - 1.28 \log_{10}(DN)$
	Unsoaked samples	$\log_{10}(CBR) = 2.83 - 1.33 \log_{10}(DN)$

TRL: Transport Research Laboratory (1993)

2.4.5 **Relative Density (%D_R)**

The relative density is a useful parameter for describing the consistency of the sand. Research by Coduto (2001) to correlate the DCP_{DN} to the % D_R produced the following formula as shown in (2.5).

$$\%D_R = \frac{189.93}{DCP_{DN}0.53} \tag{2.5}$$

The data is shown in Figure 2-12 below and illustrates an excellent correlation.

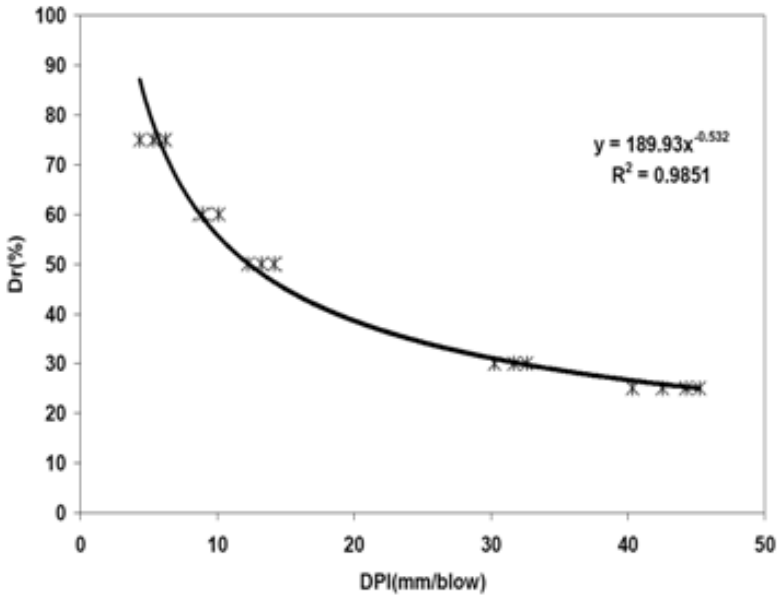

Figure 2-12 % D_R vs DCP_{DN} (Coduto, 2001)

Meyerhof (1959) suggested that the % D_R could also be correlated with the internal angle of friction for normally consolidated sand, as shown below in formula (2.6).

$$\varphi = 28 + 0.15 * D_R \tag{2.6}$$

2.4.6 **Estimating bearing capacity, Q_u**

Definition: The soils bearing capacity is its ability to withstand a vertical load placed on its foundation without failing due to shear and in some cases, uncontrolled settlement. Ultimate bearing capacity (Q_u) is the minimum gross pressure at the base of the foundation at which soil fails in shear (Das, 2010). The DCP has been used in the past to relate its penetration rate to the in-situ bearing capacity and four models are presented below.

- Model 1 (Kessler, 2010)

For analysis of shallow foundations an estimate of bearing capacity can be made from the equation adapted from the Portland Cement Association (PCA, 1955) showing the relationship between bearing capacity and CBR.

$$\text{Bearing capacity, } Q_u = 26.16 \times \text{CBR}^{0.664} \quad (2.7)$$

The CBR value is determined from the DCP_{DN} number as: CBR = 292 / $DCP_{DN}^{1.12}$ (Kessler, 2010). It should be noted that this equation is not suited for soils classified as CL or for clays with very low CBR values (<10%).

In South Africa Kleyn (1975) suggested using Log CBR = 2.628 - 1.273 log(DCP_{DN}). This formula has been used successful for road rehabilitation assessments and is suitable for natural gravels with relatively low plasticity.

- Model 2 (Paige-Green, 2009)

The DCP penetration rate has also been correlated in foundations, predicting the bearing capacity of soils for founding structures. This method provides a general indication and should not replace conventional testing, but can be a useful addition to extend the results of other tests using a cheap in situ test method. This model s based on the formula (2.8):

$$\text{Bearing capacity, } Q_u = 3426.8 \times DCP_{DN}^{-1.0101} \quad (2.8)$$

- Model 3 (DN converted SPT_N value)

Attempts in the past have been made to predict the SPT_N value by inverting the penetration rate of the DCP (Rosenthal, 2002). The number of blows is recorded to drive a SPT split spoon sampler and its cone through 305 mm and is usually done at the bottom of a pre-drilled bore hole. If the DCP_{DN} number is divided into the SPT depth (305 mm), and ignoring moisture influence, a DCP correlated “N” value is obtained, i.e. DCP_{DN} of 45mm/blow can correlated to 305/45 = 6.7 (unadjusted for a water table). The SPT method has been adopted by the ASTM in their standards (ASTM, D1586-64).

With the x DCP_{DN} value an attempt can be made at using Terzaghi's classic bearing factors for shallow foundations to assess the bearing capacity (Terzaghi's, 1967). For strip footings in sand Terzaghi's classic formula would read as shown below in (2.9):

$$\text{Bearing capacity, } Qu = CN_c + 0.5\gamma BN_\gamma + z\gamma N_q \tag{2.9}$$

Past research (MnRoad, 2002) using a direct correlation between the DCP's DN and the SPT "N" value is shown below in (2.10)

$$\log DCP_{DN} = -1.05 + 2.03 \log SPT_N \tag{2.10}$$

It should be noted that the above equation is valid only for SPT blows > 30 per 305 mm.

- Model 4 (Flat Blade Dilatometer)

This method features a direct approach that utilises the DMT's test results at the depths recorded on its control console. The method uses the 1.1 mm expansion lift off pressure readings directly without any additional interpretation of its results. Full scale load tests were used to correlate the DMT's readings. Based on these findings (Lutenegger et al, 2006), the ultimate bearing capacity formula is shown here in (2.11).

$$Q_u = ND(P_1 - P_0) + \sigma_{vo} \tag{2.11}$$

2.4.7 **Angle of friction vs angle of repose**

Mohammadi et al, (2007) proposed that a good correlation exists between the DCP's DN and the internal angle of friction in sandy soils. The formula for this correlation proposed through their research is shown below in (2.12).

$$\varphi = 52.16/DCP_{DN}{}^{0.13} \tag{2.12}$$

In recent research by Ghazavi et al, (2008) a comparison was made of the angle of repose to the angle of friction for sands. This paper presents the results of a series of laboratory experiments performed on three types of sand. Direct shear tests are also carried out on the sand at the same compaction to determine the friction angle. These two angles are then correlated. Their results show that the angle of repose can be correlated to the internal friction of the sand and the formula proposed is shown below in (2.13).

$$\theta = 0.36\varphi + 21.2 \tag{2.13}$$

(Zhou et al, 2002) presented a study on a numerical and experimental study of the angle of repose of mono-sized coarse spheres (Figure 2-13), an important macroscopic parameter in characterizing granular materials. In the Zhou study it is shown that the angle of repose is significantly affected by the sliding and rolling frictions, particle size and container thickness, and is not sensitive to density, Poisson's ratio, damping coefficient and Young's modulus. In Figure 2-14 below the predictive angle of repose is compared with the simulated angle. The predictive model however is only valid when the width of the container used in their experiments equals or is greater than 4d; "d" being the average particle size.

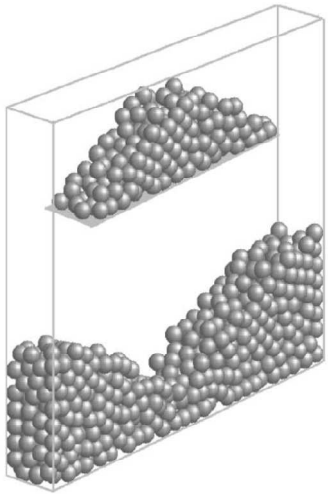

Figure 2-13 Sample container and discharge model (Zhou, et al 2002)

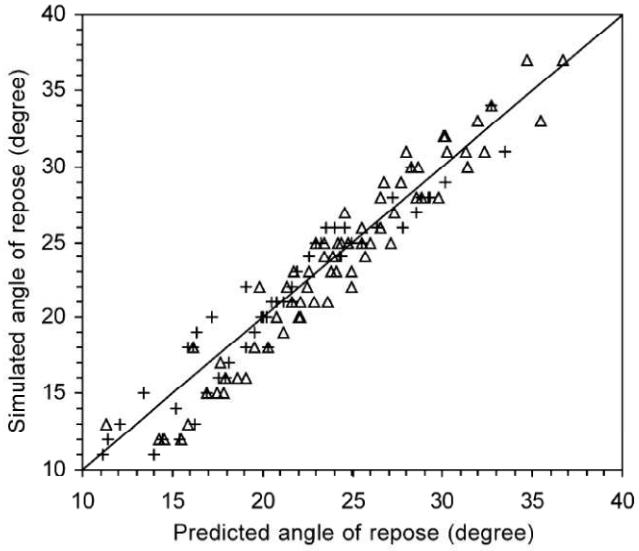

Figure 2-14 Predicted vs. simulated angle of repose (Zhou, et al 2002)

2.4.8 **Soil properties linked to liquefaction**

The Cyclic Stress Ratio (CSR) is an important soil property to consider when assessing liquefaction. Seed & Idriss (1971) introduced a "simplified procedure", which is currently used as standard practice for evaluating the liquefaction resistance of soils (Monaco, 2005). Their procedure requires the calculation of two terms: (1) the seismic demand on a soil layer generated by the earthquake, known as the cyclic stress ratio or CSR, and (2) the capacity of the soil to resist liquefaction, known as the cyclic resistance ratio, or CRR. They discovered that if the CSR is greater than the CRR, liquefaction can occur. The cyclic stress ratio CSR is calculated by the equation in (2.14).

$$\mathrm{CSR} = \frac{\tau_{vo}}{\sigma'_{vo}} = 0.65\left(\frac{a_{max}}{g}\right) * \left(\frac{\sigma_{vo}}{\sigma'_{vo}}\right) * R_D \qquad (2.14)$$

2.4.9 **Definition of Cyclic Stress Ratio**

The capacity of a soil to resist liquefaction is represented by the Cyclic Stress Ratio (CSR). If the cyclic stress ratio caused by the earthquake is greater than the cyclic resistance ratio of in situ soil then liquefaction could occur during an earthquake or sever tremor (Anbazhagan, 2009). Other in situ tests can assist here too, such as the predicted SPT_N value. The SPT_N values in this research are related to the DCP penetration rate and are the amount of blows required from the 8 kg hammer to drive the cone a distance of 300 mm through the sand. The Cyclic Resistance Ratio (CSR) can be evaluated from research data, as displayed in Figure 2-15; in this case the CSR vs. SPT_N was a method developed by Seed and Idriss (1982). The assessments were based on expected levels of an earthquake magnitude equal to 7.5.

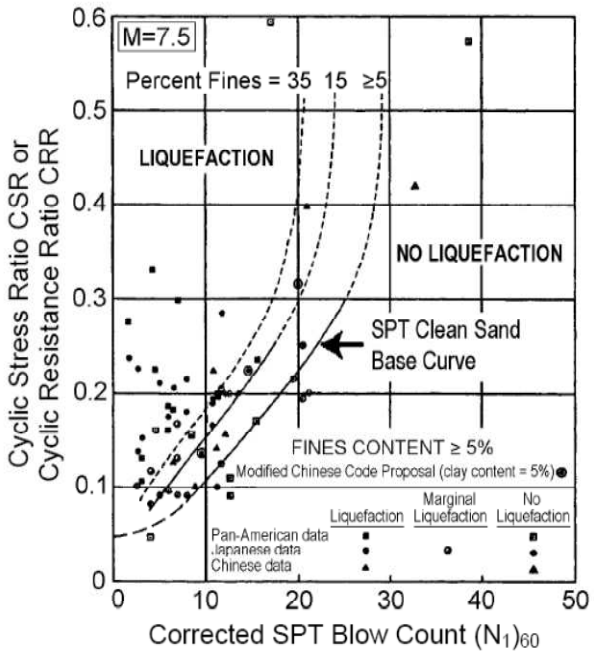

Figure 2-15 Correlation between SPT_N -values and CSR

(Seed & Idriss, 1982)

2.4.10 **Estimating the Cyclic Resistance Ratio**

- Evaluate the % D_R corresponding to the values of Q_c for the "CPT Clean Sand Base Curve" in Figure 2-16 using various D_R -Q_c correlations Baldi et al, (1986) and Jamiolkowski et al, (1985).
- Estimate the values of K_D corresponding to the above calculated values of Dr using the K_D -D_R correlation by Reyna & Chameau (1991) shown in Figure 2-17.
- Evaluate CSR corresponding to the values of corrected SPT_N for the "SPT Clean Sand Base Curve" in Figure 2-15 using the D_R–SPT_N correlation by Gibbs & Holtz (1957).

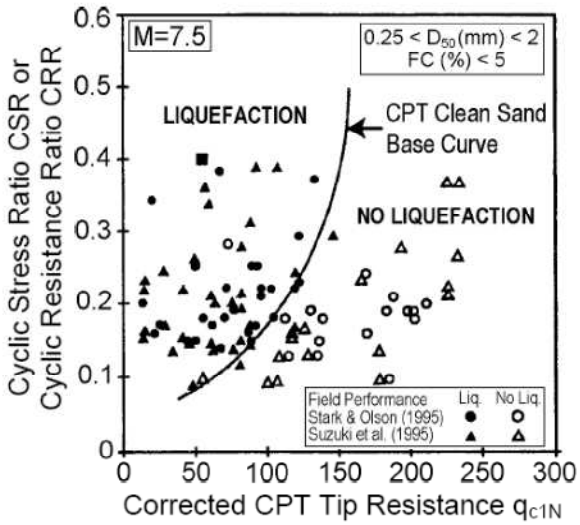

Figure 2-16 CSR vs CPT Q_c

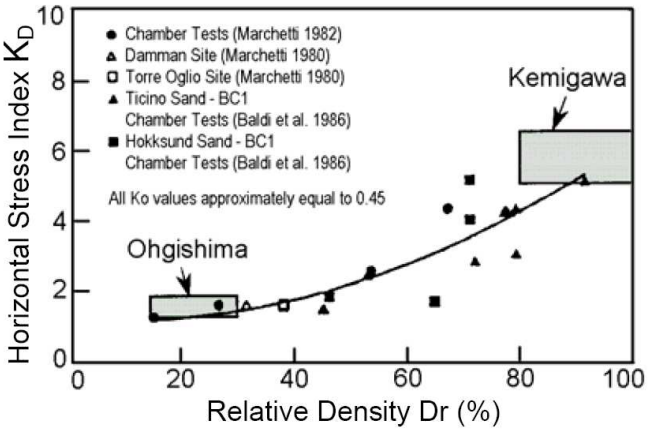

Figure 2-17 % D_R vs DMT K_D

2.4.11 **Definition of liquefaction**

Liquefaction occurs when the strength and stiffness of a soil is reduced dramatically by earthquake shaking or a form of rapid loading. Liquefaction and related phenomena have been responsible for tremendous amounts of damage in historical earthquakes around the world. The subsequent damage occurs when the strength of the soil decreases and the ability of the soil deposit cannot support foundations for buildings or bridges.

Liquefaction occurs in saturated soils, in which the voids between individual particles are completely filled with water. This water exerts a pressure on the soil particles that influences how tightly the particles themselves are pressed together. Prior to an earthquake, the water pressure is relatively low. However, earthquake shaking can cause the water pressure to increase to the point where the soil particles can readily move with respect to each other.
(http://www.ce.washington.edu/~liquefaction/html).

Based on the above criteria for liquefiable conditions, the water table of the surrounds in the study area would have to rise significantly. The sand would have to be uniform in gradation with rounded particles, a very loose density state, must be recently deposited with no cementation between soil grains, and no prior preloading or seismic shaking.

2.4.12 **Earthquakes and expected liquefaction**

Earthquakes in areas such as Bhuj on 26 January 2001, resulted in several structures being damage in Ahmedabad City, which is located about 300 km away from the epicenter (Bhandarij & Sharma, 2001). Large areas were examined and found be underlain with unconsolidated sediments. The structural damages in this location were attributed to the response to violent shaking. This event serves as a reminder that liquefaction of sandy soils and sand with non-plastic fines as a result of earthquake ground shaking pose a threat to the safety of civil engineering structures (Sitharam et al, 2004). Liquefaction will of course not occur without the presence of a high water table.

If a load is applied to a sandy soil it will become compressed and the onset of settlement will occur immediately. Total settlement is not as deep as in clay (Al-Khafaji and Andersland, 1992). The sand has a much higher permeability than clay, getting rid of voids quickly. Terzaghi and Peck (1967) discovered that if a large, expensive structure is being erected, the project needs to start by placing a fill on the area

where construction takes place. This increases the load to the site and speeds up the rate of settlement. Once the calculated depth of settlement has been achieved, the fill can be removed and construction can start.

Non-uniform sand deposits, which are common along any coastline that suffers from strong onshore wind, are found in dunes to varying depths. These areas have become popular for building development and choosing the correct founding levels can be difficult. The dunes may be undulated and soft zones of unconsolidated sands can form deep pockets filled with organic debris (as is the case in the Atlantic Beach Golf Estate). The client will have to bear the financial burden of having to approve either very deep reinforced strip footings, or install micro-piles, to transfer the loading to firmer ground below.

The deposits can vary from thinly spread to thicker stratum. The densities of these deposits are deceptive, being dependent upon the moisture content and level of contamination. For example, shallow investigations, less than 2*B (where B= footing width in meters) in the West Coast dune sand, can produce unreliable results. The SPT_N values may seem acceptable, i.e. above 15 for loading of less than 75 kPa. The influence factor of the pressure bulb is important to evaluate as well (Rosenthal, 2002). Relative densities should be checked deeper down to identify the collapse potential in the softer dune sand deposits. If ignored and in the presence of a high water table, the structure may be in serious situation in the event of a significant tremor. According to Terzaghi and Peck (1967) when a structure is erected on homogeneous strata settlement should take place uniformly. This analysis is largely based on the theory published by Boussinesq (1885) and is discussed further in the next paragraph. The method can be utilized in the presence of multiple layers. With this method the effective depth of influence is accepted to be three times the width of the foundation.

In 1809, a series of three earthquakes occurred, one with the epicentre on the farm Jan Biesjes Kraal, in the vicinity of the Paddocks shopping centre in Milnerton. A report written in 1832 by a visiting naturalist, Von Buchenroder, included actual visual inspection of fissures extending for about 1.6 km from the epicenter. Upon reviewing, an earthquake of magnitude 6.5 was suspected, which is an assessment made by Dr C. Hartnady (http://www.umvuto.com).

2.4.13 **The need for deep soil layering investigation**

Problems arise when part of a structure's underlying strata consists of sand pockets or organic deposits found in between suitable compressible soil or clay. These areas do not have the same bearing capacity. What may occur is that the deposits will compress differently to the other surrounding strata causing the softer dune sand to be forced into vacant pockets or voids. This leads to differential settlement and can cause some of the biggest problems known to construction settlement according to Al-Khafaji and Andersland (1992). When differential settlement takes place, the structure will settle more in some places causing greater strain on some of the superstructure than other parts, and will inevitably cause major cracks and structural failure. This once again points to the importance of a proper subsurface investigation.

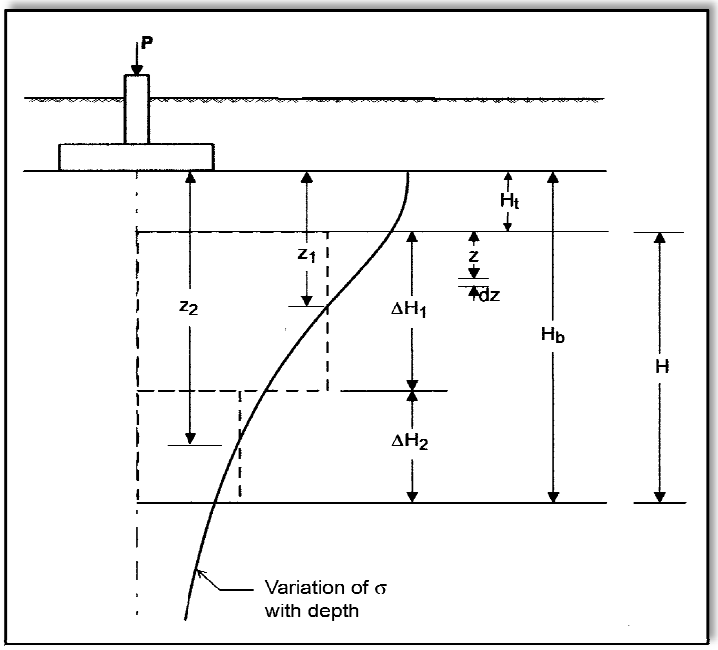

epth influence (Shamrani, 2004)

A layered soil stratum and its individual magnitude of primary settlements are essential to calculate. These are all dependent upon the stresses built up in each layer. Shamrani (2004) illustrates this in the layered system shown in Figure 2-18. At the centre of each sub-layer the Boussinesq stress influence coefficient, "*I*", is calculated for a square footing subjected to a uniformly distributed load (Shamrani,

2004). The individual sub-layer influence factor, "*I*" is calculated by dividing each of the coefficients by the accumulative sum of all the coefficients. This is completed up to the depth of influence, namely 3 x B, as was suggested by Rosenthal (2002). Therefore, when architects design footings, the prescribed size B is often a fixed dimension based on the choice of local standard being applied, whether SABS (South African Bureau of Standards) or the local SAICE (South African Institute for Civil Engineers) Struct. E Codes. What is equally important is the specification governing the depth of soil investigation. When on-site work is established over several layers of sandy deposits (such as windblown dunes), each of the layers will present its own stress related history, and thus individual attention is to be paid to the total accumulative settlement predicted in the trial holes on site. The method incorporated by Boussinesq's (1885) stress influence coefficient, "I", makes full use of this fact and is useful for calculating settlement.

2.5 The Flat Blade Dilatometer (DMT)

The DMT device is a tool used to assess the lateral stresses that are built up below ground and is useful in deep layered soil with varying degrees of lateral stresses. Also known as "The Marchetti dilatometer", after its original designer, Dr S. Marchetti, the DMT is an in-situ testing device, the results of which have been interpreted chiefly through empirical correlations based on the results of field tests. The original design was conceived back in the 1980s. The interpretation of the results has involved the use of two readings, P_0 and P_1, though recently a third reading, P_2, has been introduced. P_0 and P_1 are simply corrected pressure gauge readings, for readings *A* and *B* respectively; the units being in bar. It entails using simple mechanical-electrical principles in contrast to a few of the alternative devices which use electronic sensors. The corrected readings for each are calculated as shown in equations (2.15) and (2.16) below.

$$p_0 = 1.05 * (A - Z_M + \Delta A) - 0.05 * (B - Z_M - \Delta B) \quad (2.15)$$

$$p_1 = B - Z_M - \Delta B) \quad (2.16)$$

Z_M = Gauge reading when the DMT is vented to atmospheric pressure. The manufacturer recommends that if ΔA & ΔB are measured with the same gauge for current readings *A* & *B*, then Z_M is set to 0 (i.e., Z_M is compensated for).

2.5.1 **Fundamentals of the Flat Blade Dilatometer**

The DMT has been found to be extremely versatile and robust during laboratory and field testing. Delicate components, such as the Perspex tubing (Figure 2-21) and internal conductive wiring performed above what was expected (Marchetti, 1980). The internal components of the diaphragm do need careful inspection on a regular basis, so that fine sand and dirt do not interfere with the electrical signals between the blade and reading monitors (Marchetti, 2001). The DMT can be linked to a laptop computer which records all data related to the pressure readings during a test procedure. An illustration of this setup is shown in Figure 2-19.

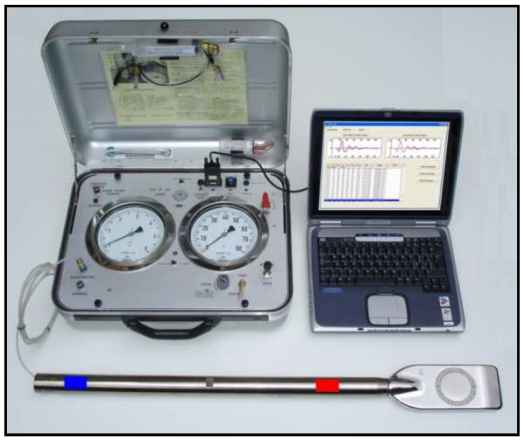

Figure 2-19 DMT Components (Marchetti, 2001)

2.5.2 **Operation of the DMT**

The DMT is constructed to yield a stainless steel blade that has a flat, custom fitted circular membrane mounted level on one side (Figure 2-20). Before the test begins, the surface of the steel diaphragm is level with the adjacent flat surface of the blade. The dilatometer is hydraulically controlled and jacked below the surface using a rig or via a Kentledge system of ballast weights similar to that used for a plate bearing test. The device can search deep down into any soil stratum and reveal what properties the soils have in its original undisturbed state. In this manner, the soil's stress history (or aging process) is to a large degree not disturbed. The blade is attached to a console on the upper surface by an internally wired Perspex pneumatic-electrical tube, to transferring gas pressure and electrical continuity that passes down through the insertion shafts. A pressurised gas cylinder, connected to the console by the hollow Perspex cabling, supplies the controlled pressure required to inflate the steel diaphragm.

Nitrogen gas is typically used, as this is the driest gas available that will not allow moisture into the system to enhance corrosion. The console is supplied with a regulator, pressure gauges, an audio-visual signal (an alert for the user for readings to be taken) and to a vent valve. The flow of pressure is controlled so that the inflation occurs within 30 seconds. It is reported by the designers that a test takes little time to complete; a thirty meter borehole's profile may take less than 2 hours to complete (Marchetti, 1980).

Figure 2-20 (DMT blade components, Marchetti, 2001)

Shafts, similar to those used for the CPT test, are used to transfer the thrust from the control rig to the dilatometer's blade. The principle working layout of the dilatometer test is shown in Figure 2-21. A test will begin by advancing the dilatometer's blade into the ground until the audio signal warns the user that lateral stresses are being detected. Soon after, the user can inflates the membrane from the controls on the console and begins to takes two important readings. These are firstly:

- the *A*-pressure, i.e., the recorded pressure reading required to initiate the first movement of the membrane
- the *B*-pressure, i.e., the recorded pressure reading at the point when the membrane reaches 1.1 mm into the soil.

The above readings provide the raw data and equations (2.15) and (2.16) are utilised for corrections.
An optional third reading "*C*", also referred to as the "closing pressure" (Marchetti, 2001), can be recorded by carefully deflating the membrane after the final "*B*" reading. The blade can then be incrementally advanced into the ground (typically at a rate of 2 cm per minute). Depth increments are typically 100 to 200 mm. The A, B readings are again repeated at each test depth. These two readings

have to be corrected via the calibration of the membrane. This is needed to account for membrane stiffness. The values are then termed as ΔA, ΔB. From here the final values are termed P_0 and P_1. The dilatometer's usefulness is wide, allowing the geotechnical engineer to evaluate soil parameters across a wide range of soils.

The dilatometer is suitable for all fine grained soils. The surface area of these soil types is well suited to the small membrane diameter of 60 mm. It is however not suitable for coarse gravels as the large and irregular surface area of the aggregate allows for poor contact with the membrane. The blade is tough enough to push through gravel layers of about 500 mm thickness.

What is unique about the DMT is the zero pressure measurement method. This means that at the start of the next incremental test depth, no pressures are built up from the upper layers (due to the retraction of the diaphragm) and the stresses measured remain unique to that layer only. The DMT readings have been identified as highly accurate even in extremely soft, nearly liquefied or paste-like soils. The blade is however tough enough to absorb stresses up to 250 kN of pushing force and can break though soft rocks and even asphalt. The cohesive strengths of clayey soils can be evaluated from C_u = 2 kPa to 1000 kPa. The range for the DMT moduli, E_D, can be tested from 400 kPa and can detect stiffness up to 400 MPa. The formula for calculating the E_D modulus is shown here in equation (2.17).

$$E_D = 34.7\ (P_1 - P_{0)} \tag{2.17}$$

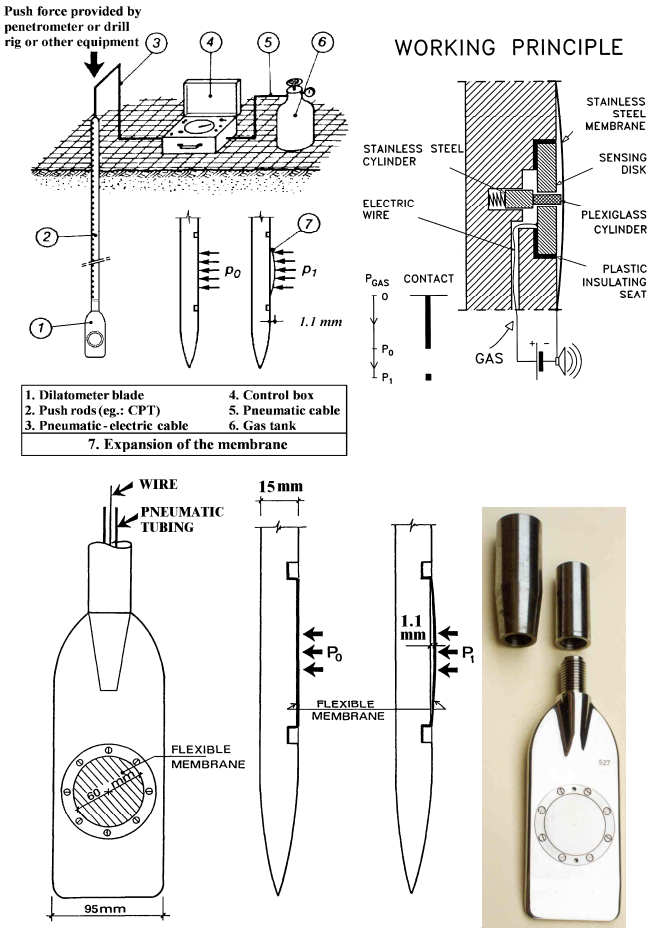

Figure 2-21 DMT Working principles, (Marchetti, 2001)

2.5.3 **Applications of the Flat Blade Dilatometer**

Predicting settlements of shallow foundations is probably the main application of the DMT, especially in sands, where undisturbed sampling and estimating compressibility provide extreme challenges. Where piles need to be driven down to acceptable refusal depths, the DMT can provide design parameters used in lateral stress calculations. Low skin friction in calcareous sand is known to develop, resulting in very low lateral pile capacity. The low K_D values measured at depth by the DMT in calcareous sands can possibly provide an early warning of low skin friction.

The DMT gives the engineer continuous depth-profiles of the important soil properties, such as current horizontal stress, angle of friction, soil type, stiffness and strength parameters (vertical constrained modulus and bearing capacity). Both researchers and practitioners have complimented the accuracy and application scope of the dilatometer (Marchetti, 1997). The acquisition of such a device and the testing of local soil conditions should benefit all in the geotechnical research industry. Many structures are built close to or on coastal beaches, which can initially provide good founding stability if the site is located away from the dunes itself. The flat blade dilatometer, with its unique soil type identification, I_D, can provide details related to the soils behaviour when subjected to vibration. The parameter I_D is discussed in paragraph 2.12.

Sensitive soil parameters such as stress history, aging, and the cementation structure are more readily detectable with the DMT as opposed to other in-situ devices, in particular the K_D value (defined in paragraph 2.7). Marchetti (1999) says that parameters, in particular the K_D value, is hardly noticeably, or poorly recognisable with comparative devices such as the Q_c parameter (cone penetration resistance) from the CPT. It is widely reported that in-situ tests offer an "inverse boundary conditions problem" (Marchetti, 1999), since these tests (CPT and SPT) measure "soil response" instead of soil properties. The laboratory chamber calibration test offers an experimental and empirical way to interpret results of the DMT. Uniform sand specimens have been prepared before in a calibration chamber with known stress conditions and density (Hsu & Huang, 1999).

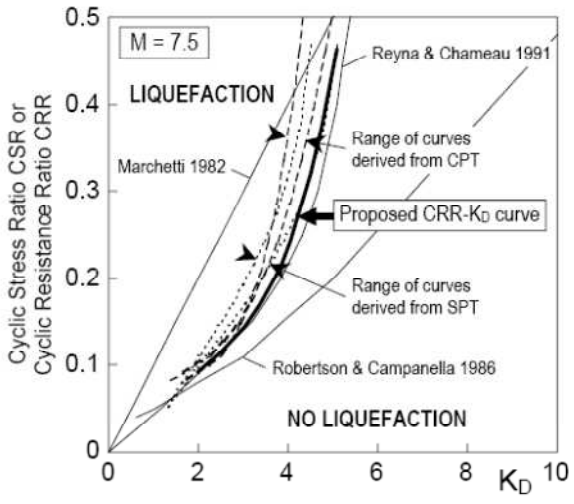

Figure 2-22 Recommended curve for estimating CSR from K_D (Reyna & Chameau, 1991)

Figure 2-22 was established after the research done by Reyna and Chameau (1991) and compared the Dilatometer's K_D value to the recorded CSR in a calibration chamber. After the CSR is evaluated, it is used in liquefaction analysis with the methods developed by Seed and Idriss (1971). A detailed step-by-step procedure can be found in documentation provided by the US.DOT (1992).

2.5.4 **Horizontal stresses and the uniqueness of the K_D value**

When the DMT blade enters the soil, the sensors begin to interact with the internal pressures on the steel membrane. The initial horizontal pressure is the current pore water pressures at the penetration depth. The pressure varies with depth and is defined here as P_0. This pressure is larger than the original H_o (horizontal stress) due to the insertion process of the blade. The pore water pressures can be normalised to σ_v (or brought to equilibrium). u_0 is the pre-insertion pore water pressure. This leads essentially to the defined K_D value, and is defined in (2.18) as:

$$K_D = p_0 - u_0/\sigma'_{vo} \tag{2.18}$$

Where,

σ'_{vo} is the effective overburden stress

The K_D value is a dimensionless and empirical number for comparative purposes, and more useful to use than P_0. In dry sand, as in this research, the abovementioned equation is reduced to:

$$K_D = p_0/\sigma_{vo} \tag{2.19}$$

Despite the dynamics involved when the blade penetrates the soil, the reaction of the soil to the blade can be seen as an indicator of the soil's resistance to volume reduction. For example, a loose collapsible soil will not show much resistance to a low horizontal stress due to the insertion of the blade (hence a low K_D value).

By assessing the reaction of the windblown sand against the penetration of the DMT blade, the K_D values will assist in determining the CSR values. The research work already done in this regard supports this part of the research and is crucial to assessing when sand becomes liquefiable. The correlation for evaluating CSR from the K_D value and using the method proposed by Seed and Idriss (1971) simplified

procedure was proposed by Monaco et al, (2005). Monaco combined previous CRR vs K_D correlations with the past experiences by other researchers who investigated methods based on CPT and SPT tests. This was supported by extensive field performance databases. Cyclic stress properties were translated using the % relative density D_R as an intermediate parameter. In this research methodology the SPT_N value will be replaced with the DCP_{DN} value.

2.5.5 Monitoring soil densification with the Flat Blade Dilatometer

The high sensitivity of the DMT in monitoring densification has been demonstrated through several studies. The DMT is twice as sensitive as the CPT to densification (Schmertmann, Baker, Gupta & Kessler, 1986; Jendeby, 1992). The DMT can also sense sand liquefiability (Schmertmann, 2006) because of the ability of the DMT to measure a change in horizontal stress with depth. The DMT sensitivity can sense the increase and the reduction of soil pressures and thereby both the positive and the negative range in pressures can be assessed.

2.5.6 Using the DMT to assess sand liquefiability

Soil liquefaction is defined as the loss of strength due to the pore pressure build-up in saturated fine grained soils, subjected to ground shaking (Seed & Idriss, 1982). Efforts aimed at identifying and understanding the basic parameters affecting the liquefaction phenomenon date only to the early 1970's. Since then, numerous cases of earthquake-induced liquefaction have been documented in which significant damage to man-made facilities were reported. The soils which have been identified as "liquefiable" are mostly fine and silty sand (these assessments having being based on actual field observations). A definitive understanding of the effect of fines (type and relative amount) on the liquefaction potential of sand has yet to be reached. Past research has been committed to this question, as near-shore reclamation and development projects have increased in number and scale (Sadek & Saleh, 2004).

The effect of fines content on the liquefaction behaviour of sand has been investigated by a number of researchers, most of whom used the relative density and/or gross void ratio as a basis for comparison of the generated results. Troncoso and Verdugo (1985) performed cyclic shear strength tests using tailing sand tested at different silt contents ranging from 0 to 30% at a constant void ratio of 0.85. The cyclic shear strength decreased with increasing fines content. Koester (1993) extended the work reported by

Troconso by reproducing the original laboratory testing program while using a constant void ratio of 0.48. The results reported by Koester confirmed the trends identified in the earlier work of Troncoso and Verdugo for specimens containing up to 20% fines (% <0,075). However, the trends were reversed for the fines content exceeding 20%; and the Cyclic Stress Ratio (CSR) causing liquefaction increased with increasing fines content. Although the West Coast and Philippi sand to be used in the chamber have low fines contents (< 5% passing the 0.075 mm sieve), possible liquefiable conditions may exist when exposed to saturated conditions. This study will attempt to measure parameters related to liquefaction with the DMT.

The abovementioned statements by past researchers contain evidence that the fine sand content of sandy soils play a crucial role in assessing whether the sand has the potential of becoming liquefiable, and the stress history associated with its condition seems to be seen in the cyclic stress ratio. These criteria can be measured, or correlated, with the DMT device, making the apparatus very suitable for this purpose.

2.5.7 **Identifying soil types**

A unique feature of the DMT is its ability to predict the soil type. The formula used for the material index, I_D, is not all inclusive, identifying only fine grained soils such as sand, mud and clay. The reduction formula is shown here in (2.20).

$$I_D = (\mathrm{p_1} - \mathrm{p_0})/\mathrm{p_0} - \mathrm{u_0}) \tag{2.20}$$

The term, u_0, is used by the designer (Marchetti (2001) to refer to the pre-insertion in-situ pore water pressure and a value (which is close to zero) is only applicable in free draining soils such as sand. The above formula (2.20) for I_D was introduced after the DMT designers recognised that the difference between the P_0 and P_1 readings for clayey soils were analytically small but far apart in sands (Marchetti, 1980). The various fine grained soil types can be identified as follows and is described in the report by Marchetti (2001):

Clayey soil	$0.1 < I_D < 0.6$
Silty soil	$0.6 < I_D < 1.8$
Sandy soil	$1.8 < I_D < 10$

In general, I_D provides an expressive profile of the soil type. In Marchetti's report (2001) it is noted that the I_D value may misinterpret silty soils as clay and vice versa, and a clay-sand mixture would generally be described by I_D as silt. The I_D value should not be confused with the grading characteristic parameter; the co-efficient of curvature, generally known as C_C. This parameter reflects the mechanical behaviour (a kind of "stiffness index"). For example, if particular clay behaves in a stiffer manner as opposed to other softer clayey soils, the former will most likely be classified by the I_D parameter as silt.

The I_D value would seem then to compliment the standard grain size distribution and can possibly assist in the overall classification of the soil type, currently determined by the USCS or AASHO methods. If permeability flow is preferred, then the I_D value should be accompanied by $U_{o,}$ the pore pressure index (Marchetti, 2001). Figure 2-23 provides an easy interpretation of the material index value, as well as an estimate of the unit weight. The I_D index is related with E_D (in bar). E_D is the DMT's modulus value. The E_D value is obtained from P_0 and P_1 by the theory of elasticity (Gravesen, 1960).

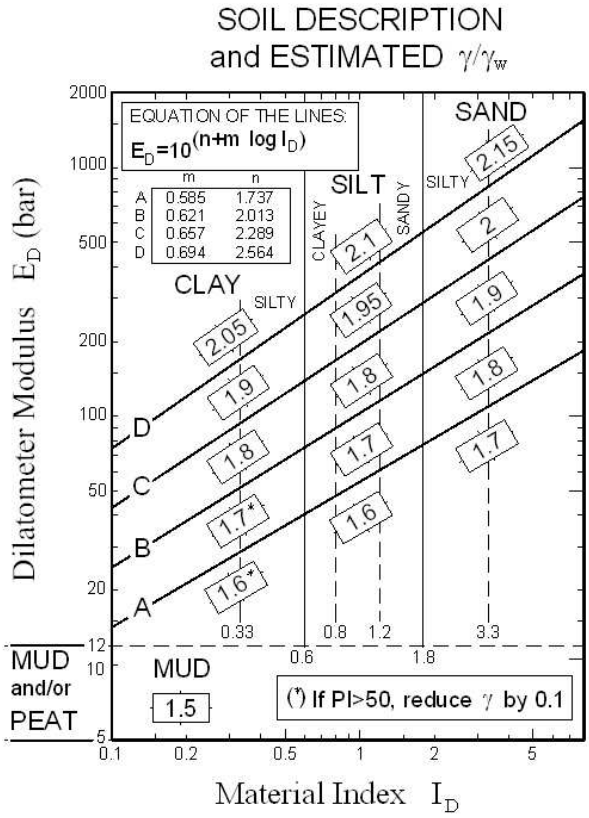

Figure 2-23 Chart for estimating soil type, I_D (Marchetti & Crapps, 1981)

The software provided with the DMT negates the use of Figure 2-23 and provides its own printout for this parameter. Examples of these printouts are found in the Appendices Schedule and Table A.8.

2.6 Calibration of the Flat Blade Dilatometer diaphragm

The manufacturer and promoter of the DMT strongly recommend that the diaphragm be regularly calibrated to suit the prevailing conditions. As this process is fairly simple in complexity, a brief explanation is offered here.

It requires that the ΔA and ΔB pressures necessary to overcome membrane stiffness be established. Under atmospheric pressure, the membrane is at rest. The membranes also have a slight natural convex curvature. The process to calibrate the membrane is seen in Figure 2-24 where a syringe is used to apply pressure to the membrane, under suction and inflation. ΔA is the syringe pressure applied to the membrane that will cause collapse against its nylon seating (i.e. A-position). ΔB is the syringe pressure that will push the membrane outward to 1.1 mm from its rest position. Figure 2-24 illustrates the setup

principle of how the DMT blade can be directly attached to the control unit for calibration purposes. A simple syringe inflates and deflates the membrane, recording the ΔA and ΔB pressures.

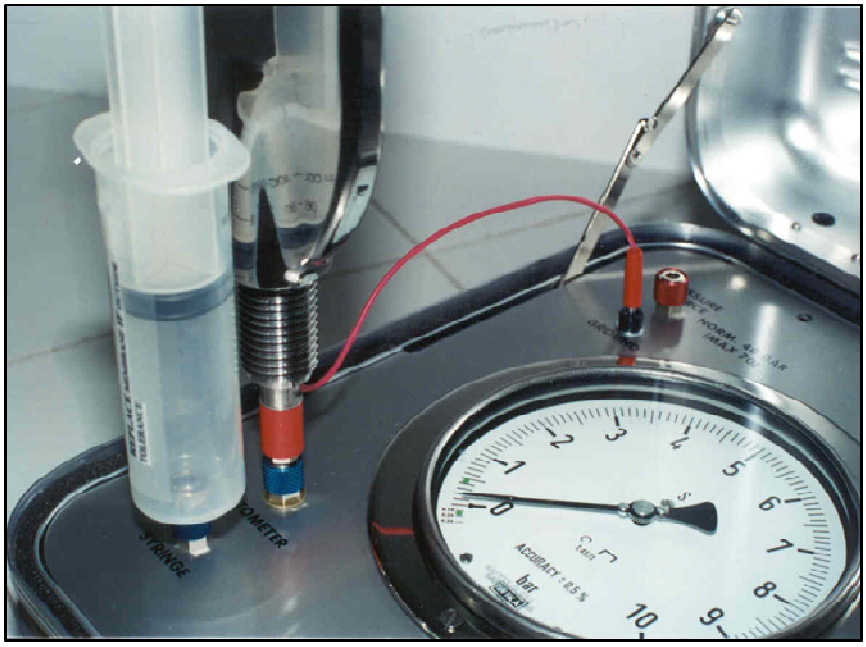

Figure 2-24 DMT Calibration setup (Marchetti, 2001)

The dilatometer's membrane calibration is effectively described by Marchetti (1999) and Marchetti and Crapps (1981). Accurate and regular ΔA, ΔB measurements in soft soils is mentioned often (Marchetti, 1999). Inaccurate ΔA, ΔB is practically the only potential source of erroneous instrumentation readings. The establishment of the correct ΔA, ΔB correction readings are crucial and will affect all other data if incorrectly applied. The correct procedure is to calibrate the DMT before and after each test session, ensuring that a strong signal (electrical conductivity) is obtained when inflating and deflating the diaphragm. This ensures continuity. The user is encouraged not to over inflate the membrane, so by insuring that the membrane's integrity remains intact. This will ensure that ΔA and ΔB remain within tolerance. If the membrane undergoes excessive inflation it will require about 30 kPa suction to close and return to the rest position.

The dilatometer reduction formulae and correlations are summarised in the Appendices, Table A1. The two readings (*A* and *B*) are firstly corrected for membrane stiffness. Variables such as zero gauge offset and feeler pin elevation can influence the final outcome. The reduction formulae (2.15) and (2.16) are used to achieve this (Marchetti, 2001).

The early research correlations done by Marchetti (Marchetti, 1980) were obtained by calibrating dilatometer results versus crucial parameters such as CSR, % D_R and SPT_N. These correlations have been used in other important interpretations, such as stress history, and were confirmed by follow up research (Marchetti & Crapps, 1981).

2.7 Methods to evaluate liquefaction

2.7.1 Cyclic tests in a laboratory

Several methodologies to evaluate the potential for liquefaction have been considered in the past. The commonly employed methods are the cyclic stress and cyclic strain approaches to evaluate the liquefaction resistance of soils. These methods can be both evaluated in-situ on site or in a well equipped soils laboratory that can monitor pore water pressure. The cyclic stress approach characterises both earthquake loading and liquefaction resistance. The cyclic triaxial test, simple cyclic shear test and cyclic torsional shear test are common laboratory tests. Over and above these tests, other approaches such as energy release, “effective stress based response analysis” and “statistical approaches” have also been developed. Anbazhagan (2009) refers to the relationship between pore pressure ratio and cyclic repetitions; an example can be seen in the chart displayed in Figure 2-25 that may be used to determine the cyclic resistance ratio of the in-situ soil. When the graph flattens out the soil becomes liquefiable. This chart was developed from observations after in-situ investigations of a number of sites that had liquefied. From these plots it is clear that even after 120 cycles, the average pore pressure ratio is about 0.94 and deviatory stresses vs. strain plots have not become flat, indicating no liquefaction.

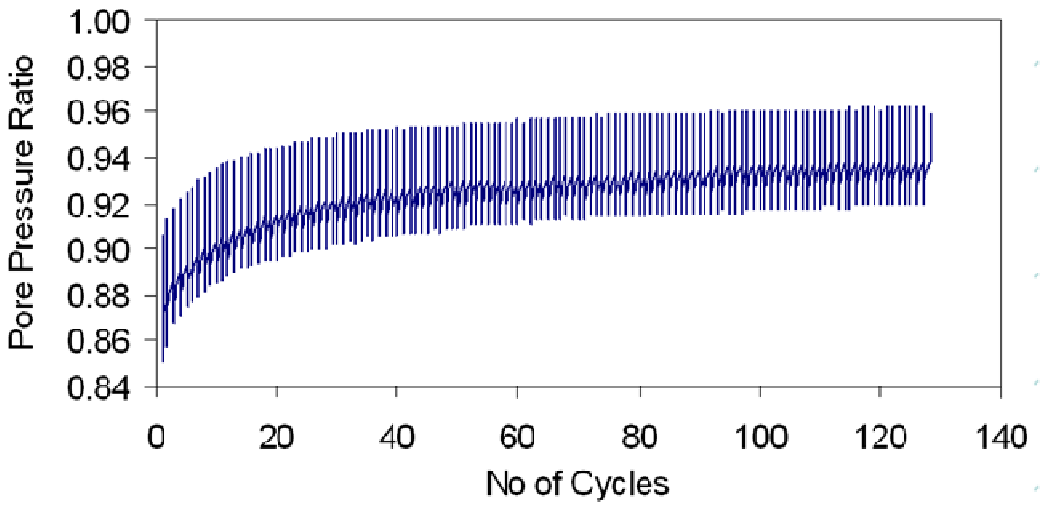

Figure 2-25 Typical pore pressure ratio plots with no of cycles (Anbazhagan, 2009)

2.7.2 **Grading analysis**

Particle size distribution is essential to evaluate. Figure 2-26 is an illustration of one proposal to analyse whether sand with a particular grading is a candidate for liquefaction or not.

Yamamuro and Lade (1998) conducted a series of experiments on Nevada sand with 7% fines tested at a relative density D_R = 30%. Their work suggested that silty sand exhibits an increasing tendency for dilatancy (increase in volume due to shearing) and stability (with increasing confining pressures), which suggests a greater resistance to pore pressure build-up and consequently, to liquefaction.

Figure 2-26 below illustrates one proposal for the range of grading envelopes for sands susceptible to liquefaction.

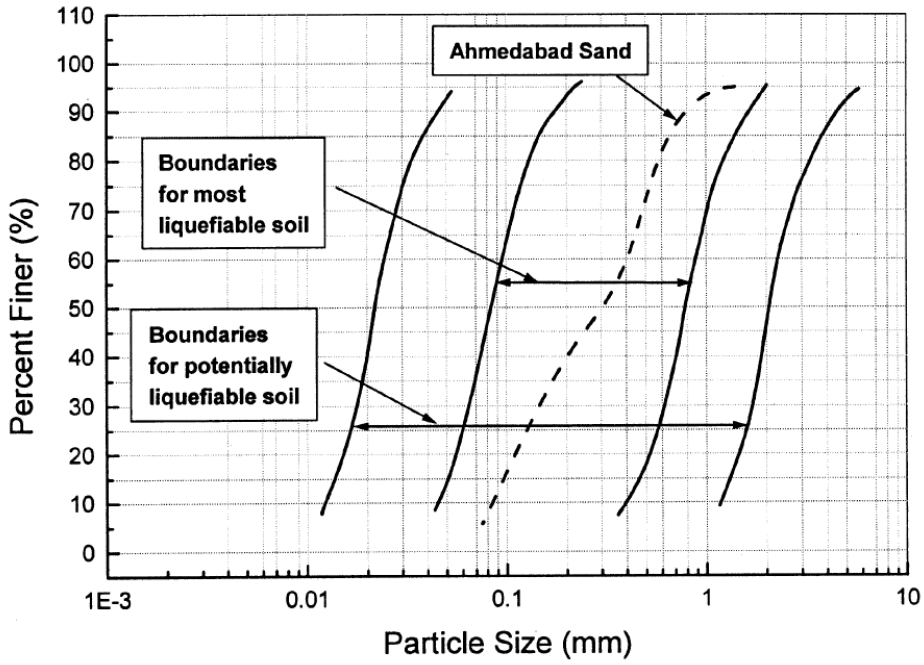

Figure 2-26 Proposal for grain size distribution of liquefaction susceptible soils (Sitharam, 2004)

2.8 Predicting settlement with the DMT

Predicting settlements in shallow foundations is, amongst other applications, the main function of the DMT, especially in sandy soils, where undisturbed sampling and estimating compressibility are difficult to assess. Settlements are calculated by a one-dimensional formula (2.21) and displayed graphically in Figure 2-27.

$S = \sum \frac{\Delta \sigma_v}{M_{DMT}} . \Delta Z \sigma_z$, the incremental vertical stress at depth *Z*, is necessary to predict the settlement using the one-dimensional method (Terzaghi). The one-dimensional settlement, *S* (mm)**,** can be calculated for each sub-divided layers, then adding the contribution of each layer as calculated in (2.21).

$$S = \sum (\frac{\sigma_z}{M}) \Delta Z \qquad (2.21)$$

$I\sigma_z$ is the depth influence coefficient caused by layering in the sand ($I\sigma_z$ is empirical, non dimensional). It represents the fraction of surface load produced at the depth *z.*

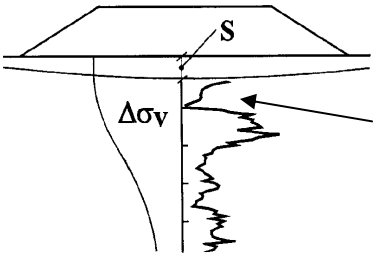

Varying modulus values as determined by M_{DMT}

$$S = \sum \frac{\Delta\sigma_v}{M} \cdot \Delta Z$$

Figure 2-27 Marchetti's DMT settlement illustration (Marchetti, 2001)

It should be noted that the one-dimensional formula (2.21) is based on linear elasticity and provides a settlement proportional to the load. Non-linear prediction is not possible (Marchetti, 2001). The predicted settlement is to be considered as applicable in working conditions. It is recommended that a safety factor (Fs) = 2.5 to 3.5 be applied.

2.8.1 **Observing Settlement**

The ability to predict settlement below foundation has been traditionally executed in the past with known in-situ apparatus such as the CPT, SPT or DCP. Researchers have in the past, since the advent of the DMT device, given a closer look at this new device, and encouraging results have been published. One researcher, Hossain (2005), revealed that the DMT device has the ability to predict more closely the actual amount of settlement when compared to the aforementioned apparatus. The site investigation included pressure meter tests, dilatometer tests, standard penetration tests (SPT), cone penetration tests (CPT), and a plate load test.

The objective of Hossain's work was to compare the bearing capacity and settlement predictions based on the different in-situ tests used for the building undergoing settlement. The field investigations were conducted by using four different in-situ tests at various locations. In order to investigate the surface conditions for the proposed development, 40 SPT's were conducted. Seven dilatometer tests were performed to evaluate soil bearing capacity and settlement characteristics. The soil resistance measured during insertion of the dilatometer blade was correlated to the strength of granular soils, while the soil

modulus, $M_{R,}$ undrained strength and other parameters were determined during deflation of blade against the soil (due to the release of the gas).

The strength parameters from the DMT test results were computed using the Schmertmann Method (Schmertmann, 1986). The bearing capacity and settlement predicted by the four in-situ methods at three boring locations were compared with the observed settlement from the plate load test. Hossain (2005) and Hayes (1990) summarised, in part that, "Predicting settlements of shallow foundations is easily determined and research in the past validates the high predictability of the DMT method, especially in sand, where undisturbed sampling and estimating compressibility is particularly difficult". It would also seem that correlating the observed and the DMT method of prediction of settlement beyond 175 mm becomes inconsistent, as was formally discovered by Hayes (Hayes, 1990). A graph illustrating this fact is seen in Figure 2-28 .

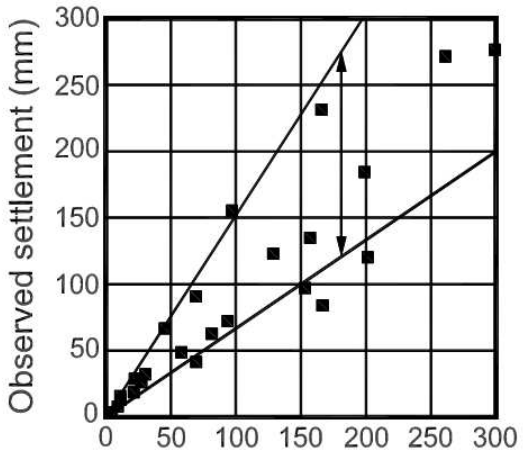

Figure 2-28 DMT vs. observed settlement (Hayes, 1990)

In-situ testing is rapidly emerging as a viable alternative to the traditional approach of obtaining geotechnical parameters required in prediction of bearing capacity and settlement (Hossian, 2005). The SPT and CPT methods seem to overestimate the predicted settlement, while DMT and PMT (Pressure Meter test) predicted settlements less than those observed in the field, done by way of the Plate Load test. A graphic representation of this comparative study research outcome is illustrated below in Figure 2-29.

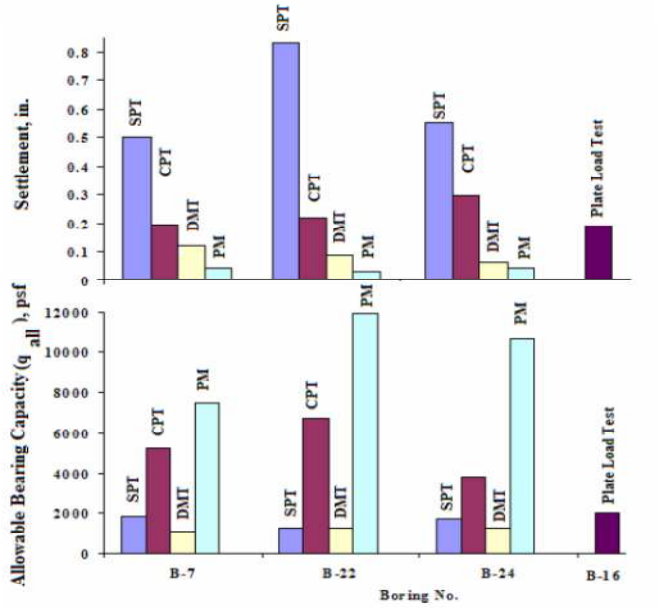

Figure 2-29 Typical In-situ test comparisons (Hossain, 2005)

2.9 Introduction to calibration chambers

Calibration chambers are nothing new to the geotechnical world and many have been built internationally at universities, such as the one depicted below in Figure 2-30. The calibration chamber built at GUT (Gdańsk University of Technology, Narutowicza) enables large-size soil samples to be tested in well-defined boundary conditions. It is a double-walled chamber with independent pressure control in internal and external chambers, which permits complex boundary conditions to be applied. The mass of the soil is confined inside a rubber membrane. Vertical stress is then applied to the specimen by the top and the bottom membranes being filled with water. The designer and operator was L. Balachowski and his findings were published in 2006 (Balachowski, 2006).

Another example of a calibration chamber was developed in Sydney to conduct laboratory controlled cone penetration tests in unsaturated soils (Pournaghiazar et al, 2011). The chamber allows independent applications of lateral and vertical pressures in an unsaturated soil specimen. Horizontal pressure is applied by cell water pressure pushing on a rubber membrane enclosing the specimen, while vertical pressure is maintained by a hydraulic loading ram at the base of the specimen (see Figure 2-31).

The concept of a calibration chamber test is to prepare a large sand specimen in the laboratory, consolidated to a desired stress level, and then to perform the experiment under given boundary conditions. Since the entire experiment is conducted in the laboratory, the test quality can be readily

controlled. The large sand specimen, with uniform deposition and known engineering properties, provides reference values for the interpretation and thus calibration of the in-situ test method (Hsu, 2008).

The calibration chamber of the Geotechnical Laboratory in Delft, Netherlands, is a 1.9 m diameter rigid wall calibration chamber. It is filled with a sand bed to an approximate height of 1.5 m. At the bottom of the chamber a number of drains are installed in a filter bed and connected to a pump. This is used to saturate the sand bed from below. The same installation is used to add water on top of the sand bed to allow percolation. After the sand bed is saturated, a couple of vibrators, fixed to the sides of the tank, can be used to densify the sand while draining the water. Two Wacker AR 06/380 vibrators were installed, each listed as yielding an effective 16 kN centrifugal force. Vibration times used are between 0 and 16 minutes. After vibrating, the remaining water can either be drained to create an unsaturated sand bed, or the sand sample can be kept partially saturated. Table 2-7 provides a list of past chambers built for calibration testing for various in-situ apparatus.

Figure 2-30 Chamber in Gdansk (Balachowski, 2006)

Figure 2-31 Chamber for CPT testing in Sydney (Pournaghiazar et al, 2011)

Table 2-7 International Chambers (Ghionna & Jamiolkowski, 1991)

Calibration chamber (Owner and location)	Specimen diameter	Specimen height	Boundary conditions		
	m		Radial	Bottom	Top
Country Roads Board, Australia	0.76	0.91	Flexible	Cushion	Rigid
University of Florida, U.S.A.	1.20	1.20	Flexible	Cushion	Rigid
Monash University, Australia	1.20	1.80	Flexible	Cushion	Rigid
Norwegian Geotechnical Institute	1.20	1.50	Flexible	Cushion	Rigid
ENEL-CRIS, Milano, Italy	1.20	1.50	Flexible	Cushion	Rigid
ISMES, Bergamo, Italy	1.20	1.50	Flexible	Cushion	Rigid
University of California, Berkeley, U.S.A.	0.76	0.80	Flexible	Rigid	Rigid
University of Texas at Austin, U.S.A.	Cube 2.1×2.1×2.1		Flexible	Flexible	Flexible
University of Houston, U.S.A.	0.76	2.54	Flexible	Cushion	Cushion
North Carolina State University, U.S.A.	0.94	1.00	Flexible	Rigid	Rigid
Louisiana State University, U.S.A.	0.55	0.80	Flexible	Flexible	Rigid
Golder Associates, Calgary, Canada	1.40	1.00	Flexible	Rigid	Cushion
Virginia Polytechnic Institute and State University, U.S.A.	1.50	1.50	Flexible	Rigid	Rigid
University of Grenoble, France	1.20	1.50	Flexible	Cushion	Cushion
Oxford University, U.K.	0.90	1.10	Flexible	Cushion	Rigid
University of Tokyo, Japan	0.90	1.10	Flexible	Rigid	Rigid
University of Sheffield, U.K.	0.79	1.00	Flexible	Rigid	Flexible
Cornell University, U.S.A.	2.10	2.90	Flexible	Rigid	Rigid
Waterways Experiment Station, U.S.A.	0.80-3.00	Variable	Flexible	Rigid	Rigid
National Chiao-Tung University, Taiwan, R.O.C.	0.51	0.76	Flexible	Rigid	Rigid
National Chiao-Tung University, Taiwan, R.O.C.	0.79	1.60	Flexible	Flexible	Flexible

Source: Ghionna and Jamiolkowski (1991)

A similar but more elaborate design was completed at Virginia Tech, USA. The calibration chamber (Figure 2-32) at Virginia Tech was built as part of a project involving the evaluation of the liquefaction potential of soil deposits using a miniature cone penetrometer. The chamber was modelled after the original CRB (Country Roads Board, Australia) chamber designed by Holden (1991).

The proposed chamber for testing the Aeolian sand in this study is discussed in Chapter 3.

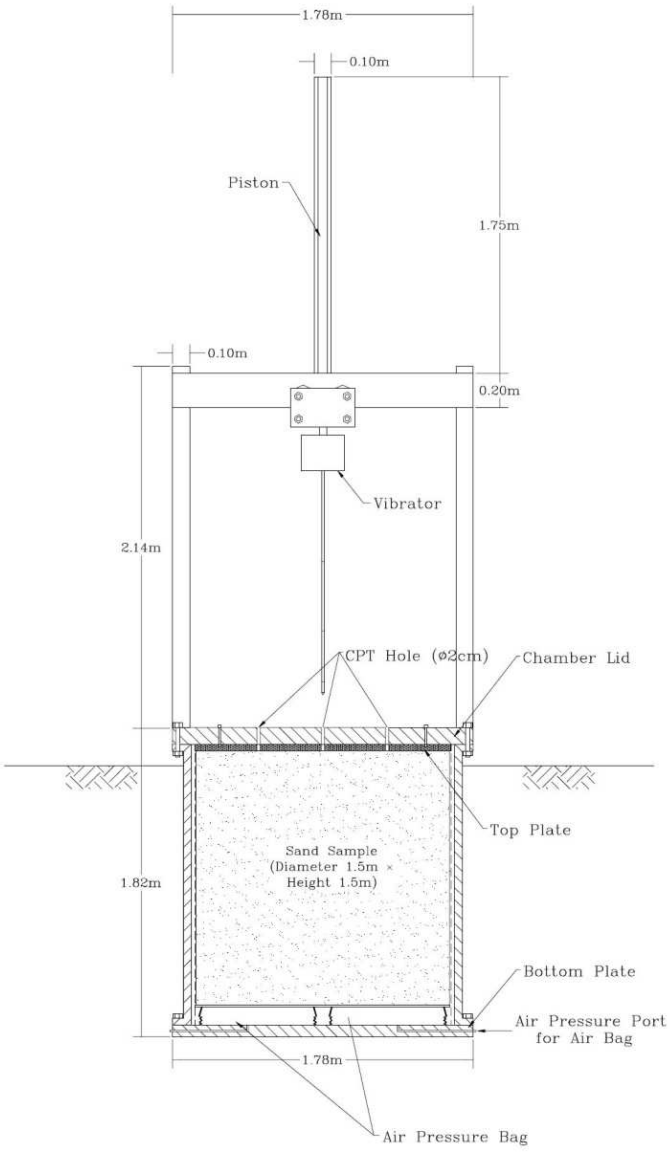

Figure 2-32 Schematic of Virginia Tech Calibration Chamber

2.9.1 **Previous research in calibration chambers**

DMT testing was conducted in the late 1980s in calibration chambers located in Florida, USA and Enel-Milano, Italy (Baldi et al, 1986). The test work was conducted in two stages, meaning that the DMT blade

was inserted before sand was placed inside the chamber. The method for sand placement was via pluviation (sifting the sand in a dry state from a standard height; in layers of equal thickness). Pre-stressing of the sand followed, after which DMT penetration continued downward. The initial state of stress, K_D, was set at 0.45 bar (the article survey does not reveal the method in which this stress was applied). The stress of 0.45 bar is also assumed to be enough for dry fine sand to become normally consolidated. The chamber was then penetrated at intervals of 100 mm and terminated half way down. The chamber used in this research is constructed to simulate varying densities and the stresses created within the chamber will have to be measured electronically via a calibrated pad transducer. The chamber testing by Marchetti (Marchetti, 1980) was set up to simulate exactly the same pre-stressing cycles in both halves of the chamber. Table 2-8 below indicates some relative densities obtained by Broere (2001) in a calibration chamber at TU Delft University. The void ratios achieved for the four types of sand used in the chamber can be seen in Table 2-9. Particle size distribution for the sand types 2-4 are displayed in Figure 2-33.

Table 2-8 Density vs Vibration (Broere, 2001)

Vibration time (s)	Relative Density
None	0.182
30	0.311
60	0.376
120	0.444
180	0.578
300	0.687

Table 2-9 Void ratios (Broere, 2001)

Sand Type	e_{min}	e_{max}
1	0.470	0.818
2	0.498	0.801
3	0.454	0.749
4	0.431	0.746

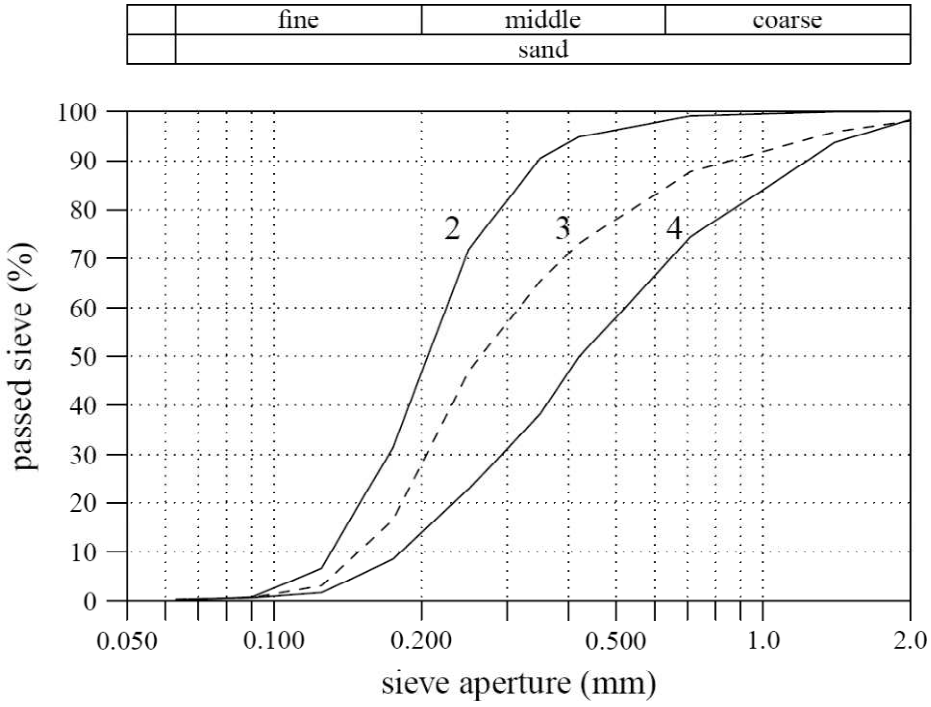

Figure 2-33 Sand grading for chamber sand in Delft, TU (Broere, 2001)

2.10 Sample preparation in calibration chambers

To prepare uniformly graded, clean sand chamber specimens, the sand first air dried and then sieved from inside the chamber and from a fixed height. The chamber density of the sand specimen is related to the drop height and volume of sand deposited per unit of time. However, when the sand contains

fine particles, these dry pluviation methods may cause particle segregation (Hsu, 2008). The sand is lightly spread and levelled with a straight edge before continuing with the next lift.

2.11 The problem of boundary effect

Boundary effect can affect the readings dramatically, as past research has demonstrated. Hsu and Huang (1999) have researched that the main obstacle in reaching a conclusion is that the conventional calibration chamber imposes significant boundary effects on the CPT. Theories and empirical methods have been proposed to correct the boundary effects (Baldi et al, 1982; Mayne & Kulhawy, 1991; Salgado, 1993). Marchetti (2001) states, in effect, that the cone distortion effect of the CPT is more dramatic than the wedge shape of the DMT, so little distortion can be expected. This assessment was based on research completed by Baligh and Scott (1975) and is graphically shown in Figure 2-34.

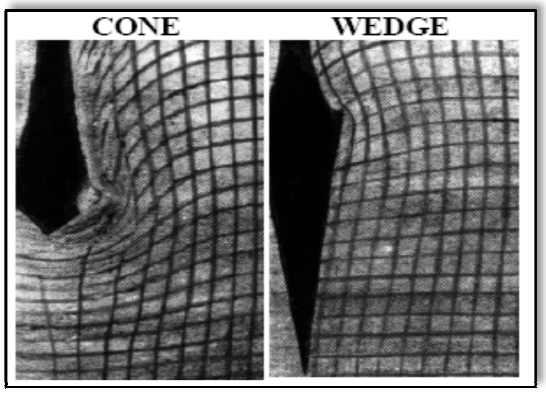

2.12 Extending the Flat Blade Dilatometer's capabilities

The DMT, due to its sensitivity to σ_h (horizontal stress), is particularly suitable to monitor soil improvement. Several studies present comparisons of results of CPT's and DMT's performed before and after a compaction treatment. Schmertmann (1986) observed that the increase in M_{DMT} after dynamic compaction of a sandy soil was approximately twice the increase in Qc (CPT cone resistance). This is useful in predicting the long-term effects of continual loading that result in slip failures (Lacasse & Lunne, 1986). When water flow increases through filling, such as in the subgrade below road works,

instability may result, leading to catastrophic failure similar to piping below earth dams. The liquefaction properties of the problematic soils need to be established so that better control of the compaction process can be monitored (Hayes, 1990).

A case can be made for the examination of the now known contaminated Aeolian sand within the confines of the study area. Early investigations have uncovered contamination of up to 15% in some areas with the Atlantic Beach Golf Estate. The DMT would be ideal to monitor the in-situ K_D parameters, as the results will easily predict the soft spots within the drift sand (about 1.5 m below ground level). The design of a suitable rig to push the DMT into the sand remains the only challenge so far, that is, to design a rig that can exert at least 15 kN force.

2.12.1 **Recognition for the Flat Blade Dilatometer**

International standards and manuals for the DMT already exist. ASTM published a suggested method in 1986. A publication known as the "Standard Test Method for Performing the Flat Plate Dilatometer" is being published by ASTM. The test procedure, as of 1997, is also standardised in Eurocode 7. There are national standards in various countries like Germany and Sweden, but none exist in South Africa. An all-inclusive manual on the dilatometer was prepared for the United States Department of Transportation (US.DOT) by Briaud & Miran (1992). Design applications and current new developments are also available in a comprehensive report by Marchetti (2001).

2.12.2 **Technological advancement of the DMT**

The DMT has been used to check the effects induced in the soil by the installation of various types of piles (Marchetti, 1980; De Cock, at al, 1993). These authors describe the use of the DMT before and after the installation of Atlas piles and concluded that the DMT detects more clearly the effects of the pile installation than that of the CPT (Cone Penetrometer). All the above observations indicate that the DMT results are noticeably reactive even to slight changes of σ_h, (horizontal stresses), or in other cases, relative density in the soil.

Previous researchers (Reyna & Chameau, 1991) have produced curves and graphs which summarise, at the time, the available knowledge for evaluating sand liquefiability with the DMT (see Figure 2-22). The

curves in question estimate the Cyclic Resistance Ratio (CRR) from the parameter K_D and are based, in part, on their curve K_D vs. % D_R relative to normal consolidation, NC, in sand. A correlation has been confirmed by additional data that plots further points for K_D vs % D_R and were produced by Tanaka and Tanaka (1998) at the sites of Ohgishima and Kemigawa. The *% D_R* was determined on a number of well preserved frozen samples.

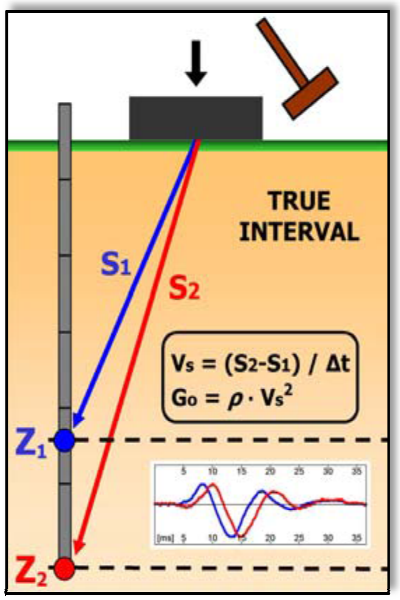

)

The S_{DMT} has been fitted with a seismic sensor that can record the magnitude of the seismic waves passing through the soils down to the blade sensor. This is an element of the research which will not be covered here but has good for further investigation.

The shear wave velocity, V_S (Figure 2-35), is recorded as the ratio between the difference in distance between the source and the two receivers (S_2 - S_1) and the delay of the arrival of the impulse from the first to the second receiver (Δt). V_S measurements are obtained every 0.5 m of depth (Zhou et al, 2005). Figure 2-36 below illustrates the method to evaluate the CSR from shear wave velocity. Figure 2-37 illustrates how the S_{DMT} data can be correlated to the rest of the DMT's parameters.

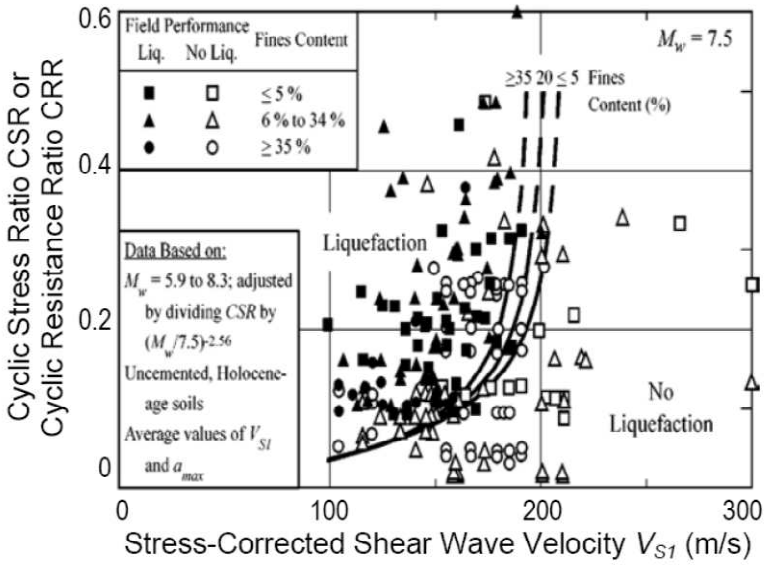

Figure 2-36 V_s to CRR for uncemented liquefiable soils (Andrus et al, 2000)

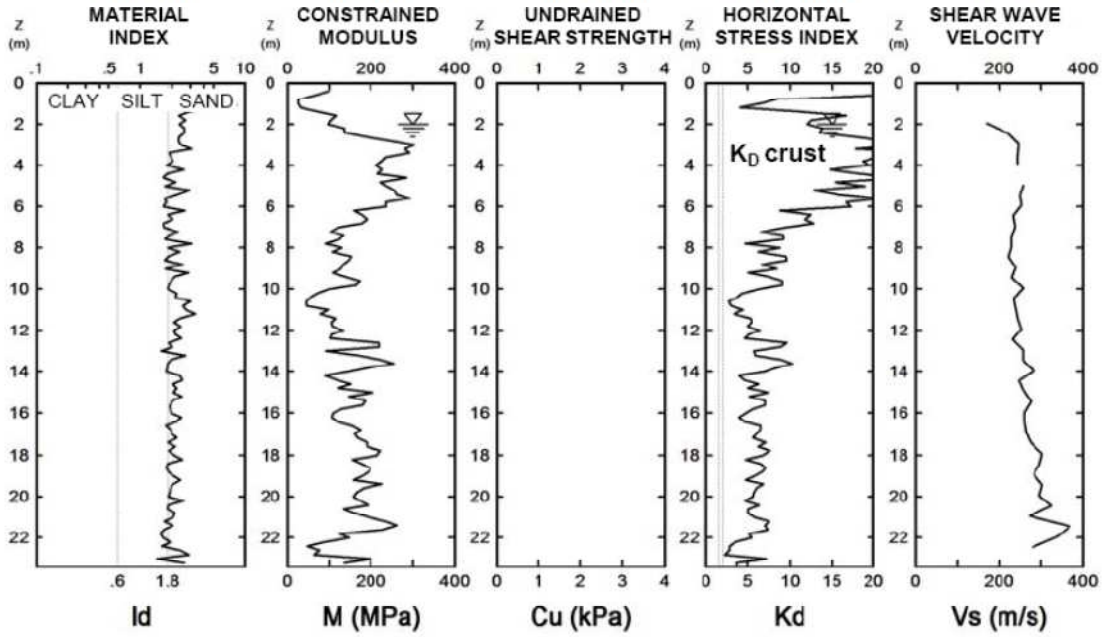

Figure 2-37 Correlation of the shear wave data with DMT parameters (Monaco, 2007)

2.13 Measuring stiffness via other in-situ methods

As a measure of comparative control over the modulus results offered by the DMT, research has been done in the past that correlated the DCP_{DN} rate with that of the plate bearing test (Murad, et al, 2004) and a summary of their analytical studies can be seen displayed in Figure 2-38. Although their curves provide low regression figures (R^2=0.62), it remains helpful to relate a modulus value to the research done with the DCP in this work. PR values of between 45 and 65 mm/blow on the dune sand translate roughly from E_{PLT} =10 to 25 MPa. The values obtained in this research are discussed in the Chapter 4. A formula (2.22) was developed and based on the DCP_{DN} rate (Murad, et al, 2004). This research work is seen in Figure 2-38. Soil samples varied from clay, cemented sand, coarse and fine sand.

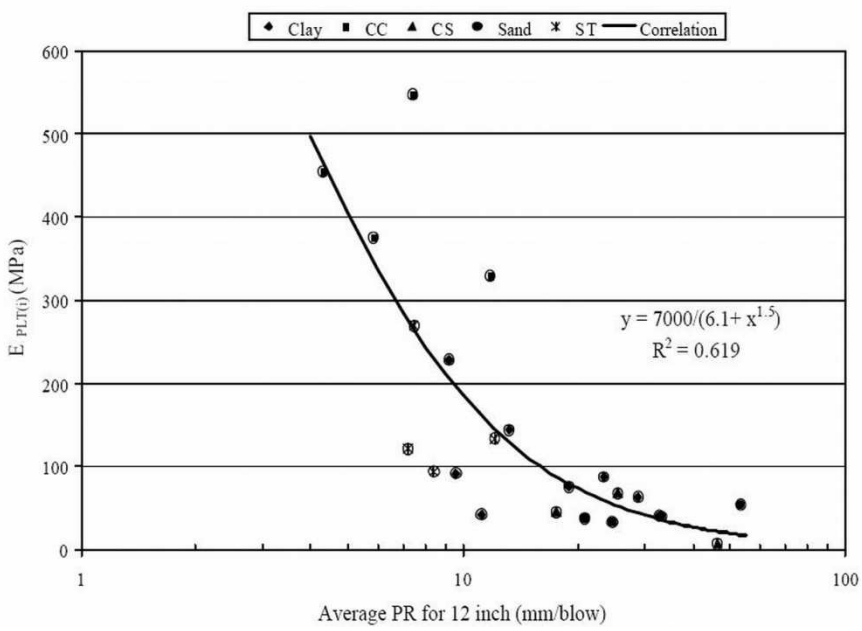

Figure 2-38 Correlation between average DCP penetration rate and E_{PLT} (Murad et al, 2004)

$$E_{PLT} = 7000/(6.1 + {DCP_{DN}}^{1.5}) \quad (2.22)$$

DCP values in mm/blow can be related (with caution) to the SPT_N values in sand with good consistency and with moisture contents evenly distributed. Rosenthal (2002) established the fact that DCP_{DN} values, when inverted over 300 mm, do roughly relate to the SPT_N value. The modulus reaction is a useful parameter when evaluating new pavement materials for road construction. In this regard, the Californian Bearing Ratio (CBR) value versus the modulus reaction has been documented in reference

manuscripts (Raymond, 1997). The DMT has the capability of interpreting the in-situ modulus, M_{DMT}, and is used in the final cumulative settlement calculations.

Figure 2-39 is an example of this researcher's past in-situ test exploration in West Coast dune sand and displays how the DCP_{DN} has been converted to the in-situ CBR value. The conversion is based on the TMH 6:ST6 Method (Technical Methods for Highways) (1984). From here the modulus (and bearing capacity) may be interpreted for further comparison to the DMT method.

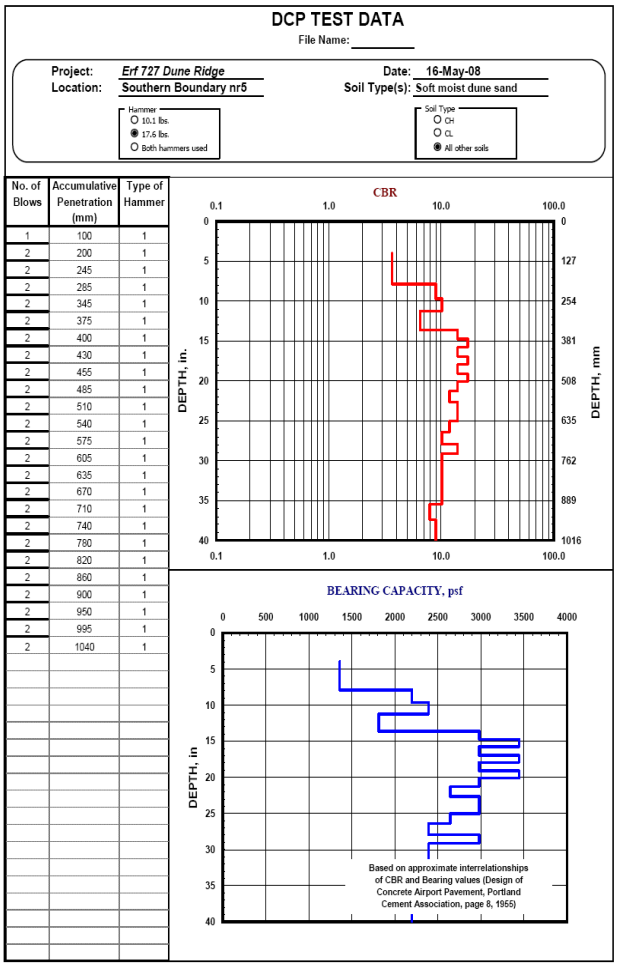

Figure 2-39 CBR vs bearing capacity graph (own work)

2.14 Comparative instrumentation

The Geogauge, Figure 2-40, is a useful and accurate tool in determining the in-situ modulus in terms of soil stiffness or the inverse, Young's E-modulus. The Geogauge is an advanced soil compaction and material strength control instrument that enables construction of higher quality and lower cost

construction works. Pavement components and layers can be compacted to engineering properties taken directly from project specifications. It was used to assess the DMT's modulus determination in the chamber.

Figure 2-40 Geogauge (CPUT Model H4140)

The stiffness values obtained with the Geogauge may be converted into Young's modulus, E, using the equation (2.23). For a Poisson's ratio of 0.35, a factor of 8.67 can be used to convert the Geogauge stiffness (MN/m) to an elastic modulus (MPa).

$$E = k * \frac{1 - v^2}{1.77} * r \tag{2.23}$$

2.15 Comparative research

Figure 2-22 (discussed previously) illustrates some of the geological interest of this study, in establishing when liquefaction becomes potentially dangerous in Aeolian sand with low horizontal stress. The resultant research and data produced recommends that the estimated Cyclic Resistance Ratio (CRR) be associated with the stress parameter value, K_D, as established by Reyna and Chameau (1991). The horizontal stress, the K_D values in uncemented or normally consolidated sand, can be plotted against the % D_R, density values, as seen Figure 2-17. Baldi et al, (1986) found that this method was less than satisfactory in that it requires both the DMT and the CPT (Cone Penetrometer Test) test to be done, with proper matching of the correspondent K_D (from the DMT) and Q_c (from the CPT). What researchers look for here is predicting when the relative density of the sand begins to reach "critical mass" as far as softness is concerned, and relating this to the horizontal stress. When no horizontal stress support is evident (shown by the K_D value), or its magnitude is not high enough to support a structure, the density will also show weakness.

2.16 Soil mechanics and liquefaction

Crucial factors govern the processes that lead to liquefaction. The most important are the intensity of the earthquake and its duration, ground water table levels, soil type and relative density, particle size distribution, fraction size and shape, drainage conditions, aging and cementation of the soil deposits (Sitharam, et al, 2004). Building on these sands and the extra loading will contribute heavily to liquefaction. Sand of uniform gradation and rounded particles has been recently deposited with no cementation of the soil grains, and no pre-stressed load or seismic activity, can be considered as potentially liquefiable. Casagrande (1936) made one of the first attempts to explain the liquefaction phenomenon in sandy soils and he based the concept thereof on critical void ratio. Dense sand, when exposed to shear stress, tends to dilate; loose sand under similar conditions tends to decrease in volume (Das, 2011).

What contributes also is the formation of the sub-stratum. Loads that are transmitted to any layered or saturated soil will trigger a collapse. In order to prevent probable destruction of structures in such areas, prediction of liquefaction potential is necessary. For the purpose of data collection, there is a need for

boreholes and performing in-situ experiments, each of which is expensive (Khozaghi & Choobbasti, 2005).

Liquefaction may also occur if dynamic loading is coupled to transitional shearing waves which can decrease part or all of the resistance of the soil. This phenomenon occurs in saturated sandy soil. Saturated sandy soil, experiencing seismic vibrations, tends to decrease in volume. If drainage conditions are not met or the hydraulic conductivity is low, the liquefaction will intensify with increased pore water pressure. The pore water pressure, u_0, will gradually equal total stress (σ), as expressed in equation (2.24).

$$\sigma' = \sigma - u_0 \tag{2.24}$$

The effective stress (σ ') reduces to zero and consequently the shear strength (τ) approaches zero as well, as shown below (2.25). In these cases, the saturated sand is reduced to "liquid" form and cannot bear any shear loading and finally results in the liquefaction of the sand.

$$\tau = \sigma' - Tan * u_0 \tag{2.25}$$

When liquefaction occurs, the resistance of the soil is overcome by the decrease in volume of loose sands, causing the collapse or incline of some structures. This phenomenon has been seen to occur in earthquakes across the world, in Alaska (1964), Japan (1964), Chili (1960, 2010) and Roodbar (1990).

2.16.1 **Past research into liquefaction**

Marchetti (1997) points out that Figure 2-41 summarises the past research for evaluating sand liquefiability with the DMT. Since then, past research by Totani et al, (1998), Monaco et al, (2005) and Marchetti and Monaco (2007) have developed further parameters for the incorporation of the K_D value in liquefiable soils. From the graph it can be seen that by using the DMT's results, a more acute liquefaction-potential line was established. This signifies the DMT's predicted horizontal stress to be a lot less for potential damage to occur should liquefaction take place during a seismic event, leading to massive settlement.

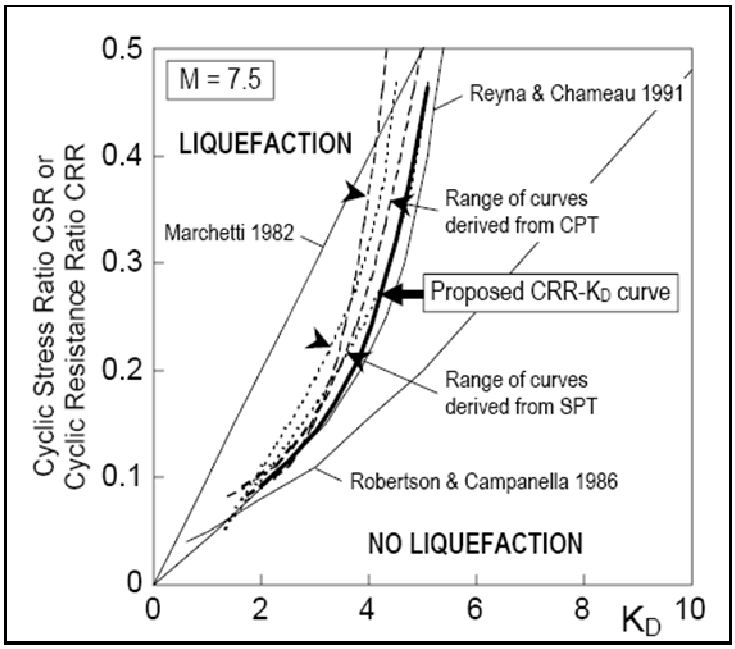

Figure 2-41 Correlation *KD* vs % D_R for NC uncemented sand (Reyna & Chameau, 1991)

Monaco and Marchetti (2005) suggest that clean sand (natural or sand fill) is adequately safe against liquefaction (M = 7.5 earthquakes). Suggested K_D values are stated in Chapter 4. This research will focus on establishing co-ordinates on a similar curve using the local windblown sand and linking this to expected settlement below light structures built on shallow foundations. No similar research in windblown sand has been attempted before in South Africa.

2.16.2 **Local seismic activities and Peak Ground Acceleration (PGA)**

The Southern African region is characterised by natural and mining-induced seismic activity (Figure 2-42). Analysis of the map indicates that high levels of hazard (red areas) are expected in parts of the Western Cape, the Free State, Gauteng and towards the eastern border of the North West Province. Moderate hazard levels can be seen in the Limpopo Province and parts of the Northern Cape. The southern part of the Eastern Cape is subject to low levels of seismic hazard (Council for Geoscience, 2002).

The Southern African region is characterised by natural and mining-induced seismic activity (Figure 2-42). Analysis of the map indicates that high levels of hazard (red areas) are expected in parts of the Western Cape, the Free State, Gauteng and towards the eastern border of the North West Province. Moderate hazard levels can be seen in the Limpopo Province and parts of the Northern Cape. The southern part of the Eastern Cape is subject to low levels of seismic hazard (Council for Geoscience, 2002).

The magnitude of a geological event is recorded as a measure of the earthquake strength. The magnitude, M, of an earthquake is determined from the logarithm to base 10 of the amplitude recorded by a seismometer. The magnitude is measured on the Richter Magnitude Scale, developed by Charles Richter in 1935. The Richter magnitude is a logarithmic scale; each whole represents a ten-fold increase in measured amplitude (US Geological Survey, 2008).

The Koeberg Power plant is situated 8km off a geological fault and is built to withstand an earthquake of magnitude 7. Its reactor footings have neoprone rubber actuators to absorb vibration. Its safety limit is most likely capable of withstanding a 7.7 earthquake. All the uncovered loose sediments were removed to bedrock (Stott, 2010)

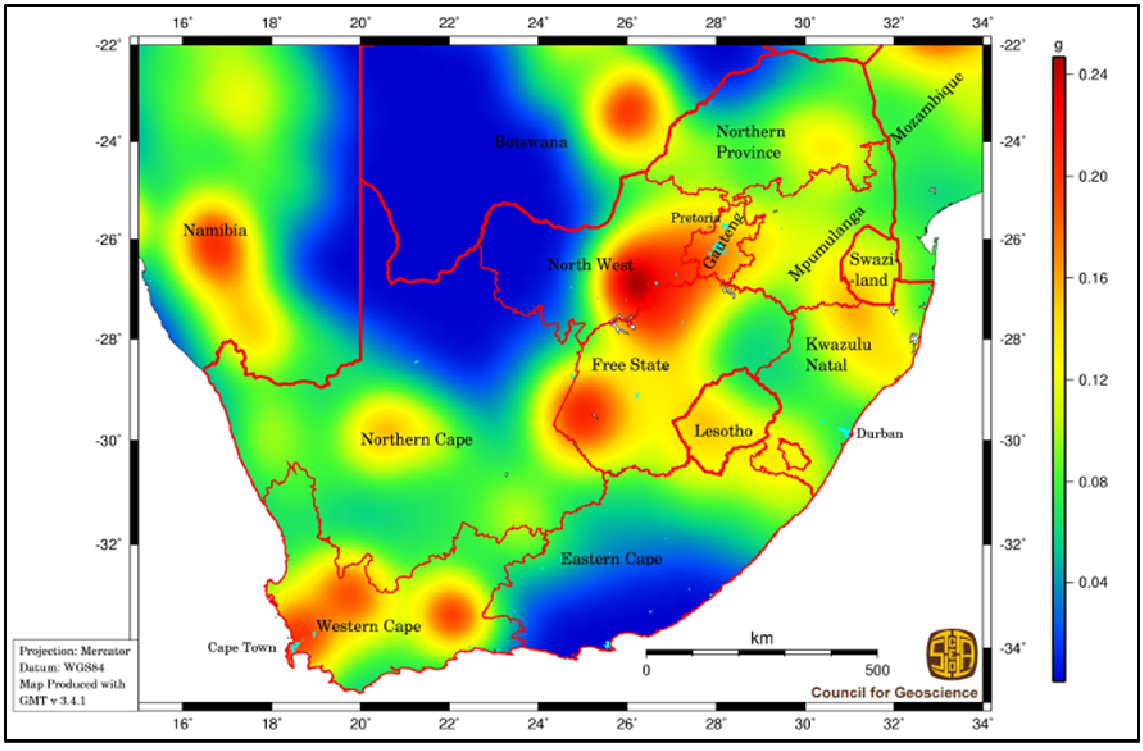

Figure 2-42 Projected ground acceleration (Council for Geoscience, 2002)

The following are facts relating to the measurement of the magnitude:

- The magnitude of an earthquake depends on the length and breadth of the fault slip.
- The Richter scale has no lower or upper limit.
- The largest known shockwaves have magnitudes from 8.7 to 8.9.
- The strength of the rocks in the earth's crust limits energy release (and hence the Richter Magnitude).

2.17 Earthquake magnitude classes

The US Geological Survey (2008) states that "earthquakes are classified in categories ranging from minor to great, depending on their magnitude". They have listed a table of expected observations and are shown below in Table 2-10.

Light tremors or excessive vibration from nearby construction plant can trigger liquefaction, which may occur in these soils and can result in more than expected settlement below these structures. This research will attempt to relate liquefiable conditions (including saturated windblown sand) to the state of densification and thereby predict a trend for possible settlement. According to the webpage of the Council for Geoscience (2007), earth tremors have been recorded from the South Western Cape since 1620. Between then and 1966 this area experienced at least 43 shock waves, 10 probably exceeding 4.5 in magnitude. Of these, 4 evidently exceeded 5.1. The last tremor was recorded on 28 September 1970 (Council for Geosciences: Historical Earthquakes, 2007).

Table 2-10 Richter magnitude scales (US Geological Survey, 2008)

Richter Magnitudes	Description	Earthquake Effects	Frequency of Occurrence
Less than 2.0	Micro	Micro-earthquakes, not felt.	About 8,000 per day
2.0-2.9	Minor	Generally not felt, but recorded.	About 1,000 per day
3.0-3.9		Often felt, but rarely causes damage.	49,000 per year (est.)
4.0-4.9	Light	Noticeable shaking of indoor items, rattling noises. Significant damage unlikely.	6,200 per year (est.)
5.0-5.9	Moderate	Can cause major damage to poorly constructed buildings over small regions. At most slight damage to well-designed buildings.	800 per year
6.0-6.9	Strong	Can be destructive in areas up to about 160 kilometres (100 mi) across in populated areas.	120 per year
7.0-7.9	Major	Can cause serious damage over larger areas.	18 per year
8.0-8.9	Great	Can cause serious damage in areas several hundred miles across.	1 per year
9.0-9.9		Devastating in areas several thousand miles across.	1 per 20 years
10.0+	Epic	Never recorded	Extremely rare (Unknown)

2.18 Motivation for this study

No documented research concerning shallow foundations in the problematic Aeolian sands of the West Coast region of Melkbos Strand has been conducted. General description of the geological formations have been adequately documented and described, but no documented laboratory evaluation of the wind blown sands in the study area could be found that highlights the problems that exist for residential homes with shallow foundations. This study documents some of the geotechnical evidence of the problematic wind blown sand and the physical evidence of consequential damage resulting from building in these conditions without the necessary precautions.

Although the Western Cape falls within the "light to moderate" category zone for earthquakes, the researched literature provides some evidence that minor tremors can trigger loose sandy deposits and cause collapse. As far as particle size distribution is concerned, the windblown dune sand of the study area falls within the category of susceptibility for liquefaction. Having stated this, it is important to link the above to a high water table. In summary the following can be established from the literature review:

- No calibration chamber has been built at a tertiary institution in South Africa for the purposes of calibrating a device dedicated to measuring horizontal stress and predicting settlement. The DMT device is not in general circulation in South Africa either and this research affords the opportunity to expose the usefulness thereof and with greater understanding the instrument can compliment further geotechnical investigations of problematic wind blown sand.

- Although alternative and established in-situ devices can be utilised effectively, this study can provide a correlation between the use of the DMT and the DCP.

- With the proper soil investigations done, which should include in-situ devices that predict potentially problematic soil, expected settlement can be more accurately predicted, thereby necessitating preventative action as far as structural damage to foundations and walls are concerned. Through trial tests with the DMT in the chamber, settlement will be correlated with the DCP under varying relative densities.

Chapter 3 Research methodology

This study was designed around the information gathered from the construction industry and the many reports of poor construction standards and foundation failure in areas where windblown sands are found. A few sites were selected in one particular area where structural failure was reported. These sites were examined and trial holes dug to substantial depths below the foundation level. In-situ tests with simple test methods such as the use of the DCP were completed and samples extracted for further geotechnical examination in a laboratory. These laboratory tests included particle size distribution, in-situ voids, relative density, dry density, shear box and % R_D. Independent laboratories were utilised to confirm some strength parameters such as the angle of shearing resistance and cohesion. A calibration chamber was designed to examine the properties of some of the Aeolian sands with the Flat Blade Dilatometer and to correlate the test results with those produced with the DCP.

All of the above was completed to evaluate why structural damage was occurring in homes built in Aeolian sand and to provide a possible solution as overcome these problems. The calibration chamber was also used to examine the phenomena known as liquefaction, which the manufacturer of the DMT device claims to be possible. Sands from two sources were placed in the chamber and the horizontal stresses (known by the DMT parameter, K_D) were examined after saturation was introduced. The research methodology is summarised below.

- Visit sites in the study areas and examine structural damage of homes by way of visual inspection and photographs. Extract sand samples and remove these to a laboratory for closer inspection and geotechnical test work.

- The study area was Melkbos Strand and the Atlantic Beach Golf Estate. A GPS was used to pinpoint the exact area. Areas outside but adjacent to the study area were selected for the examination of the windblown sand for comparative and correlation studies.

- A calibration chamber is to be commissioned and built at the Cape Peninsula University of Technology where some of the study will be conducted on sands from the West Coast and Philippi.

- Devices such as the Dynamic Cone Penetrometer were used on site. Extraction of soil samples were done with the Shelby type tube that allowed in-situ voids and density to be determined.

Bulk samples were removed at various depths to determine the grading analysis and soil classification (using the USCS method). Soil testing was based on the THM1 Methods (1986) and Head (1981). Software analysis was done with the use of Microsoft Excel, the DMT E-LAB software and interpretive correlation formulae produced by past researchers.

This chapter will focus on the field investigations, sample preparation and laboratory analysis of the Aeolian sand, the design of the calibration chamber, materials used and how the dune sand samples were confined inside the chamber. The properties of the sand samples are provided. A comparison between the DCP and DMT results are provided with settlement calculations. The measurements for the vibration frequencies are also discussed. For liquefaction prediction it is shown how the CRR values were determined and how it relates to the DMT's K_D value. The liquefiable potential of the sand was then assessed and analysed using the DMT results only.

3.1 Research design

The research involved the use of in-situ testing through the sand layers which were interpreted on site has having possible geotechnical deficiencies. Personal discussions were conducted with the owners of the properties and the builders who were contracted to complete the work. Visitation included the National Home Builders registration Council in the Western Cape who provided more evidence of structural damage for homes built in areas underlain with Aeolian sand. The building of the chamber allowed more control to be exercised as far as simulating density is concerned. The strength of the research lay in the fact that the work can be repeated and reproduced in the chamber, while in-situ testing may not. Further weakness lay in the uncontrolled boundary effect in the chamber, but research has shown that deformation below the point of contact with the blade of the DMT does not severely compromise the results. Some caution should therefore be applied in the final interpretation of the DMT result. No measurement of side stress in the chamber was planned for. The 6 mm thick Geofabric lining of the inner wall to the chamber, being highly compressible and absorbent, is expected to reduce some of the boundary effect.

3.2 Research methodology

This section of the study introduces how the work was conducted, the methods of soil examination and the equipment used on site. The design of the chamber is also discussed and how the sand samples

were examined for its strength parameters. The DMT device is also discussed in general, which will include its operation, calibration and how the data is interpreted.

3.2.1 **Data**

Data that was acquired were the accumulation of existing geotechnical test work done by past researchers in the study area and in similar conditions linked to Aeolian sand deposits. This data includes information such as particle size distribution and grading characteristics, DCP DN parameters linking sand properties to liquefaction and borehole logging data. A large data base of photographs of structural damage linked to failure of the foundations in the study area was electronically stored.

3.2.2 **Research equipment**

Equipment used during on-site investigation was the Dynamic Cone Penetrometer, small gauge Shelby Tubes, a digital camera plus various apparatus for moisture determination. Hand labour was utilised for digging purposes. The calibration chamber was designed and built at CPUT and based on the chamber built at TU Delft in the Netherlands. The DMT device was sourced from the United States of America where a bi-annual conference was attended (Washington D.C). These conferences are useful and promote research with this instrument. A Geogauge was used as a comparative device that correlated the in-situ stiffness, or Modulus, against the DMT in the chamber. Vibration motors were used to densify the sand in the chamber and its operation is discussed later in this chapter in 3.6.1

The laboratory equipment used for assessing the soil properties were the SABS listed apparatus in the TMH1 (Technical Methods for Highways Manual 1) and that recommended in KH Head's Manual for Soil Laboratory Testing, Volume 2.

3.3 Calibration chamber design

The calibration chamber was partly designed and based on the Dutch chamber built at the TU Delft University in Holland (Broere, 2001). The basic construction used at CPUT is shown in Figure 3-1. The chamber was built in the Mechanical Department of CPUT and installed above ground in the Concrete and Geotechnical laboratory of Civil Engineering and Surveying, Cape Town.

The CPUT calibration chamber is a 900 mm diameter rigid stainless steel wall calibration chamber, as shown in Figure 3.1. At the bottom of the tank, a system of filter drains connected to a pumping system was embedded in the sand. This system allows saturation of the sand bed within the tank. The geotextile below the chamber floor acts as a sand filter, so only a minute amount of fines were lost. Two commercially supplied VV05N2 380V rotary vibrators were fitted to the sides of the tank and used to vibrate the entire tank to assist compaction of the sand. They are capable of delivering 2.5 kN centrifugal force. These vibrators were fixed vertically and horizontally opposed to the outside of the wall. The inlet for the water was via a 75 mm PVC pipe. A simple centrifugal pump draws water from a gravity fed source tank and forces the water into the tank from below. The configuration of the water distributor allows the water to infiltrate upwards. The water passes through a 250 mm layer of sieved gravel (53 mm nominal size), which is protected with a layer of synthetic Geotextile, below and above the gravel layer. The gravel is supported by a platform of short galvanized pillars and steel mesh of 1 cm² in size.

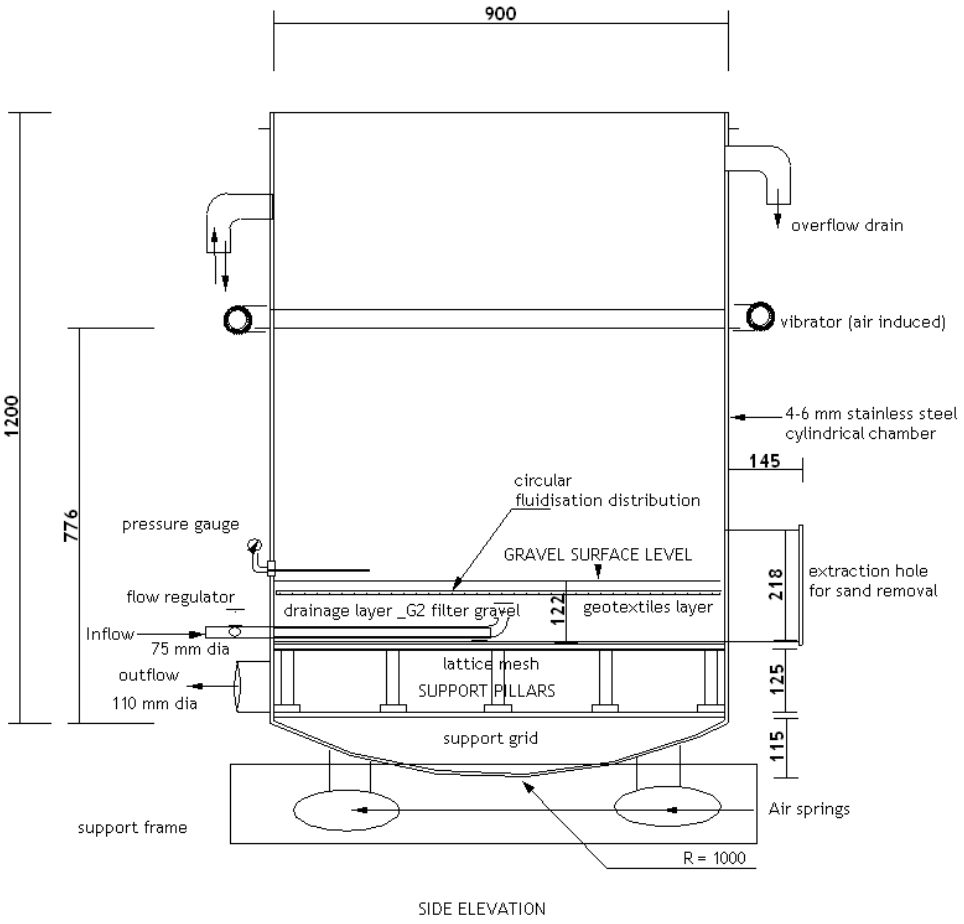

Figure 3-1 CPUT Calibration chamber design

3.3.1 **Calibration chamber preparation**

Soft dune sand was sourced from two significant areas around the Western Cape that have had problems with settlement after construction, these being the Delft and Philippi areas as well as West Beach, Blaauwberg. The uniformly distributed fine sand, has a D_{50} = 0.2 to 0.35 mm. A distribution curve for the sands can be found in Chapter 4. The chamber was cleaned before a new batch of sand was introduced.

Due to the preparation method of the sand layers and the resultant segregation that took place, it was expected that the obtained density in the tank was not uniform over the full depth of the tank.

3.3.2 **Recommended design choice of Airmount actuator**

- Step One: Load Capacity

A decision was made in selecting three isolators that could support the vertical load of the chamber at each mounting point. This was to accommodate pressures in the 400 to 550 kPa range. Type 1M1A (in the Appendix Schedule Table B.1) for single and double convoluted) was chosen as suitable for this chamber. A choice was made to fall within the range of 45 to 44800 kg. The chamber's gross estimated mass is 2800 kg.

- Step 2: Determine Isolation Effectiveness

The forced frequency was located on the vertical axis of the manufacturer supplied isolation chart (Table 3-1). The natural frequencies of the part selected was located on the chart and these values transferred onto the horizontal axis of the isolation chart. At the intersection of the forced frequency and natural frequency lines, one can determine the approximate percentage of isolation by comparing this point with the diagonal lines representing these percentages.

- Step 3: Determine Design Height

The manufacturer recommends the Airmount isolator be used at the design height as per the Appendix Schedule A14. The design height is the desired height above the isolator upon which the chamber will rest. This is about 140 mm.

3.3.3 **Air springs actuators**

Isolators are used to support and isolate external vibrations or support a vibrating load and prevent its energy from disturbing the surroundings. Air springs are designed to contain and support a column of compressed air. The rubber bellows do not provide force or support load – the column of air does this when the air spring is inflated according to the load required. Load capacity can vary from 40 to 40,000 kg. The fully loaded chamber used in this research was estimated to be 2,500 kg. Each of the three actuators carried approximately 833 kg.

Table 3-1 Airmount vibration isolation chart (Firestone, www.airsprings.com.au)

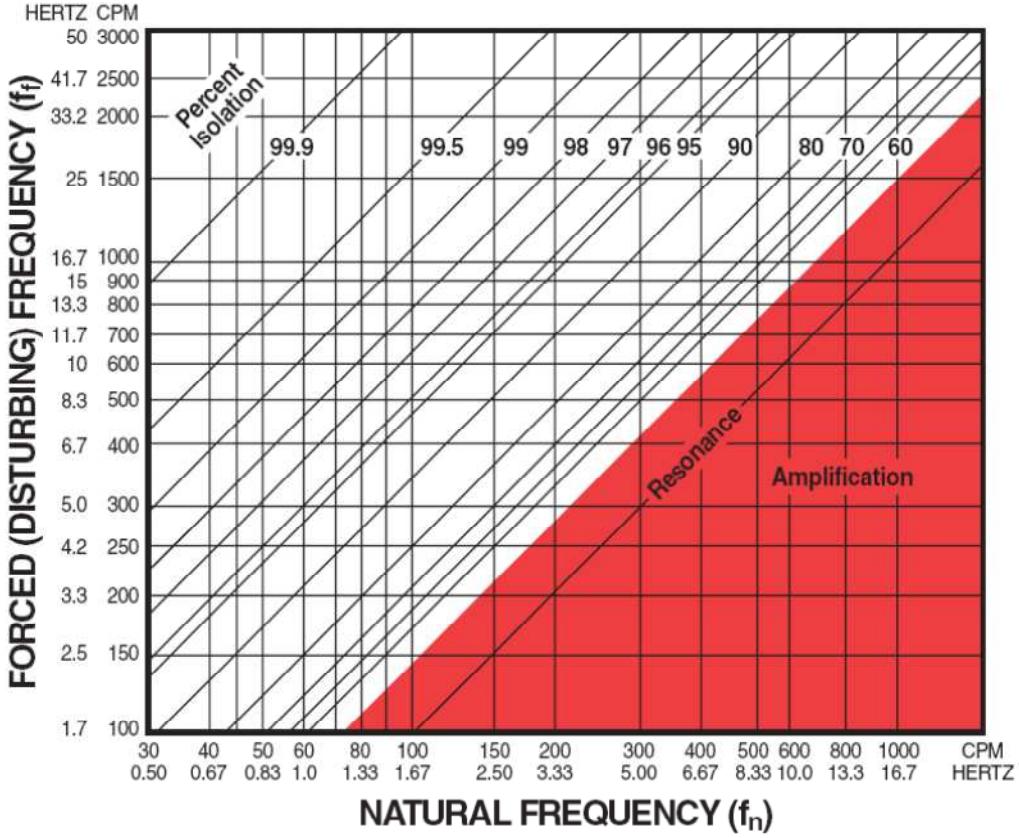

Airmount actuators have no internal rods, pistons, or sliding seals that would require lubrication or maintenance and prevents dirt or grit from destroying the seals. The type used in this research has an air valve that allows the operator to monitor air pressures. The air pressures were initially set to 250 kPa. Since the actuators have no sliding seals, there is no apparent friction and reduce structurally transmitted noise. They are quiet and present little noise disturbance, operating below the 85 dB mark.

The actuators used for the calibration chamber have elastomeric bellows with metal end fixtures. The bellows are constructed from plies of cord-reinforced rubber with standard construction utilizing two plies of special cord fabric. Airmount actuators are capable of handling loads up to 40 tons and can be designed into systems to utilize more than 30 cm of stroke. The standard air spring will operate in temperatures from 37°C to 58°C and special compounds are available on some parts to extend this range. The stroke of the actuator has been determined via trial and error, so that excessive vertical movement of the chamber would not exceed 5 mm. Air springs (as displayed in Figure 3-2) are heavy-duty bellows used for isolation tasks within industrial equipment and vehicle suspensions to provide a smoother riding suspension as an alternative to metal springs.

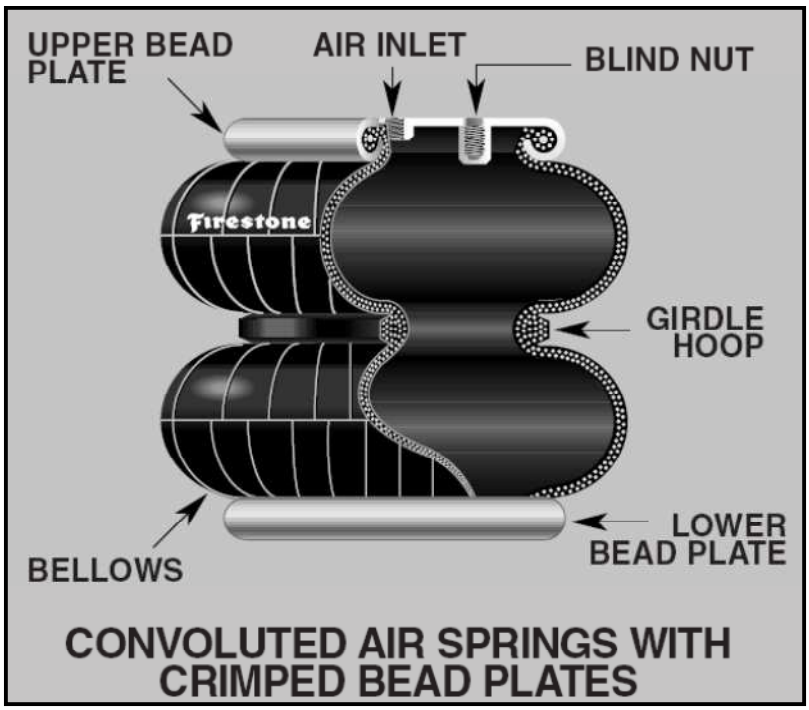

Figure 3-2 Double air spring, (Firestone, www.airsprings.com.au)

3.3.4 **Actuator Installation**

The actuators were bolted to the support pillars below the chamber and the chamber positioned on top. The designers recommended initial air pressures to be no less than 275 kPa. The actuators were pressurised before the full mass of the chamber was exerted from above. See Appendix Schedule A16.

- Start-up and Shutdown / Resonance and Amplification

The chamber was restricted to vibration duration of between 30 seconds and 2 minutes. This was useful and helped to overcome resonance, which is the forced frequency of the vibrating system at natural frequency. No amplification of movement was noticed (sideways shifting of the chamber). The chamber was never vibrated under low mass and was thereby also restricted to sideways movement.

The following information is an extract from the suppliers' notes (Firestone Air Actuators, 2003): "The maximum stroke capability of an Airmount actuator is the difference between the maximum useable height and the minimum height". For strokes of less than 75 to 100 mm, the Single Convolution parts are generally the most efficient"

- Centre of Gravity

Airmount isolator systems are inherently soft (easily deflected). Therefore, precautions were taken to ensure that the chamber was stable. Firstly, the location of the centre of gravity was considered. The laboratory floor was stable enough to support the entire chamber. Ideally, the Airmount isolators should be located on the same plane (parallel to the ground) as the centre of gravity. The suppliers (Firestone Air Actuators, 2003) recommended that the distance between the narrowest mounting points should be at least twice the height of the centre of gravity above the mounting points. The centre of gravity for the chamber was calculated to be 290 mm above the mounting points of the actuators.

3.3.5 **Water Feed System**

A 1000-liter gravity fed PVC tank was located outside the laboratory on a mounting stand. This prevented leakage from occurring inside the building and can be easily modified to allow rainwater to filter down into to the tank to replenish the water supply. A simple centrifugally operated pump (1.75 kW) draws the water via a 40 mm PVC pipe out of the tank and feeds the chamber from below.

Flow controllers were positioned in the PVC pipe and by opening and closing these, the chamber was filled up completely and thereafter the water was drained off again. An overflow drainpipe was located at the top end of the chamber to allow excess water to drain back to the source tank, in the case of an emergency (Figure 3-4).

In order to do tests on moistened sand, a water pump had to be connected to the chamber. The pump extracts water from water tanks outside the laboratory and pumps it through the inlet pipe (Figure 3-3) at the bottom of the chamber. This allows the sand to be flushed gently from the bottom of the chamber. The process is quick and saturation of the sand is completed within 2 to 3 minutes. A drain pipe was connected just above the inlet pipe and under the bottom layer of the sand to allow unexpected overflow. All the water in the chamber was thereafter sufficiently drained without the major loss of finer particles flushing past the 1.2 mm thick Geofabric liner (Appendix Schedule Figure B.2).

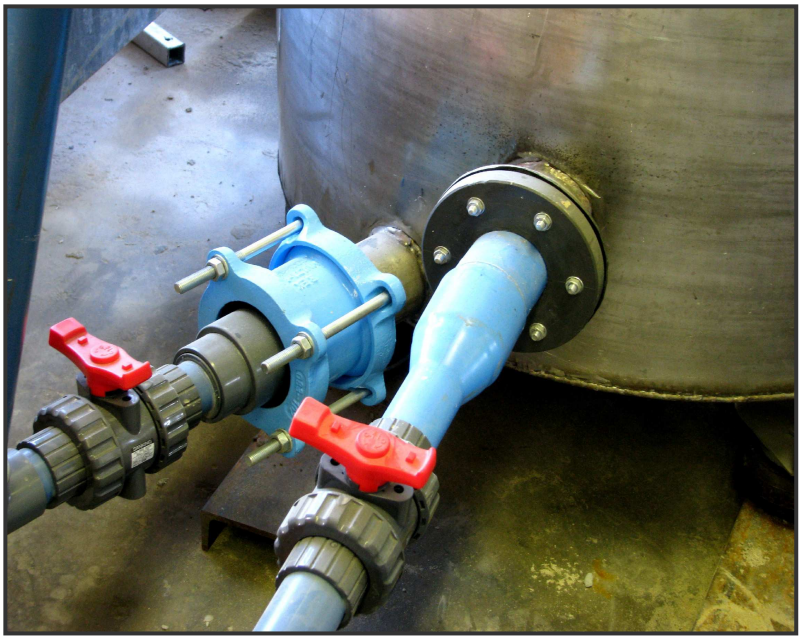

Figure 3-3 Water feed system

Figure 3-4 Water overflow drain

3.3.6 **Cross-Fluidisation Systems**

Figure 3-5 shows a view from the top of the chamber and the cross configuration of the filtration system. This is made from a 40 mm PVC pipe adapted to fit the large feeder 100 mm PVC inlet pipe. Suitable and sustainable pressures are present to force the jet stream through the stone aggregate and geo-fabric above. The cross filters are perforated with 4 mm Ø holes and 75 mm apart. After vibrating, the remaining water was drained to create an unsaturated sand bed. Appendix Schedule Figure B.2 illustrates the gravel filtration layer and Geotextile installation.

3.4 Steel chamber construction

The design was based on a rigid wall system comprised of 4 mm stainless steel. It is 900 mm in diameter and stands 1200 mm tall. It is semi-seamless, having one weld down its length. Its base was constructed from galvanised tube steel and accommodates the three actuators below. The lower side has an extraction point, 220 mm Ø, and allows soils to be removed after test work is completed or for access to allow general maintenance or modifications to take place. Support pillars below the chamber have been laid out in a grid pattern and support the stone aggregates above along with the sand mass. A collection area was created below the pillars to allow debris to collect. The collection area can be cleaned out via an extraction hole.

Above the pillars is a galvanised sieve grid, with openings of 1 cm square. On top of this grid, a round section of geo-fabric was placed to fit the diameter of the chamber. The fabric assists in preventing sand fines to filter down into the collection area, but this is at times unavoidable. A plan view of the chamber can be seen Figure 3-6.

Figure 3-5 Geotextile inside of calibration chamber

A stone aggregate media was selected (Malmesbury Hornfels, or baked metamorphic shale) and roughly 300 kg was passed through a standard 53 mm and 9.5 mm square sieve. Only the aggregates that remained between these two sieves were used. After the aggregates were washed thoroughly it was air dried and placed above the geo-fabric, in a single layer of 200 mm thickness. A second piece of geo-fabric was placed above the stone media as seen in Figure 3-5. Another picture of the fabric can be found in the Appendix Schedule Figure B.2.

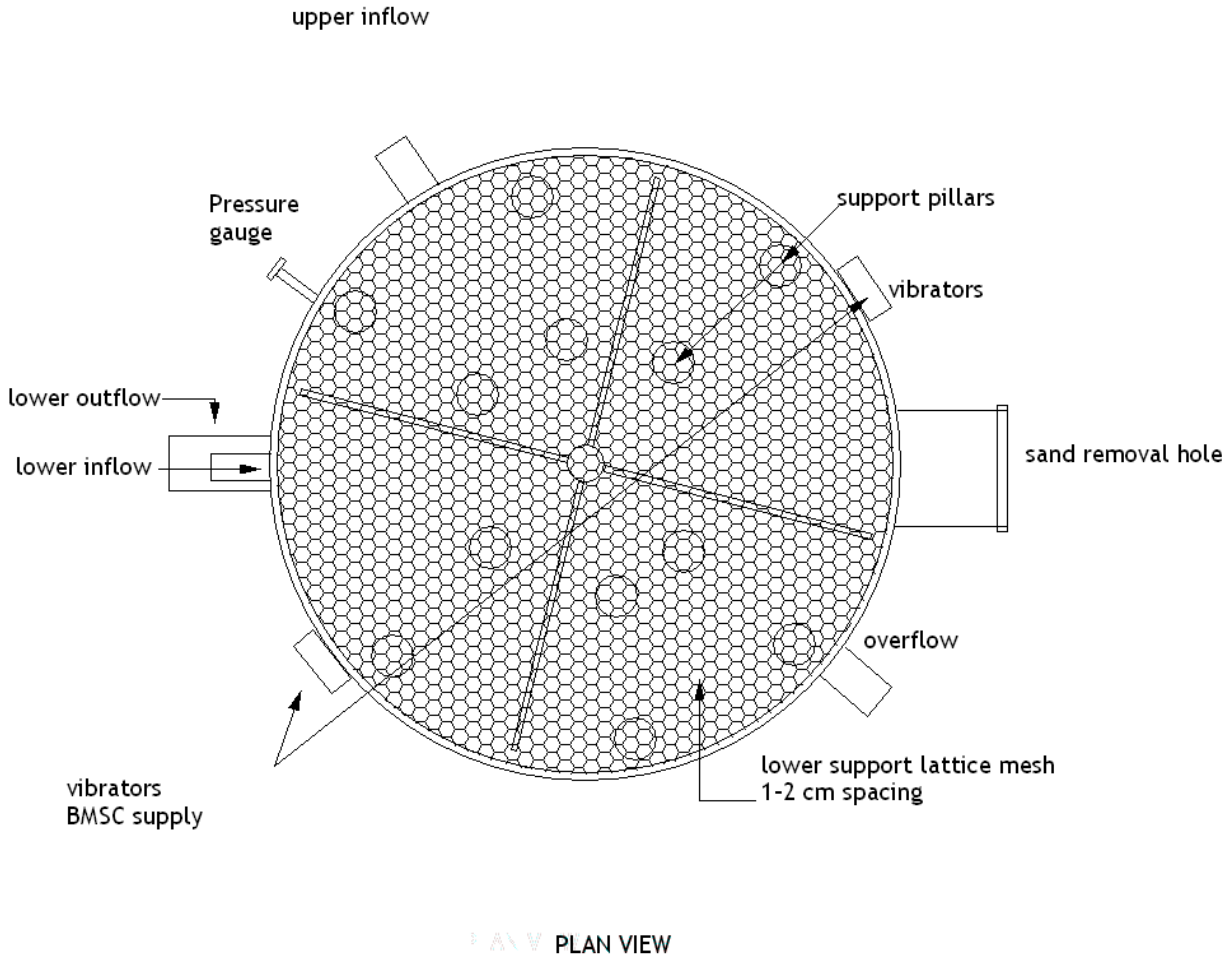

Figure 3-6 CAD plan view of calibration chamber

3.5 Calibration chamber preparation

To prepare a sample of sand to be tested, it was first air-dried and sieved into the chamber via a standard SABS size 4.75 mm sieve from a fixed height of 900 mm using batches of 30 kg at a time. Large fraction sizes of 4.75 mm and above are removed. After the full complement of layers was inserted, the tank was first saturated and, when fully liquefied, the water was allowed to drain after a rest period of 1 day. The test sand was pluviated from a standard height of 900 mm above the stone aggregate with the aid of a 4.75 mm sieve and the chamber was then filled to 100 mm below the chamber rim. The vibrators were then used for a period of 30 seconds to 1 minute (for dry condition testing), dependent on the relative density of the sand that is required. Thereafter the remaining water was allowed to drain and the density of the sample was determined by removing a sample from the centre of the layer. This was done using a sample extruder (38 mm Ø Shelby type) typically used to remove cohesive soils for triaxial testing on site.

The sand bed is fluidised while the water table is higher than the sand top level. Two vibrators fixed on the tank walls are used to vibrate the sand while the extraction pump drains water from below. A fixed phreatic level is set (15cm below the surface of the sand) to provide full saturation. Thereafter, the sand is vibrated at set intervals. Standard times of 2 and 5 min (for wet condition testing) have been chosen in previous experiments for sand (Broere, 2001).

The advantage of this method is that the preparation is not labour-intensive; as opposed to dry pluviation used in the past by researchers. New test samples can be prepared each week, requiring only one man-hour of actual work during this period.

The test samples are somewhat less homogeneous through the height of the chamber and a small amount of fines were washed out of the sand (visible in a container) during the draining phase. The level of saturation depends on the permeability of the sand and the draining time. The chamber allows for the testing of fully saturated samples. In an attempt to simulate age and stress history, this option for testing conditions was not used in this study. After testing, the sand was removed through the 220 mm Ø extraction point, situated at the bottom of the chamber.

A feature of the CPUT chamber is a rigid steel wall calibration chamber (4 mm thick), therefore the lateral boundaries are stiff and disallow any deformation of the test sample. This is in contrast to the

often-used flexible wall chambers, where a pressurised membrane is used at the lateral boundaries to keep a constant lateral pressure.

Vertical stress on the dilatometer blade was applied via a hydraulic ram piston, with a 900 mm shaft extension and 50.2 mm Ø piston (Figure 3-7). CAD design sketches are of the shaft extension are placed within the Appendices Schedule (Figures B3 to B7). The force applied from the ram piston was measured with an in-line pressure sensor that monitors the oil pressure in the hosing. The sensor type was a Senso-control, supplied by Hyflo (Pty) Ltd (Figure 3-8). A loading frame was used to provide a constant rate of penetration. The rigging consists of a loading frame fixed to two beams that provide the reaction force when the actuator pushes the DMT into the soil. A digitised loading cell recorded the pushing force required while a hydraulic actuator controls the speed of the penetration. The speed of penetration has been linked to the standard CPT push velocity of 20 mm/s. A hydraulic jack (Figure 3-7) was fitted onto a load frame rig above the flat plate dilatometer and used to force it into the sand to predetermined depths. An extension piece allows deeper test depths and was supplied by a local engineering firm, MSK Engineering. The ram and the force exerted were calibrated by the manufacturer using a load cell coupled to the in-line Senso-control. No correction factors were required as the readings on the pressure gauge and those measured from the load cell were acceptable (within 0.01 %).

The hydraulic ram was mounted onto steel I-beams above the calibration chamber. The rod has a piston with a diameter of 50 mm. This jack was used to control the rate of penetration of the flat plate dilatometer at a rate of 2 cm per second, reaching 800 to 900 mm into the chamber sample. This steel rod has a 14 mm hole running vertically through the shaft which allows the DMT inflation tubes (Figure 3.16) to enter and connect to the Flat Plate Dilatometer. An electronic pressure gauge was connected in line to the hydraulic pipes feeding the hydraulic jack (Figure 3-8). This pressure gauge provided the pressure readings. The pressure can be converted to kilogram force, allowing further calculations of the bearing capacity at the test depths.

The equipment is easy to set up and operate. The testing sequence progresses without delays and a series of tests can be completed within 6 minutes for a depth of 800 mm. At times one operator can easily manage all the test work in the chamber although for safety reasons this is not recommended.

Figure 3-7 Location of hydraulic piston ram

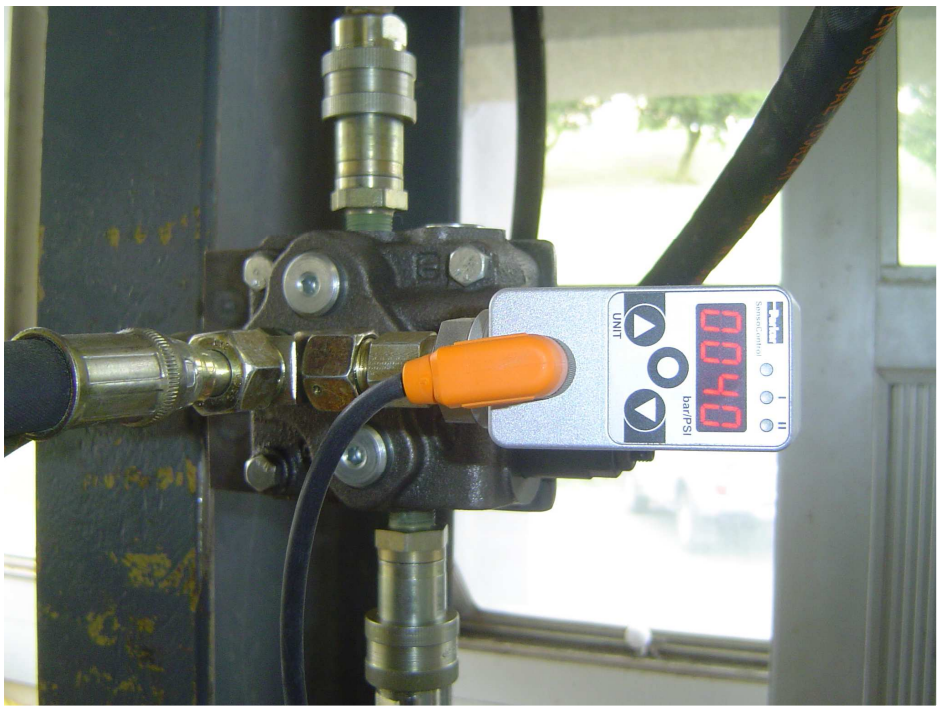

Figure 3-8 Position of senso-control device

Figure 3-9 Location of lateral vibration motors

3.6 Densification in the chamber

3.6.1 Vibro-Compaction

A local engineering supply company, BMSC Engineering Supplies, assisted in providing two vibratory motors which provided vibration for densification of the sand. The specifications for the motors have been placed in the Appendices Schedule, TableB.2. The operation of the vibratory system is discussed further in the work plan below.

Two vibratory motors (Figure 3-9) were mounted on the calibration chamber, one on each side. These motors are used to vibrate the sand in the chamber which results in the densification of the sand. The depth of the vibration readings with the accelerometer had to correspond with the depth of the Flat Plate dilatometer where test readings were done. In order to do this, a 12 mm solid steel rod was used to penetrate to the depth of the dilatometer blade. The end of this steel rod is perfectly flat with a grub screw tapped into it. An accelerometer was screwed onto the grub screw, fixing it vertically to the rod. An accelerometer is a small device which records frequencies and amplitudes. The accelerometer was connected to a sound level meter which provided a graphical output of the vibration. The data was transferred onto an EPROM interface and converted to ASCII text. A solution was found to measure the vibration within the sand at the point where the dilatometer blade rests (co-ordinated marking on the DMT blade shaft and the steel rod of the accelerometer).

3.6.2 Determining compaction in the chamber

DCP tests were done on the dry sand in the chamber in three different test holes to assess the density (and later, settlement) of the sand. The DCP (Figure 3-10) uses an 8.5 kg hammer with a drop of 575 mm and a 60° cone having a maximum diameter of 20 mm. After saturation and a rest period of 24 hours, the density was calculated by using a small Shelby type sampler.

To determine the relative density achieved in the chamber using the DCP, the formula (2.5) as proposed by Coduto (2001) was used to convert the DCP_{DN} value. These results are discussed further in Chapter 4.

Figure 3-10 DCP Apparatus (CPUT, 2007)

3.7 Operating the flat plate dilatometer

The flat plate dilatometer is used with its control unit equipped with two gauges where pressure readings are obtained. Onto the control unit (Figure 3-11) all the gas pipes and electrical continuity cables were connected. The gas inlet connects the Nitrogen gas bottle to the control unit and the outlet connects the control unit with the Flat Plate Dilatometer. The ground cable is connected to the control unit and to any other object which can conduct electricity to ensure electrical continuity. Nitrogen gas is preferred as it is the driest gas that will deter corrosion of the inside of the control unit. On the control unit, the critical A, B and C pressure readings are obtained. The first gauge gives small readings between 0 bar – 6 bars and the second gauge gives pressure readings from 0 bar – 80 bar.

The DMT is easy to manipulate into position and with the correct hydraulic equipment on site, according to the manufacturer, can penetrate to depths exceeding 90 meters in a single test. The test procedure in the CPUT chamber utilising the hydraulic ram is effortless and readings are taken soon after each depth is reached.

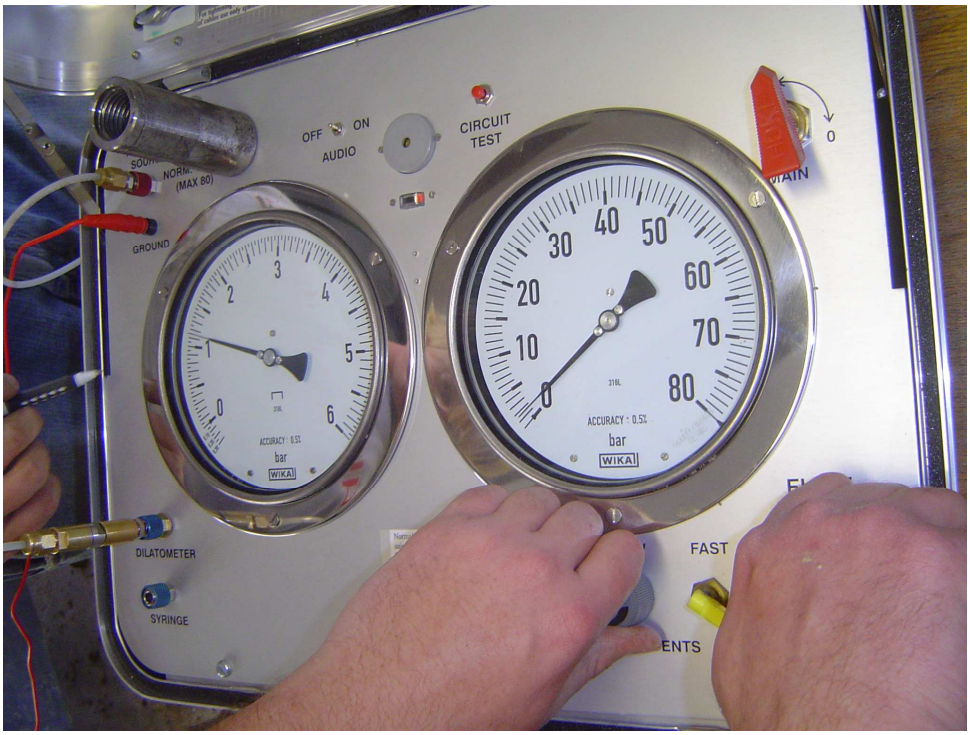

Figure 3-11 DMT Control Box

3.7.1 **Membrane calibration**

Definition of ΔA and ΔB

The membrane calibration should not be seen as only a calibration, since the term calibration may refer only to the scale of error of an instrument (Marchetti, 2001). The membrane is in effect a flexible separator of soil granules and not a device designed for measurement. The membrane acts like a "tare" button on an electronic scale and the "calibration" is in affect a return to reset position".

The calibration procedure depends upon obtaining the ΔA and ΔB pressures necessary to overcome the membrane stiffness before the actual testing is started (see Figure 2-24). During test work in the chamber the ΔA is the external pressure applied to the membrane and causes the collapse against its internal nylon seating. Thereafter gas flow was increased, resulting in the ΔB reading. This is the internal pressure that moves the membrane centre 1.1 mm from its original position. This reading is signalled with the return of the audio signal beep. In detail procedures can be found in the documents released by the originators of the dilatometer, Marchetti and Crapps (1981) and Marchetti (1999). Values of tolerance for ΔA and ΔB are: ΔA = 15 kPa, ΔB = 40 kPa. When these values are exceeded, it is time to replace a potentially worn out membrane. This research showed no sign of wear within the 6 months of

testing and was not necessary to replace. The manufacturer recommends that as long as a membrane remains within tolerance it is not required replacing it. Typical calibration values obtained during test work in the CPUT chamber are listed in Table 3-2.

Table 3-2 Typical calibration data for DMT membrane

	Test Hole 1		Test Hole 2		Test Hole 3	
ΔA	0.3 Bar		0.3 Bar		0.3 Bar	
ΔB	0.5 Bar		0.55 Bar		0.6 Bar	
	A (Bar)	*B* (Bar)	*A* (Bar)	*B* (Bar)	*A* (Bar)	*B* (Bar)
200mm	1.5	4.9	0.5	2.55	1.0	3.65
300mm	1.15	4.4	0.675	3.08	0.975	3.825
400mm	0.8	3.9	0.85	3.6	0.95	4
500mm	1.23	4.0	0.825	3.6	0.875	3.525
600mm	1.65	4.1	0.8	3.6	0.8	3.05

3.8 Field Investigations

Recent inspection of trial holes in the area of West Beach, Blouberg and the Atlantic Beach Estate has revealed low bearing capacity within the upper drift zone. Values as low as 45 kPa (inside the Atlantic Beach Estate) are not uncommon (own research) and have been determined with the DCP. Low bearing capacity can be expected in the drift zone because of the varying densities associated with the contamination therein, including spongy organic matter. Figure 3-12 below reveals the darker contaminated decaying organic matter that can be expected in the Atlantic Beach Golf Estate. On closer inspection it becomes clear that much of the contamination is charcoaled debris, most likely blown about by the prevailing winds after seasonal fires that occur regularly in the summer months, the fires being fed by the surrounding fynbos and Port Jackson brush.

Figure 3-12 Contaminated dune sand at Atlantic Beach Golf

3.9 Dynamic Cone Penetrometer testing at existing homes

The Dynamic Cone Penetrometer, illustrated in Figure 3-13, has become an industry standard since its development in the 1970s and is now an ASTM test method. Information on the structure and strength of the road pavement can be interpreted to a depth of 800 mm. However, the instrument is not particularly robust, requires a three-man crew to operate, as well as considerable technician time to process and interpret the data. The drawbacks to this valuable test are now a thing of the past. A light weight (8 kg) probe was used on site at the bottom of the trial holes at the Atlantic beach Golf Estate. Many sands occur in a loose state. When relatively dry, such sands show no DCP index values for the top few centimetres and may show increasing DCP index values with depth. Sands and gravels in an oversaturated condition (water percolating through) should be avoided. The processed results reveal the consistency of the soils density below ground and, with further mathematical models, a prediction can be made regarding correlated bearing capacity, angle of friction, shear resistance, modulus of elasticity and % density.

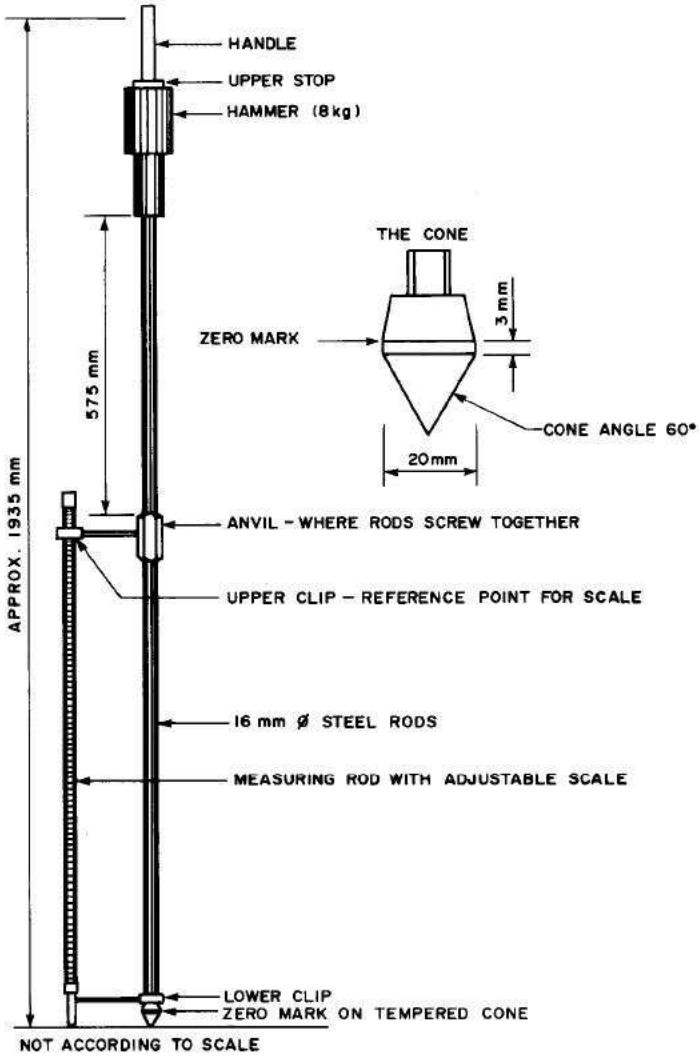

Figure 3-13 DCP Apparatus (Paige-Green, 2009)

3.9.1 **DCP Apparatus**

A Dynamic Cone Penetrometer consists of the following:

A sliding hammer of 8 kilograms

A steel rod that allows a drop of 575 mm

A measuring rod with an adjustable scale, may vary from 1 -2 meters in length

Allen keys and various spanners for bolt tightening and dismantling

A penetration cone shaped to 60 degrees (including spares)

The dual-mass DCP consists of a 19 Ø mm steel rod with a steel cone attached to one end which is driven into the soil by means of a sliding dual-mass hammer. The angle of the cone is 60 degrees. The cone is manufactured of hardened steel to increase service life. The diameter of the cone is 4 mm larger than that of the rod to ensure that the resistance to penetration is exerted on the cone only. Figure 3-13 shows an assembled DCP with a vertical scale for measuring the cone penetration depth in millimetre. The DCP is driven into the soil by dropping the 8 kg sliding hammer from a height of 575 mm.

The depth of cone penetration is measured at selected penetration or hammer-drop intervals, and the soil shear strength is reported in terms of a DCP index, usually as mm/blow (also referred to in other publications as the PR-rate “or penetration rate”). In sandy soils readings after every 2 blows is seen as adequate. Although in very loose sands, where high readings are obtained, reading after each blow is necessary. The DCP index is based on the average penetration depth resulting from one blow of the 8 kg hammer. The DCP is designed to penetrate soils to depths of up to 2 m and in some cases (without unforeseen obstacles) even deeper with extension rods attached.

The disposable cone is for use in soils where a standard cone is difficult to remove. The disposable cone mounts on an adapter and is shown in Figure 3-14. At the conclusion of the test, the disposable cone easily slides off the cone adapter, allowing the operator to remove the DCP device from the soil. The disposable cone remains in the soil. Use of the disposable cone approximately doubles the number of tests per day that can be run by two operators. The mode of operation was that if the cone did not penetrate 25 millimetres after 20 blows, the test was terminated. In none of the trial holes examined was this required. DCP tests were completed in each trial hole at a position level with the existing foundation.

Figure 3-14 Disposable cones for the DCP (Paige-Green, 2009)

The trial holes all revealed contaminated Aeolian dune sand up to a depth of about 1.2 m below the foundations. Some minor rubble and varying amounts of organic material were also evident. The imported fill and the uppermost portion, or drift zone tends to be of a loose nature as recorded by the DCP's. Table 3-3 below summarises the depth investigation, at a site called Lands End in Atlantic Beach, to a zone construed to be firm and dense enough to found foundations upon in relation to actual founding depths at the positions tested. These tests were completed by an independent consultant.

Table 3-3 Depth Investigation in trail holes

Trial Hole Nr	1	2	3	4	5	6	7
Depth to TOF	0.7	0.7	0.65	0.3	0.4	0.8	-
Depth to BOF	0.85	0.85	0.8	0.45	-	1	-
Thickness of footing	0.15	0.15	0.15	0.15	-	0.2	-
Depth to firm sand	2.2	1.25	0.85	0.85	0.9	2	1.7
Thickness of loose sand under footing	1.35	0.4	0.4	0.4	0.35	1	-

The 8 kg light weight DCP was used. Results were recorded in mm/blow and readings taken after each blow.

3.9.2 **Determination of in-situ density in study area**

A Shelby-type cylindrical tube of 260 x 38 mm Ø was used to extract sand samples for the purposes of measuring density and moisture content. The tubes were wrapped in "cling wrap" to preserve the moisture content. The tubes have conveniently placed drill holes on one end to assist the penetration and extraction process. The results from these tests were used to calculate in-situ voids and % relative density.

3.10 Experimental apparatus and laboratory data

3.10.1 Introduction to laboratory methods

Disturbed samples from a site within the boundaries of the Atlantic Beach Golf Estate were removed inside sealed plastic bags for laboratory testing. The apparatus used for test work is described below. All the apparatus were locally supplied from the laboratory at CPUT. Equipment used were the standard Bishop's 60 x 60 mm shear box , SABS recommended sieves for the particle size distribution (including the ASTM 152H hydrometer), inclinometer for angle of repose, 8 kg light Dynamic Cone Penetrometer and Flat Blade Dilatometer.

3.10.2 Direct Shear Test

This test method (ASTM D3090 – 90) covers the determination of the consolidated drained shear strength of a soil material in direct shear. The test is performed by deforming a specimen at a controlled rate on or near a single shear plane determined by the configuration of the apparatus. Generally, three or more specimens are tested, each under a different vertical load, to determine the effects upon shear resistance and displacement; including strength properties such as Mohr strength envelope.

The shear box apparatus consists of the split 60 x 60 mm shear box, vertical and horizontal loading systems, frame, proving ring and dial gauges; specimen cutter, 60 mm square, 20 mm deep wood pusher; cutting tools, spatula and straight edge; tamping rod, stop clock, balance, accurate to 0.01g, and apparatus for determining the % moisture content.

The classic Coulomb straight line curve (as displayed in Figure 3-15) for direct shear failure is used to plot the results. An Excel spreadsheet was designed to accomplish this. The failure curve is represented by:

$$\tau = C + \sigma_n \ * Tan\, \varphi \qquad (3.1)$$

Note on angle of friction.

Although the shear box is the traditional method of determining this parameter, a correlation will be made with the DCP_{DN} in predicting the same parameter, as done in past research (Mohammadi et al, 2007). Typical values for internal angle of friction are given below in Table 3-4

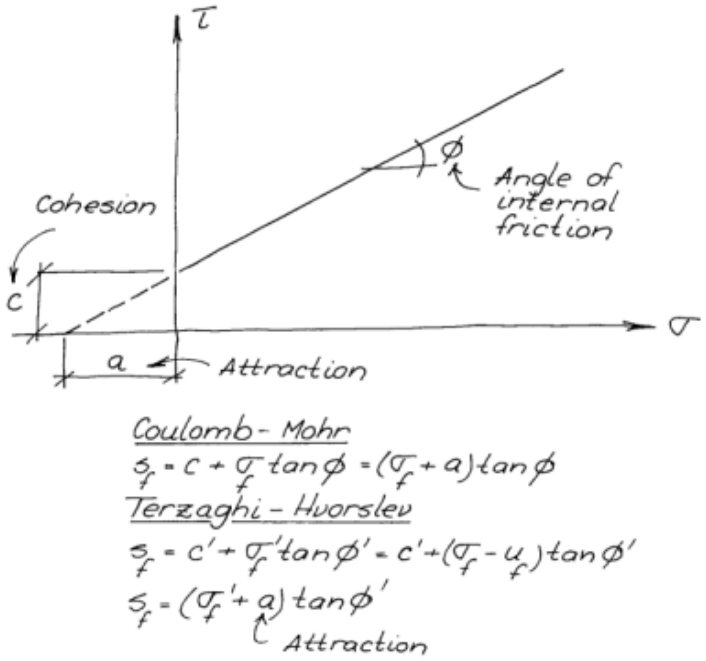

Figure 3-15 Typical Mohr-Coulomb Failure curve

Table 3-4 Friction values for φ (phi) (Head, 1981)

VALUES OF PHI FOR QUARTZ GRAINS

	Degrees		
Particle shape and grading	Loose		Dense
Rounded, uniform	28		35
Angular, well-graded	34		46

TYPICAL VALUES OF PHI FOR DRY NON-COHESIVE SOILS

	Degrees			
Type of soil and grading	Loose		Dense	
	Rounded	Angular	Rounded	Angular
Sand-				
Uniform fine to medium	30	35	37	43
well graded	34	39	40	45
Sand and gravel	36	42	40	48
Gravel	35	40	45	50
Fine clays and silts	28-32		30-35	

3.10.3 **Angle of repose of dune sand**

Tests were conducted to correlate observations in the field with experiments in the laboratory. These were done so that an order of correlation could be evaluated over the results. Discussed here are the method used for the angle of repose as measured with an inclinometer on a set of dunes in the Big Bay area close to the study area. The inclinometer results were correlated to a simulated angle of repose using extracted dune sand. A standard sand replacement funnel was used to pluviate the sand to form a natural angle of repose. This experiment was conducted to establish any relationship between the angle of repose, angle of shearing resistance (as determined with the traditional method of shear box testing) as well as by extrapolation with the DCP. The results are presented in a graph.

- Fieldwork

An inclinometer (Figure 3-16) was used to measure the natural angle of repose. A section of beach just beyond Big Bay, outside Blouberg (Figure 3-17) was selected for measurement and where sand dunes occur of various heights. The experiment was conducted to compare the angle of repose to the natural angle of friction as measured inside a shear box in a laboratory. Shelby-tube samples were removed at the positions where inclinometer measurements were recorded and dispatched to laboratories, including an independent laboratory (Geoscience Laboratories Airport Industria, Cape Town). The laboratory tests included particle size distribution and angle of internal shear resistance using the shear box. As an additional experiment, the natural angle of repose was reproduced in the laboratory using equipment as displayed in Figure 3-18 (sand replacement cone). Simulating the angle of repose (Figure 3-19) was accomplished with laboratory apparatus using calipers for height and base width measuring.

Figure 3-16 Inclinometer

Figure 3-17 Dune formations at Big Bay (North facing)

Figure 3-18 Sand replacement cone

Figure 3-19 Measuring the angle of repose

- Method for inclinometer operation

The method followed below is the same as described by the Department of Environmental Quality, State of Michigan, USA for the measuring of slopes under their sand dune protection program (Document Nr 353-96-01).

While holding the inclinometer, the operator stands at the toe or crest of the slope and sights to an object such as a survey staff at the opposite end of the slope. The object being sighted must be the same distance above the ground as the eye height of the person holding the inclinometer, thus keeping the same angle as the slope being measured. Hold the inclinometer to one eye while keeping both eyes open.

Look simultaneously through the lens and alongside the housing. A horizontal sighting line will appear in the viewing lens and extend to the side of the inclinometer housing. A bubble inside the housing appears as the horizontal comes into alignment. Raise or lower the inclinometer (by tilting your head) to place the sighting line at the object.

Read the number on the circular scale. Measurement is taken perpendicular to the contour (straight up or down the slope) so that the results are a true indication of the steepness of the feature. Determine if the angle of the slope is consistent. If the angle of the slope is not consistent, determine where the change in slope occurs and measure the steepness of the slope for each individual change of slope. This should be completed by measuring the slope from the toe of the slope to that point where the steepness of slope changes. Slope measurements were recorded on a site inspection form. GPS co-ordinates were recorded with a hand held Garmin device.

3.11 Laboratory trial tests

500 grams of dry dune sand from three areas inside the study area was used to simulate the angle of repose. A density funnel (Figure 3-18) was used to pour each individual sand portion from a height of 100 mm. A solid steel base was used below the funnel. The results of the trial tests are recorded in Chapter 4.

3.11.1 **Particle size distribution for coarse fraction sizes (>0.425 mm)**

The grain size distribution of a coarse grained soil is generally determined through sieve analysis, where the soil sample is passed through a stack of sieves and the percentages passing different sizes of sieves are noted. The grain size distribution of the fines are determined through hydrometer analysis, where the fines are mixed with distilled water to make 1000 ml of suspension and a hydrometer is used to measure the density of the soil-water suspension at different times. The time-density data, recorded over a few days, is translated into grain size and percentage finer than that size. Hydrometer analysis is effective for soil fractions down to about 0.005 mm (Das, 2010). Hand sieving was considering suitable for this test for fractions above 0.425 mm. Method A1 was followed as suggested in the THM1 manual.

-

3.11.2 **Grain size distribution in soils with the hydrometer (<0.425 mm)**

This method covers the quantitative determination of the distribution of particle sizes in soils smaller than 0,075mm and is determined by a sedimentation process, based on Stokes' law defined here under in (3.2); using a specially calibrated hydrometer (ASTM recommended 152H type). This method does not give absolute results, but gives data which are comparable and consistent if the method is followed in detail.

$$d = \sqrt{\frac{300\,nL}{980 - (Gs - Gw)T}} \qquad (3.2)$$

Readings were taken after 1 hour, 40 seconds and 18 seconds. The time related readings for each particle size is given in Table 3-5 below. Corrections were applied to the hydrometer readings according Table 3-6 below.

Table 3-5 Time interval readings vs diameter size (TMH1, 1986)

Hydrometer Readings at	**Maximum diameter of particles in mm's**	**Common term**
18 seconds	0.075	Material passing the 0.075 sieve
40 seconds	0.05	Silt & Clay
1 hour	0.005	Clay

Table 3-6 Temperature correction table for hydrometer readings

Temperature in Degrees Celsius	Correction
18.2 - 18.4	-0.6
18.5 - 18.7	-0.5
18.8 - 19.0	-0.4
19.1 - 19.3	-0.3
19.4 - 19.5	-0.2

3.11.3 **The determination of the percentage of material passing the 0.075 mm sieve**

This method covers the determination of the quantity of material passing a 0.075 mm sieve, expressed as a percentage of the total material, by washing a sample of prepared soil fines on a 0.075 mm sieve. The process is expedient for silty or clayey fines that may become clogged if sieved normally as described above. Washing of the 0.075 mm fines and the expectant result can be equated to the computed 18 second reading using the hydrometer sedimentation method. The formula for the % passing the 0.075 mm sieve is given below in (3.3).

$$\% < 0.075 = \frac{M1 - \mathrm{M2}}{M1} * \%Sf \tag{3.3}$$

3.12 Grading characteristics

A grading curve is a useful aid to soil description. Grading curves are often included in ground investigation reports. Results of grading tests can be tabulated using geometric properties of the grading curve. These properties are called grading characteristics.

First of all, three points are located on the particle size distribution grading curve:
d_{10} = the maximum size of the smallest 10% of the sample
d_{30} = the maximum size of the smallest 30% of the sample
d_{60} = the maximum size of the smallest 60% of the sample

3.12.1 **Classifying the sand**

The USCS method was incorporated in classifying the sand samples. Based on this method (ASTM, Designation: D 2487 – 06), the sand can be classified as uniform or singular, poorly graded sand.

Figure 3-20 below provides an illustration of how the grading of a soil is produced and its characteristics calculated. Useful grading characteristics are explained below.

Effective size: d_{10} = the maximum sieve size through which 10% of the sample fraction will pass by mass
Coefficient of uniformity: $C_u = d_{60} / d_{10}$
Coefficient of curvature: $C_c = d_{30}^2 / d_{60} * d_{10}$
Both C_u and C_k will yield a value of 1 for a single-sized soil
$C_u > 6$ indicates a well-graded soil
$C_u < 3$ indicates a uniform soil
C_c between 1 and 3 indicates a well-graded soil
$C_c < 0.1$ indicates a possible gap-graded or poorly graded soil

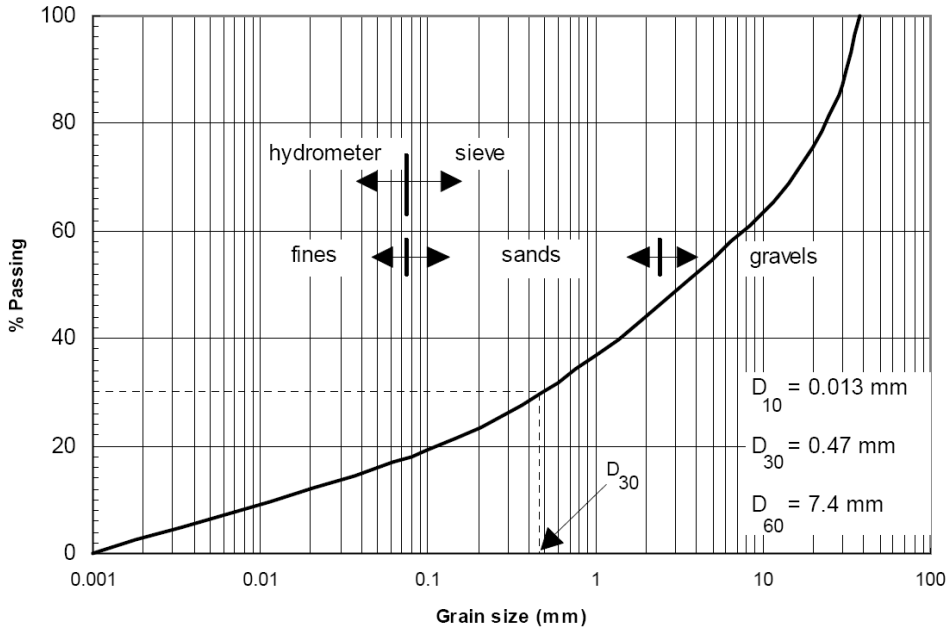

Figure 3-20 Illustration of Grading Curve

The particle size distribution curves from the study area (Figure 3-21 and Figure 3-22) are shown here. These curves have been produced and plotted as an average from 6 individual samples.

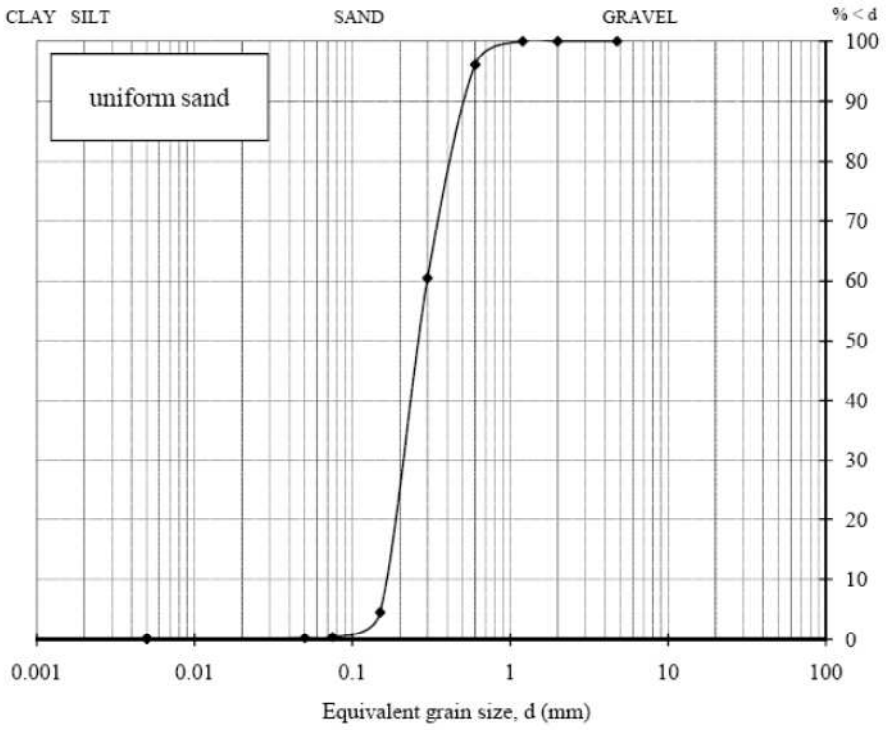

Figure 3-21 Typical grading below the drift zone Sample AB.4

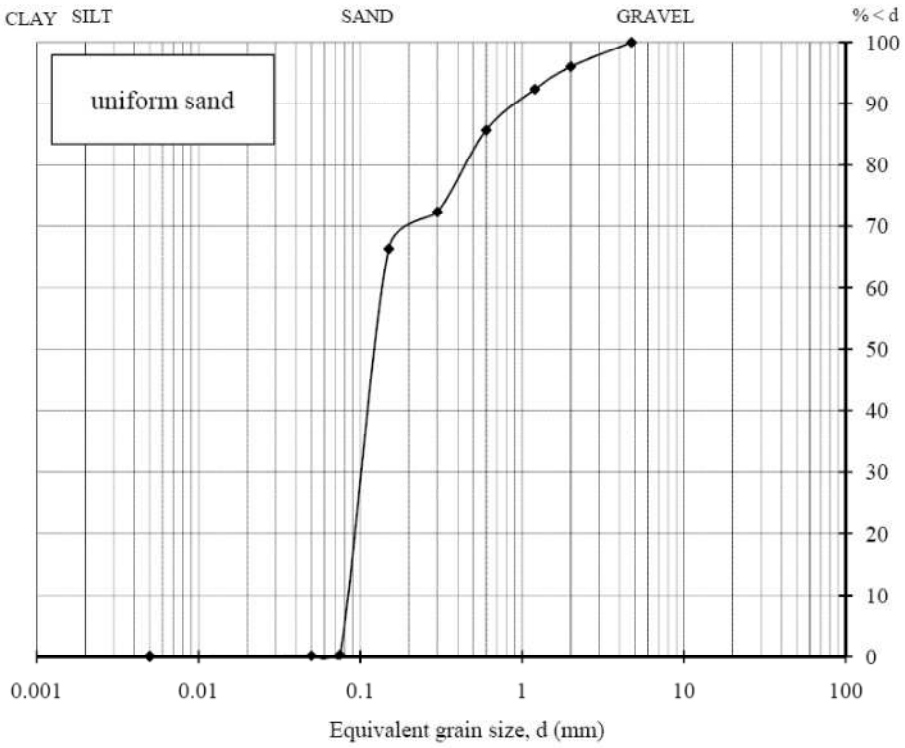

Figure 3-22 Typical grading within drift zone, Sample AB.2

3.13 Determining the in-situ density and voids

3.13.1 **In-situ density of sand**

Six Shelby type tubes were used on site to remove samples representative of the layers in the trial holes. A tube was lightly hammered into the layer after brushing a selected surface clean. The tube was then extracted via a twisting motion and marked for identification. Each tube was placed in a plastic bag to preserve moisture. In the laboratory the tubes were unpacked and cleaned. Thereafter each tube was weighed to the nearest 0.1 g. Some tubes had a small amount of sand fallout from the edges and these had to be repacked into position by lightly tamping the sand into the tube. The volume of the tubes was determined by using a calliper accurate to 0.02 mm. The difference between the two masses (tube with moist sand and clean tube without sand) was recorded. The bulk density was determined by dividing the moist sand mass by each applicable tube volume, and recorded in kg/m^3. A typical result is shown below using the formula (3.4)

$$\rho_b = \frac{Mass\ of\ Moist\ sand(kg)}{Vol\ of\ tube(m^3)} \quad (3.4)$$

Bulk density at Trial Hole At.B4 is $0.441/2.6298*10^{-4}$ =1676 kg/m^3

The moist sand was then removed from each individual tube and placed in an oven at 105°C for 24 hours. The moist sand mass was determined previously as part of the density calculations. After 24 hours the sand was removed from the oven and allowed to cool down to room temperature. It was then weighed to the nearest 0.1 g. The moisture content was then determined by the formula (3.5).

$$\%\, mc = \frac{Mass\ of\ water\ loss\ in\ sample(g)}{Mass\ of\ dry\ sand} * 100 \quad (3.5)$$

3.13.2 **Determining the minimum and maximum dry density of dry sand**

Procedure for minimum density

The guidelines as suggested by ASTM D 4253 (Standard Test Methods for Maximum Index Density and Unit Weight of Soils Using a Vibratory Table) were followed with slight modifications to the procedure. These changes were in the mould size used, surcharge weights and vibration time.

Sand was removed from the bulk sample and allowed to oven dry overnight. Dry sand was quartered out and placed inside a typical funnel cone used for the sand replacement test in field density tests (Figure 3-18). This process was selected as it duplicates the procedure used when determining the in-place field density of a compacted soil layer. The funnel was fitted over the Marshall mould (the funnel in the closed position). The sand is then allowed to drop from below the cone onto the mould below in a controlled manner. A straight edge was used to level off the sand at the rim. After cleaning and removing off excess sand the mould was weighed. This exercise was repeated six times with different batches and an average dry mass of the sand in the mould was determined.

The dimensions of the Marshall mould were determined with a caliper to the nearest 0.1 mm. The effective height was 78 mm and diameter was 101 mm.

After the final dry sand mass and mould volume calculations were completed the average minimum dry density of the sand was calculated. The formula (3.6) for density calculations is shown below.

$$\rho = \frac{[Mass\ of\ mould + sand] - [Mass\ of\ mould]}{Volume\ of\ mould} \quad (3.6)$$

A typical calculation is shown here in Table 3-7.

Table 3-7 Calculation data for minimum dry density

Mould + dry loose sand	3497
Mass dry loose sand	916
Minimum density, kg/m^3	1465.8

Figure 3-23 Marshall Hammer for compaction assistance

- Procedure for maximum density

For convenience the maximum density of the dry sand was determined with the aid of a surcharge weight in the form of a standard Marshall Hammer. The Marshall Hammer has an overall sliding weight of 4.53 kg, flat face diameter of 98 mm and has an overall weight of 8.631 kg (Figure 3-23).

The mould was filled in three layers from the same bulk representative sample of oven dried sand used for the minimum density determination. After each layer, the Marshall Hammer was placed inside the mould and allowed to rest on the surface of the sand. The Vebe vibrator table (Figure 3-24) was switched for 2 minutes and repeated for each layer (the Vebe table operates between 50 and 200 Hz). The final layer was lightly tamped down with extra sand to remove all surface irregularities. The same procedure was then followed as for the minimum dry density determination in calculating the final mass of the dry sand and final maximum dry density in kg/m^3.

Figure 3-24 Typical Vebe table (ELE Catalogue, 2010)

Typical calculations are shown in chapter 4 and Table 4-16 alongside the % relative densities.

3.13.3 **Determining the void ratio**

The in-situ void ratio is calculated with the use of the formula (3.7)

$$\rho_d = \frac{G_{s*}\,\rho_w}{1+e} \tag{3.7}$$

From (3.7),

$$e = \frac{G_{s*}\,\rho_w}{\rho_d} - 1$$

The factors that affect the outcome of the maximum and minimum void ratios for granular soils depend on:

- Grain size
- Grain shape
- Nature of the particle size distribution curve, and
- The fines content (the % <0.075 mm)

3.13.4 **Determining the % relative density, %D_R**

The void ratio of sands and gravels varies depending on how close the particles are packed in tight against each other, the variance occurring between the loosest practical state in which it can exist and the densest. Some engineering properties are affected by this, e.g. shear strength, compressibility and permeability. Figure 4-14 in Chapter 4 is a broad description of granular deposits and provides the practitioner a sense of how dense the deposit of soil is.

It was decided to measure the in situ relative density by comparing the in situ void ratio (e) with the minimum and maximum values (e_{min} and e_{max}). The density of packing is quantified through a simple parameter, relative density (% D_r) and defined as shown below in (3.8).

$$\%\, D_R = \frac{\mathrm{e_{max}} - \mathrm{e}}{\mathrm{e_{max}} - \mathrm{e_{min}}} * 100 \tag{3.8}$$

Results are shown here in (Table 4-16) for the Big Bay dune formation outside Melkbos Strand.

3.14 Investigating dwellings with structural damage

A survey of homes with external structural damage were visited and photographed to establish the cause. The NHBRC in the Western Cape have documented homes with reported damage earmarked for claims for repairs. This data can be seen in Table 3-8. The information covered only the period from 2001-2003. It is clear that an alarming trend can be seen in the number of reported occurrences of structural damage. An appointment was made with the NHBRC in Bellville for discussions of the process surrounding potential claims for damage to a homeowner's property. As a rule, structural integrity is guaranteed for 5 years while paintwork and waterproofing covers 2 years. The registered builder is responsible for the repairs covered by this agreement, or the NHBRC may appoint a contractor for this work.

Visitations were also made with home builders in the study area that were appointed to rectify structural damage. Damages include differential settlement below foundations, poor compaction below trenches and floor filling, incorrect drainage structures and general poor maintenance.

Photographs were provided by the builders of structural damage as well as own high resolution images were gathered. Figure 3-25 and Figure 3-26) are examples of damage resulting from settlement and poor construction respectively.

Table 3-8 Breakdown of structural problems (Courtesy NHBRC, 2003)

Type of Damage	Number of occurrences		
	2001	2002	2003
Foundation – settlement and failure of footings	0	0	4
Substructure – Settlement of floor slabs	1	2	7
Superstructure – Structural failure of walling	2	1	7
Roof structure – Structural failure of roof	1	4	1
Drainage – Failure impacting on structure	0	0	0
Total	4	7	19

Figure 3-25 Images of structural damage (Courtesy NHBRC, 2003)

The occurrences of light to sever structural damage to residential homes in Aeolian sands show signs of increasing. To establish the reasons why this is happening is important for the construction industry and for the local authorities.

Figure 3-26 Images of light structural damage and poor drainage

The above images are typical examples of homes built in windblown sands and where structural damage has been observed. High resolution photographs were taken with an appointed contractor. Many examples of structural damage were found and, upon inspection, it was found that the causes can vary from poor site management to low quality control of the materials used.

3.15 Analysis of in-situ test results

This section presents the results of the investigative work done on site and after laboratory work was completed. The DCP was used to analyse the sand deposit below homes with shallow foundations and undergoing settlement.

3.15.1 **In-situ data with the DCP**

The Dynamic Cone Penetrometer was used in trial holes to assess the firmness of the sand deposit below the foundations. The results are presented in (Figure 3-27) that displays the depth (vertical axis) against the DCP_{DN} (horizontal axis).

The large fall off to the right of the graph indicates a sudden loss in densification and be interpreted as loosely compacted. A better judgment in these case (e.g. trial holes AT.B1 and AT. B3) would be to assess the $\%R_D$ through the depth of the sand deposit. Loosely compacted sands would indicate $\%R_D$ values of below 25%. A correlation is made in this case, relating the DCP_{DN} to the predicted $\%R_D$ and is placed in the last column of Table 3-9.

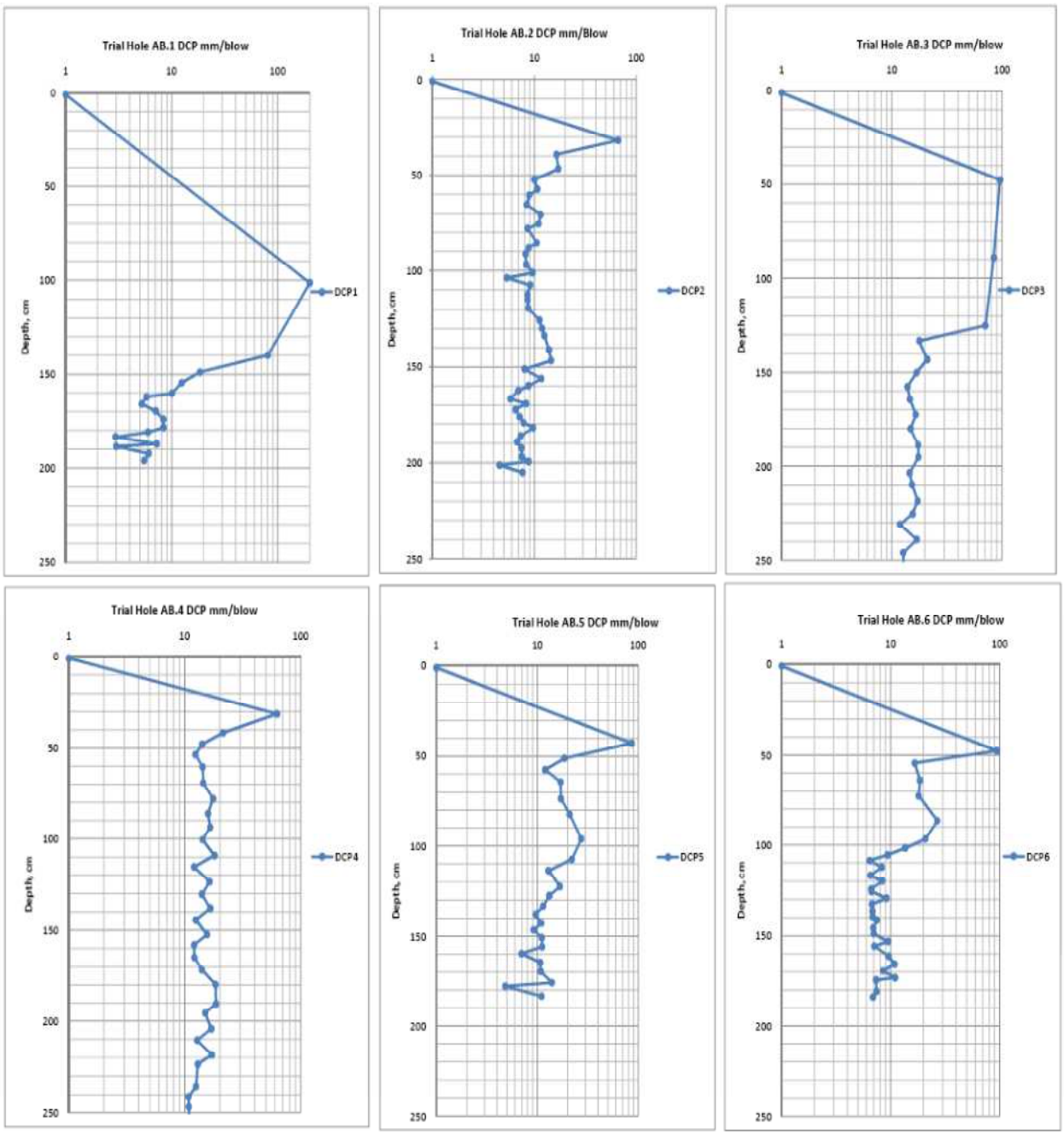

Figure 3-27 DCP data at Atlantic Beach Golf Estate

The DCP_{DN} data is presented below in Table 3-9 for interpreting the bearing capacity and relative density. The bearing capacity is based on the formula (2.7) proposed by Kessler (2009) while the relative density has been correlated to the DCP_{DN} using the Coduto formula in (2.5).

Table 3-9 Predicted strength parameters based on DCP_{DN}

Test hole AT.B1	Depth BGL	DCP_{DN}	In-Situ CBR	Q_u (kPa) Ultimate	% D_R
0.0	50.0	start	-	-	-
3.0	145.0	31.7	6.1	86.8	30.4
3.0	265.0	40.0	4.7	72.9	26.9
3.0	490.0	75.0	2.3	45.7	19.3
3.0	595.0	35.0	5.4	80.5	28.9
3.0	675.0	26.7	7.4	98.6	33.3
3.0	740.0	21.7	9.3	115.1	37.2
3.0	815.0	25.0	7.9	103.4	34.5
3.0	895.0	26.7	7.4	98.6	33.3
3.0	980.0	28.3	6.9	94.3	32.3
3.0	1060.0	26.7	7.4	98.6	33.3
3.0	1135.0	25.0	7.9	103.4	34.5
3.0	1230.0	31.7	6.1	86.8	30.4
3.0	1340.0	36.7	5.2	77.8	28.2
3.0	1420.0	26.7	7.4	98.6	33.3
3.0	1480.0	20.0	10.2	122.1	38.8
3.0	1530.0	16.7	12.5	139.9	42.8
3.0	1575.0	15.0	14.1	151.2	45.2
3.0	1615.0	13.3	16.0	165.1	48.1
3.0	1650.0	11.7	18.6	182.3	51.7
Average		26.5	9.5	113.6	34.9

3.16 Angle of friction and repose

Samples from the Big Bay dune formation were delivered to an independent laboratory to evaluate the angle of shearing resistance in a shear box apparatus. . Figure 3-28 displays a correlation between a simulated angle of repose and the shearing angle of friction with a correlation co-efficient of =0.96.The same tests were done on the Atlantic Beach drift sand in Melkbos Strand. These results were compared to a simulated angle of repose for comparative purposes. The angle of friction was used to in calculating values such as the bearing capacity. The results of these tests are displayed here in Table 3-10 and the average plot is shown in Figure 3-29

Table 3-10 Shear box results (Geoscience, 2010)

Sample Nr	Angle of Friction	Dry Density, kg/m^3	Post test voids achieved
16911	37.9°	1253-1260	1.01-1.08
16910	39.9°	1252-1257	1.08-1.11
16909	41.1°	1601-1607	0.64-0.66
16908	42.2°	1599-1601	0.64-0.66
16907	44.5°	1600-1605	0.63-0.65
16906	44.4°	1601-1603	0.64-0.67
16912	41.7°	1254-1262	1.09-1.14

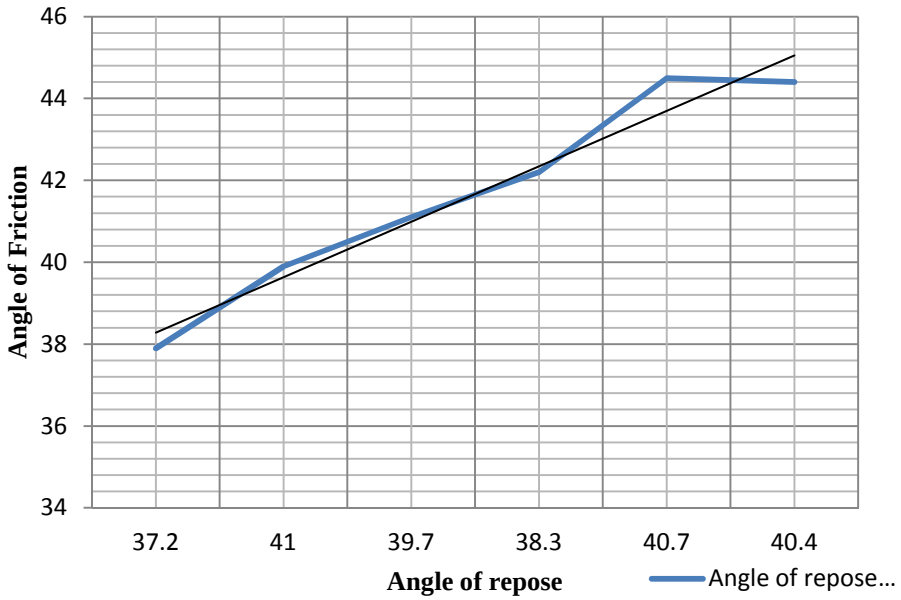

Figure 3-28 X-Y plot of angle of repose vs angle of friction

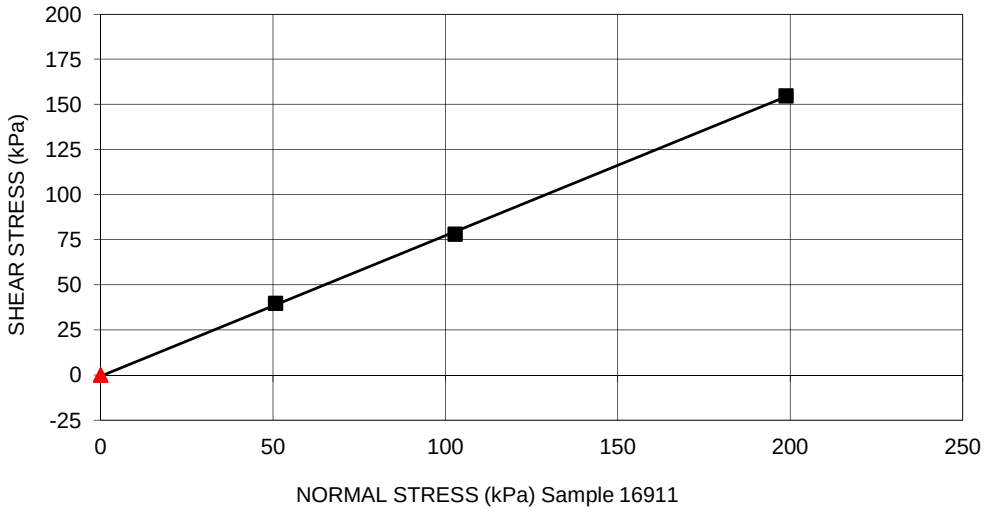

Figure 3-29 Typical direct shear data for Big Bay dune sand

The contaminated drift sand from the Atlantic Beach Golf Estate produces an angle of friction that is lower than the cleaner white sand found below. Cohesive strength is also evident as can be seen in a single test in Figure 3-30.

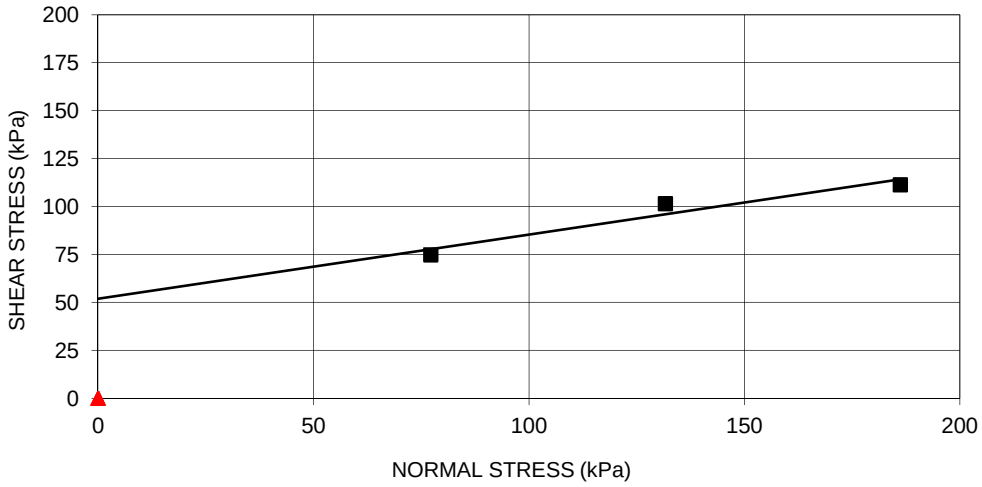

Figure 3-30 Direct shear for contaminated drift sand

The organic contamination is most likely responsible for the lower angle of friction and cohesive strength. Contamination can be as high as 21%, as can be observed in Table 3-11. The drift sand from Atlantic Beach has been transferred onto this graph. A 0.6 mm sieve was used to sift out the majority of the contamination.

Table 3-11 Contamination observation in drift sand from Atlantic Beach Golf Estate

	Contamination Estimate			
Gross sample mass	235	207	179	193
Jar	61.5	61.5	61.5	61.5
Nett sample	173.5	145.5	117.5	131.5
Sieved Sample	98	89	86.5	83
Organic debris >0.6mm	36.5	27.5	25	21.5
% Contamination	21.0%	18.9%	21.3%	16.3%
Error observation*	3%	3%	3%	3%
*sand particles on sieve				

3.9.1.1 In-Situ Voids

Research on the relationship of the maximum voids vs the % fines in the sand has produced best-fit regression lines (Cubrinovski et al, 2002) and the formula is shown here (3.9), with the expectant results displayed in Table 3-12 for two of the sand deposits in this study. The regression formula is for % soil fines between 0 and 5% and is applicable to the research sands in this study.

$$e_{max} = 0.072 + 1.53 e_{min} \quad (3.9)$$

Table 3-12 Predicted e_{max}

Sand Type	Measured in-situ	Predicted by formula (3.9)	% difference
Atlantic Beach drift sand, Melkbos Strand	0.756	0.838	9.8
Big Bay dune sand, Blaauwberg	0.804	0.9112	11.8

3.16.1 **Evaluating settlement with the DCP**

The first step in the method of assessing the predicted settlement with the DCP is calculated by converting the DCP_{DN} to the SPT_N value. For example if an average DCP_{DN} through a layer of firm sand deposit was 10 mm/blow, this would be converted to a SPT_N value of 30.5 (calculation value = 305/10). It is important to stress the fact that the SPT is performed after a successful borehole has been drilled through firm ground, thereafter driving the SPT's split spoon sampler further down at the bottom of the borehole. The amount of blows is recorded to hammer the sampler through 305 mm. The converted SPT_N value can then be used in the general settlement formula made popular by researchers such as Terzaghi & Peck (1967).

When considering the Terzaghi & Peck method (with reference to Figure 3-31) their original formula for calculating settlement is as shown here in (3.10).

$$\delta\,(footing) = \delta(plate)\left[\frac{2B}{B+0.3}\right]^2\left[1-\frac{1}{3}*\frac{D_f}{B}\right] \qquad (3.10)$$

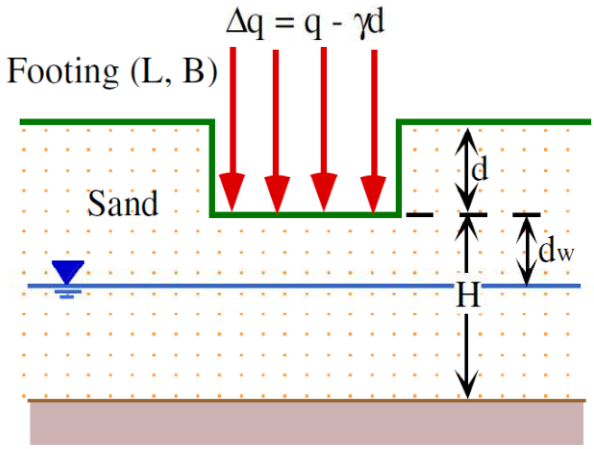

Figure 3-31 Parameters for SPT data

The value for SPT_N is obtained by averaging blow counts over the depth of influence, *Iz*. Past research correlated the vertical pressure with the settlement measured with a plate bearing test (Leonard et al, 1988). The last term in equation (3.10) is to account for the reduction in settlement according to the depth of the sand deposit. Sand deposits in the study area may be 22 meters thick (the sand deposit below the Koeberg Power plant can be as much as 35 m).

When using equation (3.10) to calculate settlement at the Atlantic Beach Golf Estate site, the following values were estimated and the results are placed in Table 3-13. Variables used in this calculation are as follows:

B = 0.8 m

L = 5 m

δ plate = settlement estimated from Figure 3-32 in mm (from GA Leonards, University Purdue)

Loading = 125 kPa

Z = from 0.8 m BGL and increments of 0.2 m

N = uncorrected SPT_N values as an average through the layers (no water table is accounted for)

D_f = 1 (a depth factor of 1 is assumed, as the actual depth is unknown)

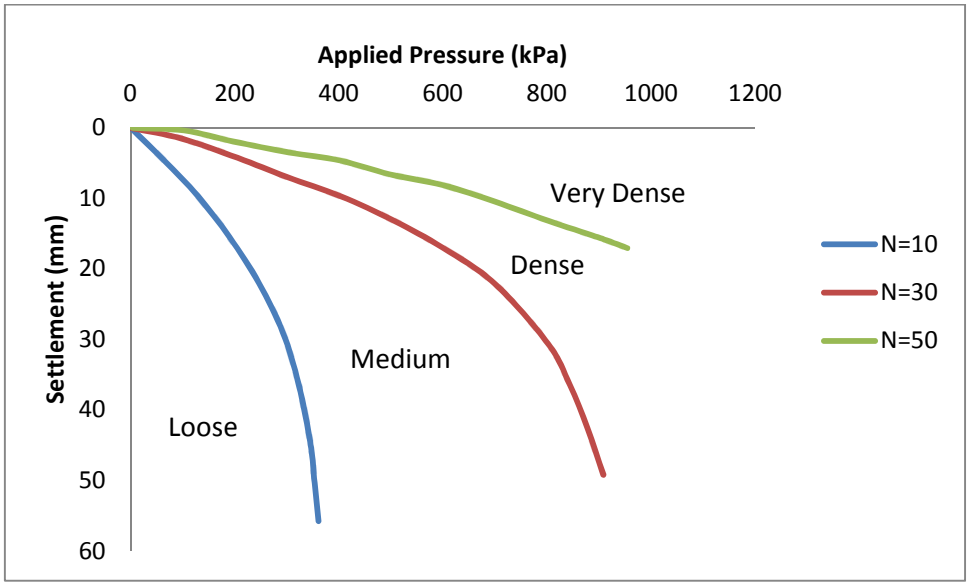

Figure 3-32 Settlements of 300 x 300 plate tests in mm (Leanards et al, 1988)

Table 3-13 Settlement predictions

Depths for settlement predictions (m, BGL)	Trial Hole AT.B1 SPT_N =6.1	Trial Hole AT.B2 SPT_N = 15.2	Trial Hole AT.B3 SPT_N = 7.6	Trial Hole AT.B4 SPT_N = 20.3
	Settlement using (3.10) (mm)			
0.8	19.4	9.7	24.3	12.1
1	15.7	7.9	19.7	9.9
1.2	12.8	6.4	16	8
1.4	10.3	5.1	12	6.5

From Table 3-13 it is clear to see that the depth at which the foundation has been placed is not suitable with the conditions as discovered on site. A more appropriate founding level would have been deeper down. Further discussion regarding appropriate action is discussed in Chapter 4 under Results.

With more than 40 different footing settlement prediction models to choose from, it becomes clear that it is important to include the factors that have the most influence. These factors would be soil stiffness (Young's modulus, E), applied pressure, footing width, depth of influence and footing shape. Terzaghi and Peck (1967) include all of the aforementioned in their prediction model and the outcome for this study bears testimony to acceptable accuracy.

3.17 Error Analysis

Error analysis on laboratory measurement is provided here. No certification of compliance was available on any of the equipment used such as scales or sieves. Inspection was carried out by visual assessment for suitability. Standard weights were used to calibrate the electronic scales. Table 3-14 to Table 3-16 provides an error analysis for readings performed by hand.

Table 3-14 Shelby tube error measurement

Tube Nr	Measurement diameter, mm	Typical specification, mm	Typical range of error	% error	Remarks
1	37.2	Supplied specification = 38	0.8	2.1%	Callipers used, accuracy 0.02 mm/div
2	37.4		0.6	1.6%	
3	38		0	0.0%	
4	38.2		0.2	0.5%	
5	38.5		0.5	1.3%	
6	38.5		0.5	1.3%	

Table 3-15 Inclinometer error measurement

Test Nr	Measurement Slope angle, degrees	Typical specification	Typical range of error	% error	Remarks
1	29	Field reading to nearest 1 degree	0.4	1.37%	Inclinometer 1 div = 0.2 degree
2	27		0.4	1.48%	
3	31		0.4	1.29%	
4	25		0.4	1.6%	
5	28		0.4	1.43%	
6	31		0.4	1.29%	

Table 3-16 Direct shear strain gauge error measurement

Test Nr	Measurement Strain gauge, divisions	Typical specification,	Typical range of error	% error	Remarks
1	11	Reading to nearest 1 division	1.5	13.6%	Strain gauge 1 div = 0.71 Newton Speed 0.5 mm/min. Dial gauge moves quicker at early stage
2	22		1.5	6.8%	
3	35		1	2.9%	
4	83		1	1.2%	
5	125		0.5	0.4%	
6	138		0.5	0.4%	

3.17.1 **DMT diaphragm response**

The reliability of accurate A and B readings are heavily dependent upon regular calibration checks, especially in softer soil types (Marchetti, 1999). The incorrect calibration data of the membranes will result in inaccurate final readings for the adjusted P_0 and P_1. Two types of membrane diagrams are supplied with the DMT device, a hard and a soft version. The choice is dependent upon any fore knowledge of the soil type earmarked for testing. The soft version was used for the Aeolian sand as the hard counterpart did not respond to the low K_D values in the chamber.

Maintenance is important to maintain low error readings between the sensing disc and the insulating seat. Regular measurements of this gap were taken during a period of 10 weeks of testing using the tripod gauge developed for this purpose. The tolerances were set up prior to testing and re-checked 5 days later. The legs of the calibration tripod rest on the surrounding steel plate and the micro dial gauge is used to measure any changes in elevation above this plane. Marchetti (2001) recommends the following tolerances:

- Sensing disc - Nominal elevation above the surrounding steel plates: 0.05 mm. Tolerance range: 0.04 to 0.07 mm.
- Feeler - Nominal elevation above the nylon sensing disc: 0.05 mm. Tolerance range: 0.04 to 0.07 mm. (The results are recorded below in Table 3-17).

Pressures recorded less than 5 bar during test work in the chamber. The manufacturer specifications for the Senso-gauge are provided in the Appendices Schedule, Table B3. According to the manufacturer pressure readings may differ from the actual by 0.5%. Marchetti's comments regarding the correction of membrane pressures are stated in Chapter 2 under "Calibration of DMT Diaphragm".

Table 3-17 Error Analysis of Sensor disc

Dilatometer	Sensing Disc	Feeler Gauge
Initial setup (mm)	0.05	0.05
Cycle week 1	0.055	0.06
Cycle week 2	0.053	0.076
Cycle week 3	0.056	0.072
Cycle week 4	0.054	0.07
Cycle week 5	0.055	0.06
Cycle week 6	0.056	0.066
Cycle week 7	0.056	0.067
Cycle week 8	0.057	0.065
Cycle week 9	0.058	0.067
Cycle week 10	0.058	0.065
Arithmetic mean	0.0558	0.067
Standard Deviation	0.0016	0.005
Maximum	0.058	0.076
Minimum	0.053	0.06
Maximum % Error	0.3%	0.8%

3.17.2 Sample disturbance

-

The degree of disturbance of the sample collected by the Shelby type tube can be expressed by the term called the A*rea Ratio, Ar, and* is expressed as a percentage (Das, 2010); its formulation is displayed here below as:

$$Ar(\%) = \frac{D^2{}_o - D^2{}_i}{D^2{}_i} * 100 \qquad (3.11)$$

For a standard split-spoon sampler, D_i = 35.05 mm and D_0 = 50.8 mm.

Therefore,

Ar (%) = $\frac{50.8^2 - 35.05^2}{35.05^2}$*100 = 110%

For a Shelby type tube sampler, D_i = 36.5 mm and D_0 = *38* mm. Therefore,

Ar (%) = $\frac{38^2 - 36.5^2}{36.5^2}$*100 = 8.38%

The sampling done with a split spoon type is highly disturbed while fewer disturbances for a Shelby type tube can be expected. Six similar Shelby type tubes were used on site for in-situ sampling and the results are displayed here in Table 3-18. For practical purposes the result can be accepted for being representative of an undisturbed sample. Some sand loss was discovered and had dislodged from the tube ends and had to be lightly recompacted into position. The amount of sand replaced was about 25 grams.

Table 3-18 % Area Ratio for Shelby tubes

Shelby Tubes Nrs	Outside Diameter	Inside Diameter
Tube sampler 1	39.7	38.4
Tube sampler 2	40	37.8
Tube sampler 3	40.2	37.6
Tube sampler 4	40.1	37.7
Tube sampler 5	40.1	37.8
Tube sampler 6	40.2	37.8
Averages	40.05	37.85
Std. Dev	0.187	0.281
Variance	0.035	0.079
% Area Ratio	12%	

Chapter 4 Results and discussion

In this chapter the results of the geotechnical properties of the windblown sand is presented. Gradations, percentage relative density, void ratios and DMT readings in the chamber will be presented and discussed. The DMT method of determining the horizontal stress, K_D will be related to the Cyclic Stress Ratio and how the possibility of liquefaction can be determined from the presently established graphs set up by Reyna and Chamaue (1991). The in-situ field investigations are also discussed and appropriate action or remedial work will be suggested.

4.1 Field investigations

Recent inspection of trial holes in the area of West Beach, Blouberg and the Atlantic Beach Estate has revealed low bearing capacity within the upper drift zone. Values as low as 45 kPa (inside the Atlantic Beach Estate) are not uncommon (own research) and have been determined with the DCP. Low bearing capacity can be expected in the drift zone because of the varying densities associated with the contamination therein, including spongy organic matter. On closer inspection it becomes clear that much of the contamination is charcoaled debris, most likely blown about by the prevailing winds after seasonal fires that occur regularly in the summer months, the fires being fed by the surrounding fynbos and Port Jackson brush.

4.1.1 **Sand gradation analysis for chamber sand**

The bulk sample for the West Coast sand was extracted from an excavation of between 4 to 6 m in depth and 55 m from the coastline below ground level on a construction site in the Blaauwberg area outside Cape Town. The GPS co-ordinates are S 33.810369, E 18.469418 (Figure 4-1). The Philippi sand sample was obtained from a site adjacent to land designated for low coast housing. The GPS co-ordinate is approximate (S-34.052339, E 18.536682) and could not be accurately recorded for this site .The area is also quarried for sand used in concrete works for the housing construction industry.

The moisture content was fairly low when placed inside the calibration chamber. Both sand types have low fines content (0.075 mm <10%). The D_{50} size fraction size for the Philippi and West Coast sand is 0.15 mm and 0.22 mm respectively. Figure 4-3 and Figure 4-4 displays the plotted average particle size distribution for the two chamber test sand samples. 6 samples were used for each sand type in this determination.

Figure 4-1 West Coast sand site (S 33.810369, E 18.469418)

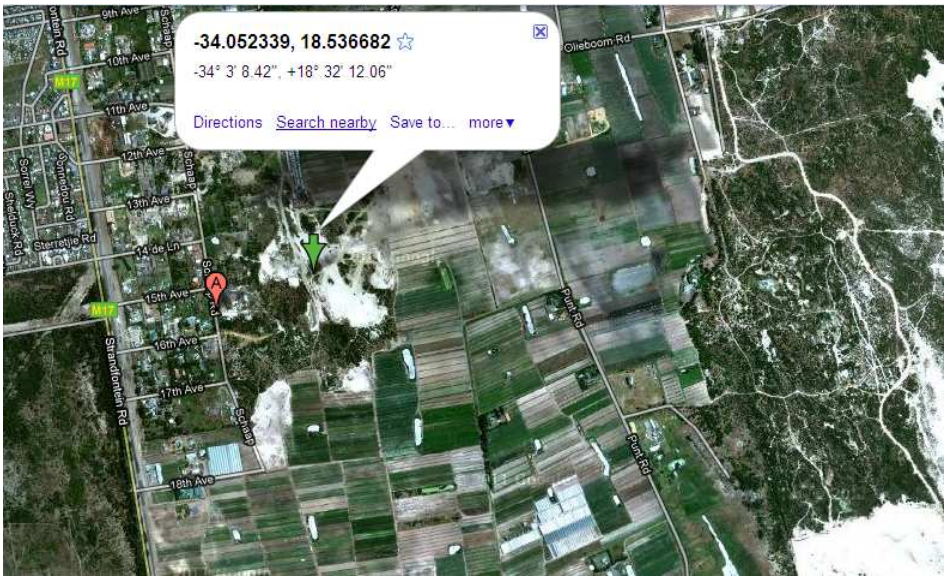

Figure 4-2 Dune area near Philippi (S-34.052339, E 18.536682)

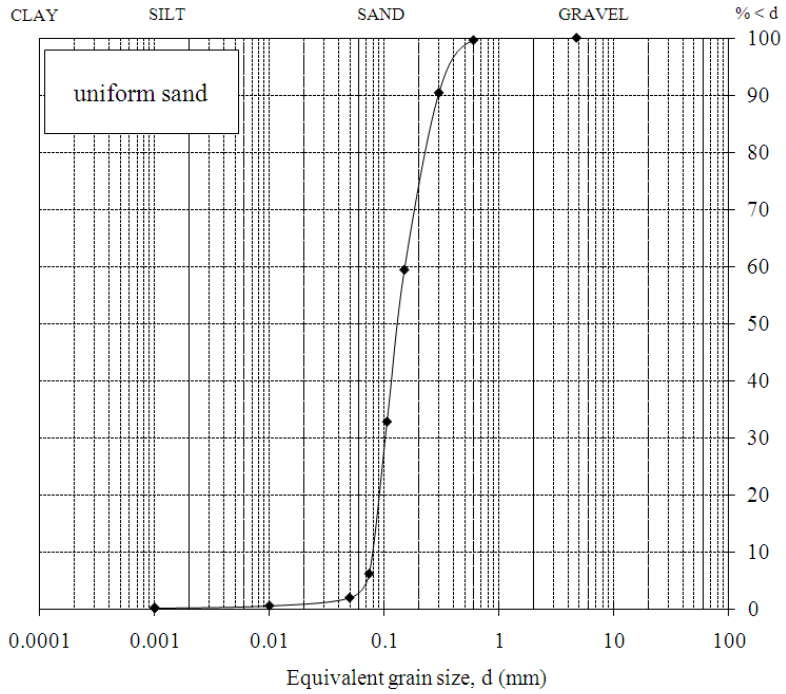

Figure 4-3 Particle size distribution for Philippi dune sand

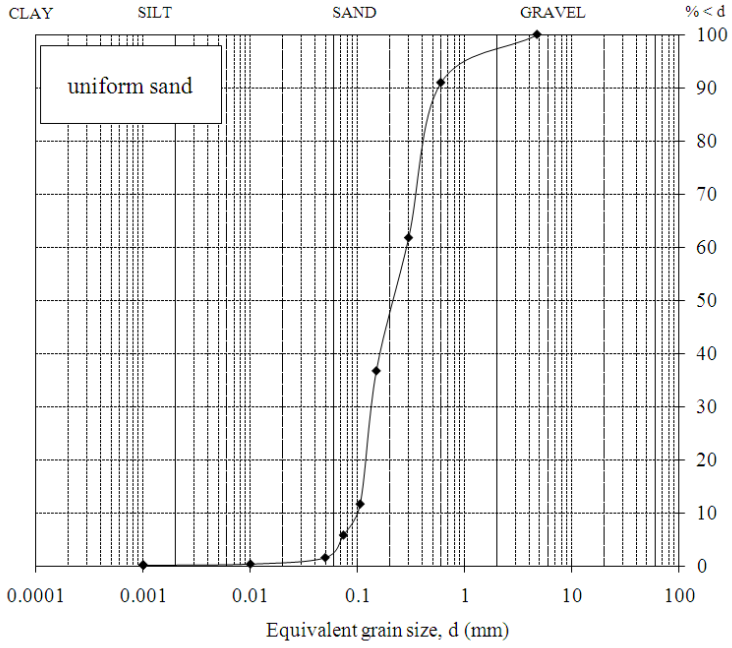

Figure 4-4 Particle size distribution for West Coast dune sand

4.1.2 Sand gradation analysis for study area in Melkbos Strand

The average grading analysis for 6 samples of the dune sand at Big Bay is displayed in Figure 4-5. Very little variation was observed in the grading characteristics (C_u and C_c). Figure 4-6 displays the plotted average of 4 samples for the upper drift sand in the study area in inside the Atlantic Beach Golf Estate. The sand has a low fines content, being <5 % by mass.

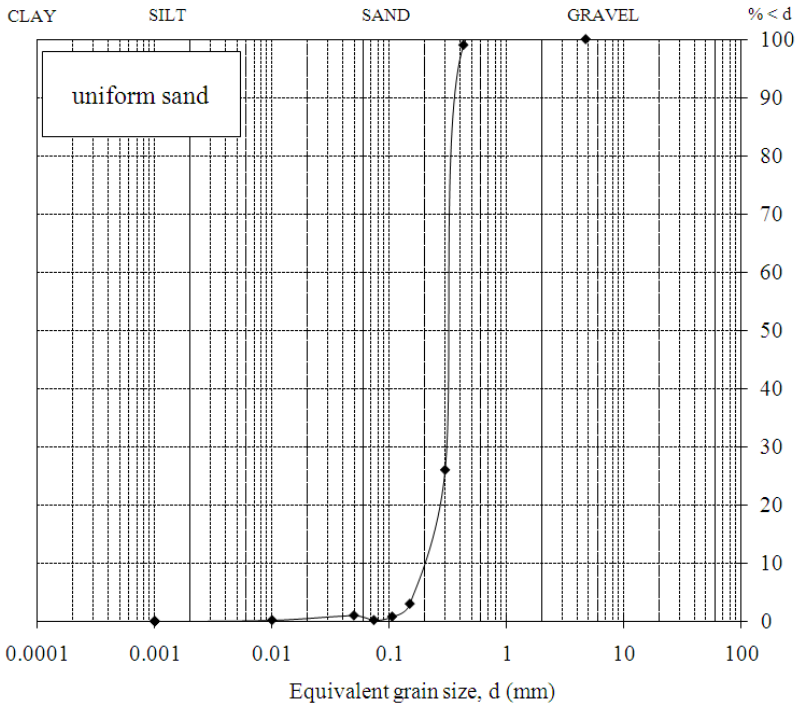

Figure 4-5 Particle size distribution for Blaauwberg Dune sand at Big Bay (Sample 16911)

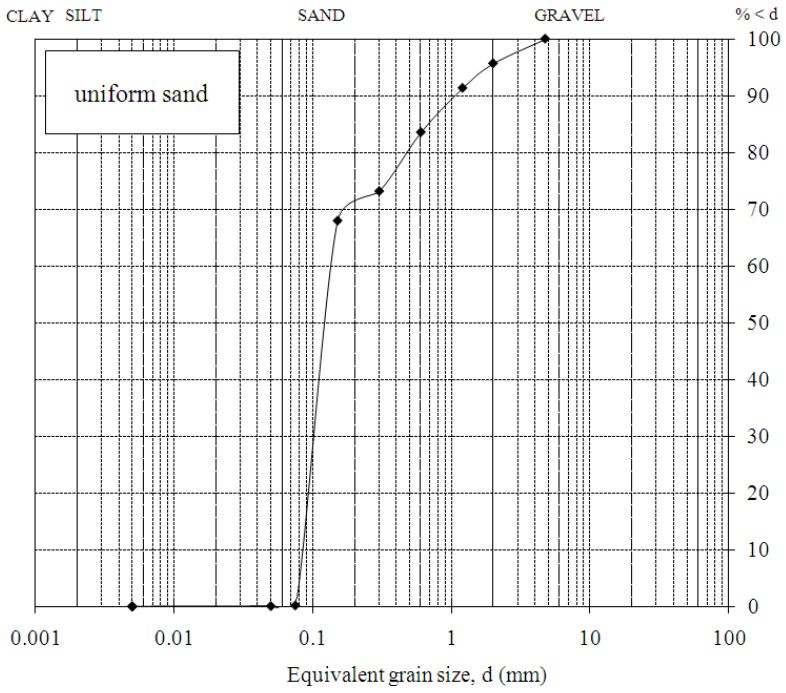

Figure 4-6 Particle size distribution for contaminated drift sand

Table 4-1 displays the grading characteristics for the chamber sand samples as well as the dune sand from the study area outside Melkbos Strand.

Table 4-1 Grading characteristics of chamber sand

Criteria	Philippi sand	West Coast sand	Big Bay dune sand	Atlantic Beach drift sand
Uniformity Coefficient (C_u)	1.95	2.98	1.52	1.67
Coefficient of Curvature (C_c)	1.25	0.67	1.04	0.67
USCS Classification (Uniform sand)	SW	SP	SW	SP
AASHTO Classification	A-3 (non plastic fine sand)			

4.1.3 **Liquefaction of sand based on particle size distribution**

The particle size distribution of the study sands were plotted against the suggested boundaries as proposed by Sitharam (2004) and shown below in Figure 4-7. The final results and conclusions are discussed in Chapter 5.

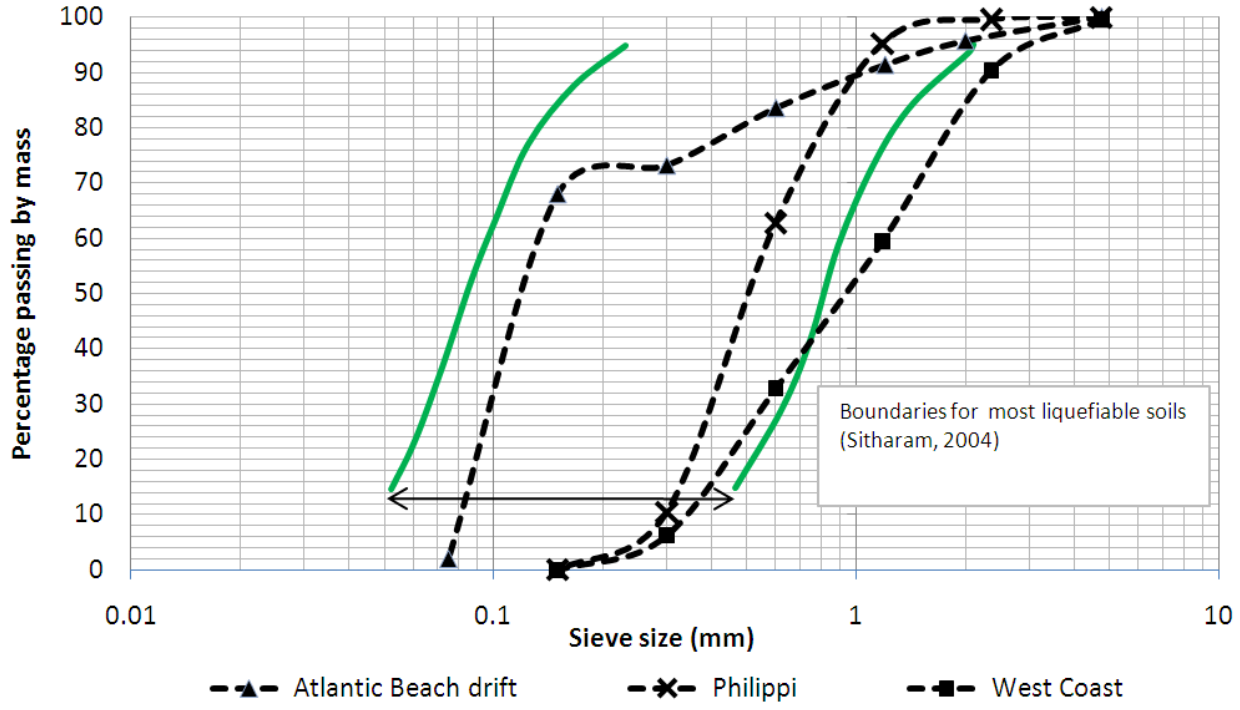

Figure 4-7 Boundaries for liquefiable sands

4.2 Sand density in the test chamber

Samples were extracted with a Shelby tube for the determination of the bulk density of the chamber test sands. After a 24 hour rest period the samples were withdrawn in the middle section. The results are displayed from Table 4-2 to Table 4-5.

Table 4-2 Chamber sand density

Density of dry Philippi sand		Density of moist Philippi sand	
Mould	2969 g	Mould	242 g
Mould & Material	6867 g	Mould & Material	685 g
Volume	2626 ml	Volume	273 ml
Density	1484 kg/m^3	Density	1620 kg/m^3
Density of dry West Coast sand		Density of moist West Coast sand	
Mould	2971 g	Mould	233 g
Mould & Material	6805 g	Mould & Material	697 g
Volume	2626 ml	Volume	273 ml
Density	1460 kg/m^3	Density	1698 kg/m^3

Table 4-3 Philippi sand dry moisture analysis

Dry loose West Coast sand Moisture content of West Coast sand	
Mass of container	431 g
Container and wet sand	1899 g
Container and dry sand	1875 g
Dry sand	1444 g
Wet sand	1468 g
Moisture content	1.63 %

Table 4-4 Philippi sand moisture analysis

Densified moist Philippi sand after vibration Moisture content of Philippi sand	
Cylinder and dry sand	482 g
Cylinder	242 g
Dry sand	240 g
Pan and dry sand	611 g
Pan	424.5g
Dry sand	186.50 g
Total dry sand	426.50 g
Total wet sand	443. g
Moisture content	3.72 %

Table 4-5 Moisture content after vibration

Densified West Coast sand after vibration Moisture content of West Coast sand	
Mass of container	423 g
Container and wet sand	1461 g
Container and dry sand	1414 g
Dry sand	991 g
Wet sand	1038 g
Moisture content	4.53 %

4.2.1 **DMT parameters for chamber sand**

The West Coast and Philippi dune sand is classified as uniform sand. The West Coast sand is coarser with more angular particles. The percentage passing the 0.425 mm sieve is about 65%. From its fraction size alone it would appear that this sand will be more resistant to settlement as the smaller particles will fill the voids quickly during any tremor of significance, filling voids and densifying the layer, giving a dense mass of interlocking particles with high shear strength and low compressibility. The natural moisture content of the sand was determined before any tests were conducted in the chamber and a moisture content of 1.63% was recorded. Due to the interlocking nature of its particles, the sand densifies easily and with enough moisture present, should resist higher vertical stress (the horizontal stress index, K_D, measured with the DMT yielded values of ≥ 1.

Philippi sand is finer when compared to the West Coast sand, being more singular in shape and size. Foundations in areas containing this sand type (and with a high water table) will need special attention to safeguard against possible structural cracking if excessive vibration leads to settlement. The DMT test classifies the material index, I_D, as clean sand (Table 4-6) and the horizontal stress index, K_D, can be read off this table. The moisture content of the sand was determined before any tests were conducted in the chamber and a moisture content of 0.95% was recorded under air dry conditions.

Table 4-6 records typical DMT results for the Philippi sand tested in the chamber. The I_D values range from 13.43 to 17.33, placing the soil type within the “Clean Sand” range. This value compares well with the standard grading classification and USCS method for soil type analysis. K_D values are low and range from 0.9 to 1.1 and signify that the sand does not tolerate high horizontal stress at the densities that were achieved in the chamber (%D_R = 62%).

Table 4-6 Typical DMT data for Philippi sand (CPUT, 2008)

Water Level below end of sounding
Reduction formulae according to Marchetti, ASCE Geot.Jnl.Mar. 1980, Vol.109, 299-321; Phi according to TC16 ISSMGE, 2001

Z (m)	A (kPa)	B (kPa)	C (kPa)	Po (kPa)	P1 (kPa)	P2 (kPa)	Gamma (kN/m^3)	Sigma' (kPa)	Uo (kPa)	Id	Kd	Ed (MPa)	Ud	Ko	Ocr	Phi (Deg)	M (MPa)	Cu (kPa)	Philippi Dry DESCRIPTION
0.28	20	260		15	220		16.7	14	0	13.43	1.1	7.1				29	6.0		SAND
0.34	15	290		12	250		16.7	15	0	19.83	0.8	8.3				27	7.0		SAND
0.41	15	270		12	230		16.7	16	0	18.17	0.7	7.6				26	6.4		SAND
0.58	20	270		15	230		16.7	19	0	14.33	0.8	7.5				26	6.3		SAND
0.62	20	300		15	260		16.7	20	0	16.33	0.8	8.5				26	7.2		SAND
0.65	25	350		18	310		16.7	20	0	16.22	0.9	10.1				27	8.6		SAND
0.69	25	350		18	310		16.7	21	0	16.22	0.9	10.1				27	8.6		SAND
0.71	25	370		18	330		16.7	21	0	17.33	0.9	10.8				27	9.2		SAND

As far as the DMT's ability to predict the soil type it can be stated that the I_D value is correct and can be assumed to be trustworthy. The E_D value (in-situ modulus, in MPa) is low. This indicates the sands stiffness, which is an important factor used to calculate settlement.

4.2.2 **The effect of vibration on dune sand**

The effects of vibration are significant. The rotary vibratory equipment fitted to the sides of the chamber is capable of producing frequencies in excess of 8000 Hz. It would seem that, in reference to the data recorded for the dune sand, only 250 Hz is required to densify the sand to an acceptable level for shallow foundations. The SPT_N values improve by about 45% which must assist the bearing capacity of the sand and improve the E-modulus, so thereby improving the soil stiffness.

Figure 4-8 displays the readings and results of the vibration test on the dry Philippi sand on the first depth increment of 220 mm. These vibration tests were done with each DMT test on both sand types. These readings were obtained with an accelerometer and a sound level meter. The accelerometer measures vibration acceleration (related to force). The sensitivity is in mV per m/s^2.

The probe on which the accelerometer was fixed was forced into the sand to the same incremental depths as the DMT blade, to obtain a vibration reading at the same level in the sand. The peak in the graph (Figure 4-8), as seen between frequency ranges 31.5 to 250 Hz, is the optimum range to compact the sand to achieve its lowest void ratios. The actual recorded data from the accelerometer used during the vibration of the Philippi sand can be viewed in the Appendices Schedule Table A.2. The vibration range responsible for the most vibro-compaction is similar to the light trench compactors found on site today.

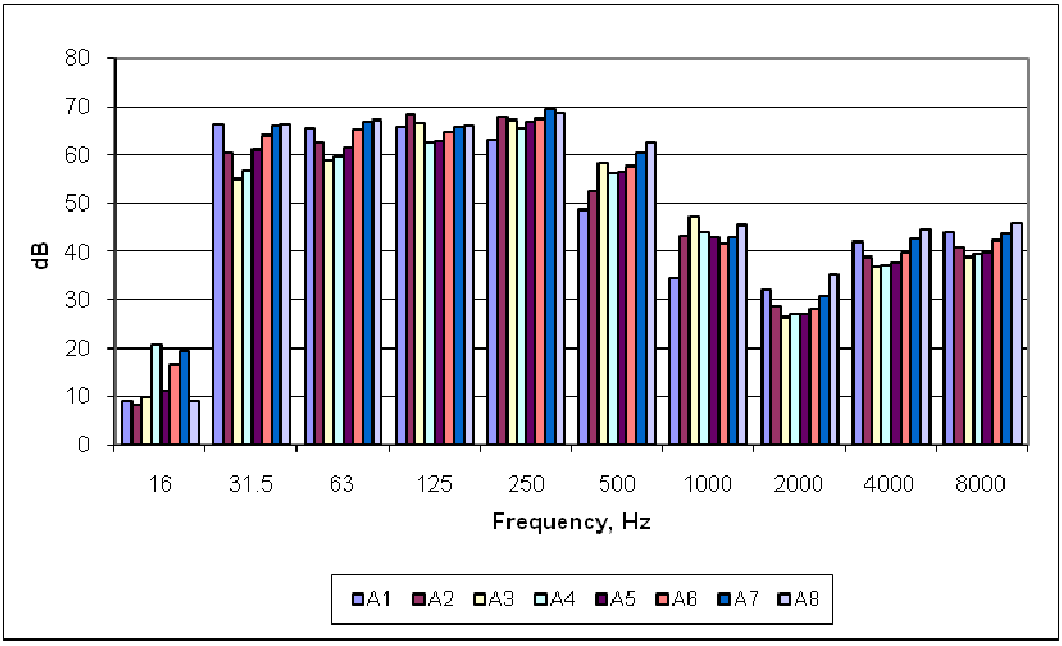

Figure 4-8 Vibration frequencies in Philippi sand

4.2.3 **Densification of the chamber sand samples**

The test series designated A1 to A8 in Figure 4-8 are indicative of the range of frequencies measured in the calibration chamber during vibration of the Philippi sand. The accelerometer only measured vibration in the vertical axis, thus no information regarding vibration in any other plane is displayed. Figure 4-8 also displays the vibration energy (dB) in one octave (1/1 Oct) frequency bands for each of the different depths of the rod. There seems to be a trend visible in the 31.5 Hz and 125 Hz octave bands in that in most test cases the two sand types show higher densification.

The sand was vibrated in a fairly dry state (moisture contents less than 1.5%, by mass) and thereafter fully saturated. The water pump was switched on and the pipe distribution system forces the water through the stone media and upward through the sand sample. Once the water appears above the surface by (roughly 50 mm), the pump is switched off. Immediately thereafter the vibratory motors are switched on for 30 seconds. The outlet drainage pipes are opened after about 8 minutes to allow excess water to drain back into the holding tank. The chamber is then placed at rest for 24 hours before test work begins. Table 4-7 reflects the DMT results that were obtained after hand compaction. The sand yields the expected higher K_D values when vibrated.

Table 4-7 DMT readings after hand-compaction

Calibration	Test Hole 1		Test Hole 2		Test Hole 3	
ΔA	0.3 Bar		0.3 Bar		0.3 Bar	
ΔB	0.5 Bar		0.55 Bar		0.6 Bar	
Depth, mm	*A* (Bar)	*B* (Bar)	*A* (Bar)	*B* (Bar)	*A* (Bar)	*B* (Bar)
200	1.5	4.9	0.5	2.55	1.0	3.65
300	1.15	4.4	0.675	3.08	0.975	3.825
400	0.8	3.9	0.85	3.6	0.95	4
500	1.23	4.0	0.825	3.6	0.875	3.525
600	1.65	4.1	0.8	3.6	0.8	3.05

4.3 Bearing capacity in the chamber

4.3.1 **Bearing capacity design with the DMT**

Assessing the bearing capacity with the DMT is accomplished with the application of the corrected A and B readings, known as P_0 and P_1. In this case, P_0 represents the DMT lift-off pressure and P_1 represents the DMT's 1.1 mm expansion pressure. These values are recorded directly off the DMT control console in bar. Since the DMT blade is of fixed dimensions, the use of P_0 and P_1 represent pressure values that are repeatable from any DMT equipment and are not subject to arbitrary graphical interpretation. *ND* is analogous with the DMT's own "bearing capacity factor", not dissimilar to the CPT's "K"-factor for the depth to footing width factor (D/B). For square footings D/B is accepted to be in the range of 0 to 1, the factor "K" varies from about 0.22 to 0.30, depending on the sand density. The application formula for the ultimate bearing capacity with the DMT is given in (2.11).

Table 4-8 compares the bearing capacity of the same sand type (Philippi) using hand compaction as opposed to loose pluviation. The blows were administered with an 8 kg circular (150 mm Ø) dead weight on a 1.5 m steel pole. Lifts were 200 mm and blows amounted to 25 blows per layer.

The bearing capacity results observed in the chamber after vibration are listed in Table 4-9. The DMT bearing capacity factor of 0.7 was used, as suggested by Lutenegger et al, (2006). The bearing capacity is the ultimate value and a safety factor of 2.5 is suggested. This reduces the working bearing capacity average through the depth of the chamber to 72.9 kPa. For light construction (single story dwellings using standard masonry and light roofs), this bearing capacity may seem adequate if line loads are expected to reach 50 kPa. With added contamination on site, it has been seen how unit weight is reduced, thereby reducing the DMT bearing capacity as well.

Table 4-8 DMT Bearing Capacity (loose-medium)

Depth in Chamber, mm	Hand Compaction	Loose pluviation
Philippi sand		
200	146.4	45.3
300	172.6	52.2
400	198.2	63.2
500	201.4	70.7
600	204.6	81.4

Table 4-9 DMT Bearing Capacity (after vibration)

Depth in Chamber, mm	Bearing Capacity, Kpa
Philippi sand	
280	147.5
340	173.6
405	159.8
585	158.9
615	181.7
650	185.7
685	215.6
710	230.6

Increased bearing capacities were observed on wet vibrated sand as opposed to dry un-vibrated sand. Higher horizontal stresses were recorded in the moist vibrated sand. The K_D value is used from the

Marchetti formula to determine the friction angle (see Appendix Schedule Table A.1) and which can be used to calculate the bearing capacity of the sand. The friction angle for the DMT is shown here in (4.1).

$$\varphi_{safe(DMT)} = 28° + 14.6° log K_D - 2.1° log K_D \quad (4.1)$$

The friction angle was used to obtain the bearing constants N_q and N_γ, sourced from a well documented soil mechanics reference table (Terzaghi and Peck, 1967). Vibration in the chamber increased the horizontal stress in the sand, therefore resulting in an increase in the bearing capacity of the sand. The angle of shearing resistance, $\varphi_{safe(DMT)}$ for Philippi dune sand was in order of 27.4° to 29.6°, which is surprisingly low for fine sand.

Angle of friction tests in a standard shear box showed values of above 38°. This is probably due to the higher sustained vertical stress which is not the case on site. The K_D values are low (<1.1) leading to lower frictional angles. An increase in bearing capacity of 20% was observed between the dry unvibrated Philippi sand.

4.3.2 **Bearing capacity using Eurocode 7**

The angle of friction used here was determined from the DMT. The Eurocode 7 Limit state method for strip foundations is shown below in Table 4-10. This method is explained in detail by Smith (2006) with functional Excel spreadsheets available from the publisher's website [http://sbe.napier.ac.uk/esm]. In this method the foundation size is required, including vertical stress, unit weight of concrete and soil. The software spreadsheet determines it's bearing capacity factors accordingly. Angle of friction was selected as per the DMT method and 28° was selected. Input parameters selected were: γ_{conc} =24 kN/m^3; γ_{soil} =14.56 kN/m^3; Vertical load = 50 kPa (standard loading test stress); B =0.8 m; Depth to BBF, *Z* =0.8 m; Thickness of concrete = 0.23 m

Table 4-10 GEO Limit State Method on strip shallow foundation (Eurocode 7, 1997)

Bearing Capacity results:	Term	Value	Unit
Ultimate bearing capacity	Q_u	256.4	kPa
Ultimate bearing capacity/m run	Q_u	205.1	kN/m

4.3.3 **Bearing capacity using the Terzaghi classical formula**

The standard formula proposed by Terzaghi (1967) is the general bearing capacity equation for a strip footing and is shown here (4.2) below.

$$q_u = CN_c + 0.5\gamma BN_\gamma + qN_q \quad (4.2)$$

Using the above formula the bearing capacity was calculated for the finer Philippi sand with the standard bearing capacity factors linked to the angle of friction determined by the DMT. The φ -angle used was determined with the DMT as it penetrated the bottom zone of the chamber. The results are recorded in Table 4-11.

Table 4-11 Bearing Capacity using Terzaghi method

Sand Type	Q_u, Kpa	Bearing capacity factors			φ phi angle
	DMT	N_c	N_γ	N_q	
$Q_{u\text{-Philippi}}$	444.2	0	30.22	23.18	32
$Q_{u\text{-West coast}}$	664.9	0	48.03	33.3	35

4.3.4 **Bearing capacity using the Dynamic Cone Penetrometer**

The method used here was based on Kessler and the Paige-Green formula for bearing capacity using the light probe (8.5 kg hammer). The formula (2.7) is not suited for soils classified according to the USCS method as either CL or CH (clayey soils). To calculate the bearing capacity the % in-situ CBR value is required for the Kessler method. The CBR value is conveniently determined using the DCP_{DN}. Three DCP tests were done in the chamber (pre and post- vibration) for which an average bearing capacity was

calculated. The Paige-Green formula does not require the CBR value. The results are displayed in Table 4-12.

Table 4-12 Bearing Capacity based on DCP_{DN}

Chamber Depth	Test Hole 1		Test Hole 2		Test Hole 3	
	% CBR	Q_u (kPa)	% CBR	Q_u (kPa)	% CBR	Q_u (kPa)
	Loose density (pre-vibration)					
Kessler (2009)	4.2	74.8	4.8	82.0	4.2	75.9
Paige- Green (2009)	-	74.6	-	85.0	-	75.6
	Medium density (post-vibration)					
Paige- Green (2009)	-	158.2	-	219.3	-	148.3

A brief summary of the bearing capacity results is displayed in Figure 4-9. The average bearing capacity has been calculated for each individual device through the depth of the chamber.

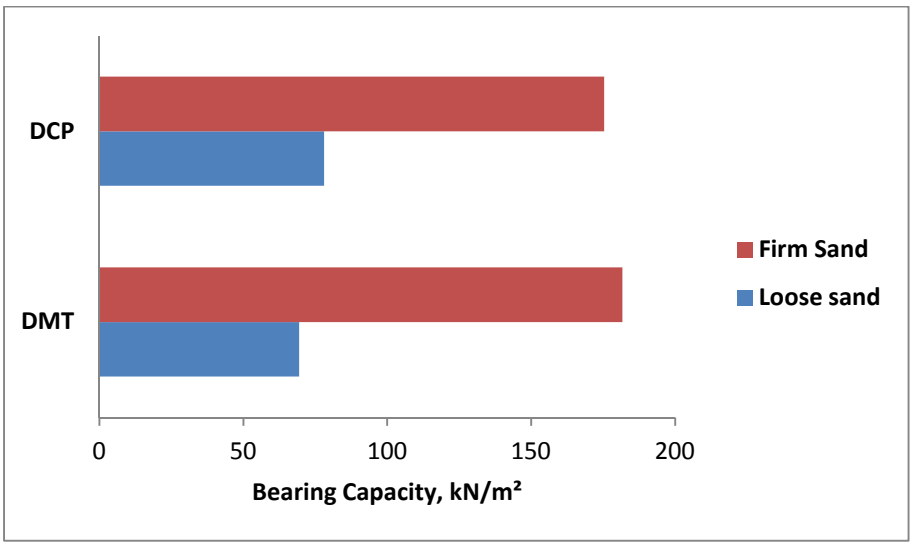

Figure 4-9 In-situ correlation of bearing capacity

4.3.5 **Laboratory results on sand from study area**

Independent shear box tests were conducted by Geoscience Laboratories (Pty) Ltd and the average results for direct shear are displayed here in Figure 4-10 to Figure 4-13. The results are typical for clean windblown sand with an internal angle of friction of about 39°. In-situ moisture contents in the drift sand of the study area varied from 3.25 – 11.94 %. The higher moisture contents were from the upper drift zone where higher concentrations of organic matter were found. The lower moisture content was found below the level of 2 meters. It is assumed that the higher moisture content can be attributed to the concentrations of organic debris that is present in the drift zone

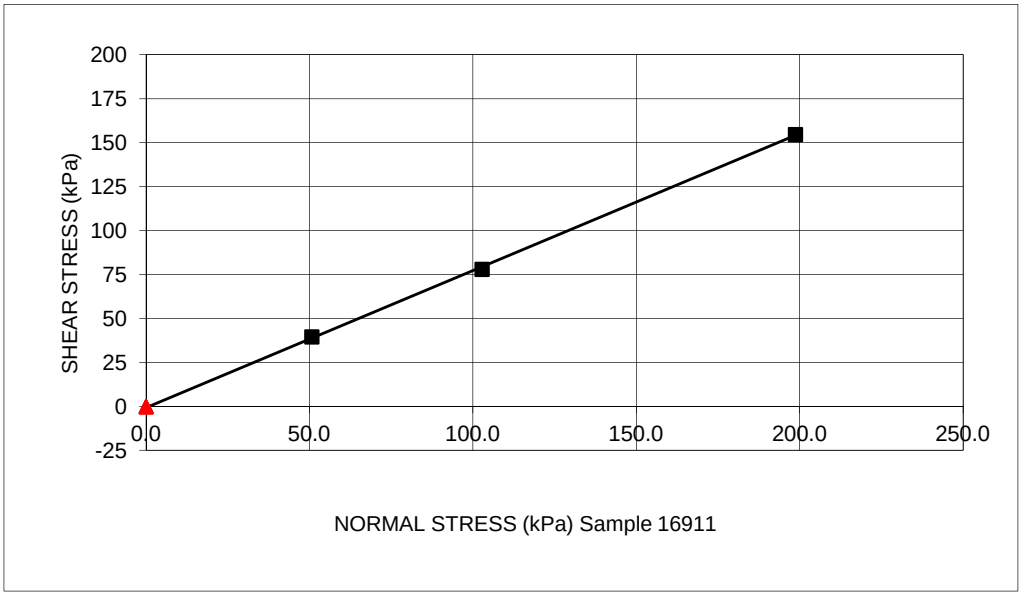

Figure 4-10 Direct shear data for Big Bay dune sand

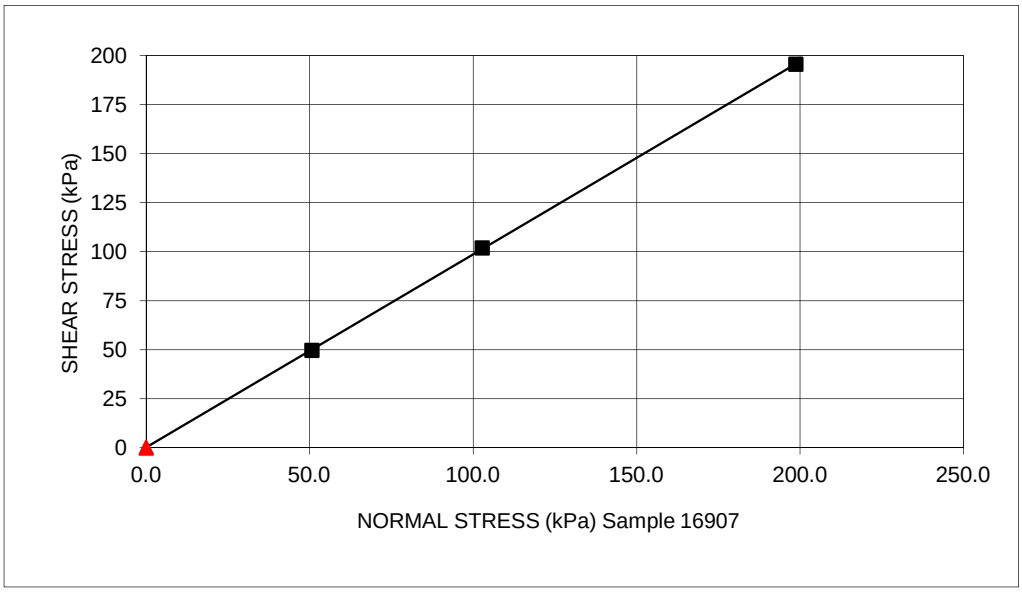

Figure 4-11 Direct shear data for Big Bay dune sand

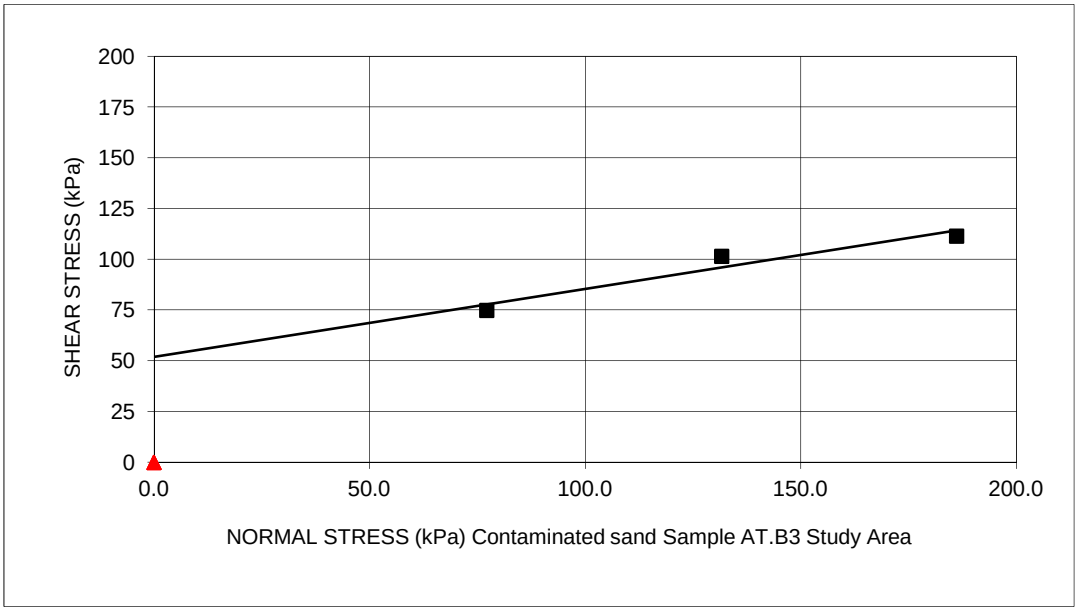

Figure 4-12 Direct shear data for contaminated dune sand in the drift zone

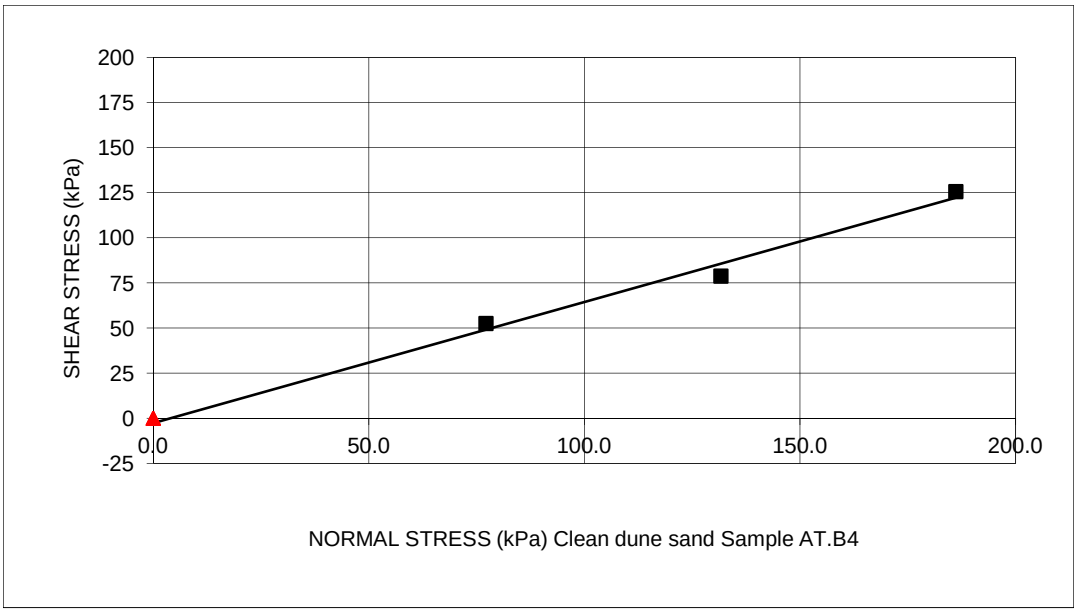

Figure 4-13 Direct shear data for clean dune sand below the drift zone

The results for the dune sand formation at Big bay are all consistent with little variance. Of interest is the contaminated drift sand from the Atlantic Beach Golf Estate that yielded significant cohesion of 50 kPa (Figure 4-12). It is assumed that the high concentration of organic debris in the sand will negatively affect the shear strength parameters.

4.3.6 **Inclinometer results for dune formation**

A series of tests have been conducted to correlate observations in the field with experiments in the laboratory. These experiments have been done for correlation purposes. Discussed here are the results for the angle of repose as measured with the inclinometer on a few dunes in the Blouberg area and how this is correlated to a simulated angle of repose using dry sand and a sand replacement funnel. This experiment is correlated to the angle of friction as determined with the traditional method of shear box testing as well as the DCP. The inclinometer results are recorded in Table 4-13.

Table 4-13 Inclinometer readings

	Dune 1 North Facing	Dune 2 East Facing
Position	S 33.47.06.4; E 18.27.06.6	S 33.47.06.3; E 18.27.08.0
Inclinometer angles	29°,27°,31°, 33°	25°, 28°, 31°

4.3.7 **Correlation for angle of repose**

Only the Big Bay dune site outside Blaauwberg was chosen for correlations to be done. A correlation was attempted to see whether the field inclinometer observations and laboratory readings were compatible with each other. Average readings for the inclinometer angle in a small area of dune formation at the Big Bay site was 29.1°as compared to the simulated angle of repose in the laboratory which yielded and angle of 39.5°. The simulated angle of repose for the three sand samples show little variance and is displayed Table 4-14. Table 4-15 displays a correlation between the angles of repose and internal friction for dune sand from Big Bay near Blaauwberg Strand. It is clear to see that the field observations were substantially lower than those observed during the simulated angle of repose.

Table 4-14 Laboratory trial tests for angle of repose

Test nr	Big Bay dune sand	Atlantic Beach contaminated drift sand	Atlantic Beach clean white dune sand
GPS Position	S 33.47.06.3 E 18.27.08.0	S 33.74.42.63 E18.45.10.98	S 33.74.41.58 E18.45.09.45
Test 1	37.2	34.9	39.2
Test 2	41.0	40.4	38.9
Test 3	39.7	39.1	40.1
Test 4	38.3	38.3	38.7
Test 5	40.7	42.0	38.5
Test 6	40.4	42.1	39.7
Average	39.5°	39.5°	39.2°
Standard deviation	1.5	2.704	0.614

Table 4-15 Angle of repose and shear resistance correlations for dune sand in study area

	Angle of repose	Shear box Friction angle
	37.2	37.9
	41.0	39.9
	39.7	41.1
	38.3	42.2
	40.7	44.5
	40.4	44.4
Standard Deviation	1.5	2.36
Average	39.5°	41.7°

The correlation of the angle of repose vs the angle of shearing resistance shows a close relationship. The date is displayed in Figure 3-28.

4.3.8 **In-situ voids and relative density**

The in-situ voids and the relative density data for the Big Bay dune formation is provided in Table 4-16. The dune formation is assumed to be newly formed and the high % relative density from some samples is surprising. The range of density, with reference to the guide in Figure 4-14, is dense to very dense.

Table 4-16 Voids and % D_R for Big Bay dune formation

Voids, maximum						
voids, e_{max}	0.808	0.806	0.806	0.802	0.802	0.798
Voids, minimum						
voids, e_{min}	0.549	0.559	0.542	0.539	0.564	0.538
% D_R data						
In-situ wet density	1726	1735	1729	1723	1716	1722
In-situ moisture content	3.61	3.2	3.6	3.7	3.2	3.4
In-situ dry density	1665.9	1681.2	1668.9	1661.5	1662.8	1665.4
In-situ voids, e	0.591	0.576	0.588	0.595	0.594	0.591
% D_R	83.9%	93.2%	82.6%	78.8%	87.4%	79.4%

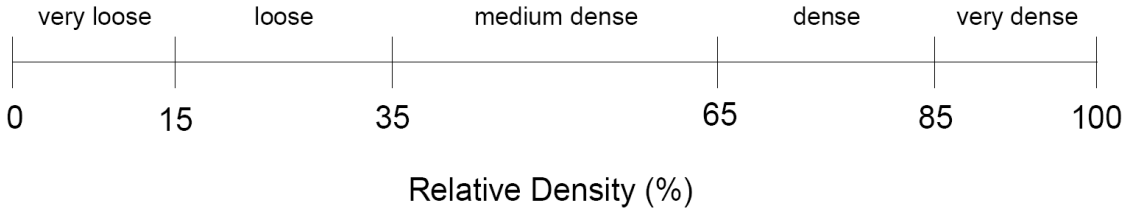

Figure 4-14 Designations based on relative density, D_R (AS Nr 1726)

A more descriptive table that incorporates the DCP is displayed blow in Table 4-17.

Table 4-17 DCP densification

Average DCP_{DN} (in blows per 100 m)	Founding level description	In-Situ Sand Description	% D_R (Skempton, 1988)
0-1	Poor founding levels	Very loose	<15%
1-3	Not good founding levels	Loose	15 – 35%
3-8	Suitable founding levels	Medium dense	35 – 65%
8-15	Good founding levels	Dense	65 – 85%
>15	Excellent founding levels	Very dense	>85- 100%

The in-situ voids for problematic areas in the study area of Atlantic Beach Golf Estate are displayed in Table 4-18. The in-situ voids are on average above 0.7 and the % D_R is consequently dangerously low, as much as 17.2% on average. These results are indicative of sand that is loosely compacted and therefore cannot support a structure of significant size. Homes in the study area having founding levels in the contaminated drift sand (without preparatory work first being done) are exposed to severe settlement. Sand that is loosely compacted has a low modulus of elasticity (Das, 2010) and can be in the order of E_s =10000 – 28000 kPa (these are representative values). Corresponding Poisson ratios are 0.2 – 0.4.

Table 4-18 Correlation of voids, % D_R and settlement for Atlantic Beach drift sand

Trial Holes at Atlantic Beach Golf Estate	Average Bearing Capacity (kPa)	Standard Deviation (kPa)	Predicted differential settlement (mm)	DMT Settlement 50/50 mixture	In-Situ Density (kg/m^3)	Density Classification (% of maximum)	NHBRC Site Classification
Test AT. B1	71	34	20*	29	1510	85 - 90	S2
Test AT. B2	22	12	28*		1509	<85	S2
Test AT. B3	208	57	11*		1560	90 -95	S1
Test AT. B4	176	61	2	-	1570	90 -95	S
Test AT. B5	85	17	7	-	1555	85 - 90	S
Test AT. B61	127	37	3	-	1568	90 - 95	S

*Sites with organic contamination

4.3.9 **In-situ density of windblown sand in study area**

The in-situ densities (Table 4-19) were measured with the use of an extraction Shelby tube. Data revealed that the in-situ densities vary from 1529 kg/m^3 in the upper drift zone where contamination exists (0-1.3 m BGL) to 1723 kg/m^3 in the lower regions (1.2-1.4 m BGL). A significant amount of contamination exists within the drift zone where shallow foundations have been founded (refer to Table 3-11 in Chapter 3).The lower densities were found in the contaminated zone, while the cleaner, white sand at the lower level, recorded higher densities.

Table 4-19 In-situ densities D_R for Atlantic Beach drift sand

Position	Site Lands End: GPS -33.74425,18.451055			
moisture, %	6.11	6.11	3.25	11.94
ρ_b, kg/ m3	1828.4	1824.6	1740.4	1711.9
ρ_d, kg/m3	1723.1	1719.5	1685.6	1529.3

4.3.10 **Predicted settlement in the chamber**

All bearing capacity and settlement data in the chamber was calculated using the method proposed by Burland and Burbridge (1985). The software program, Correct Bearing Capacity, utilises this method and incorporates the SPT_N value. The DCP_{DN} was converted first to SPT_N before the analysis was completed. Due to the added vibration an increase in the SPT_N value was observed with a resultant decrease in settlement. Table 4-20 records the settlement prediction on the chamber sands, alongside the expected allowable bearing capacity and K_D. Miscellaneous data related to this table is displayed in the Appendices Schedule from Table A.3 to A.6. The settlement has been calculated for a strip footing with dimensions of 0.8 m wide, 8 m in length and a vertical load (without eccentricity) of 50 kPa. The frictional angle used was the same as predicted with the DMT using formula.

Table 4-20 DCP vs DMT Settlement prediction

Parameter	West Coast sand		Philippi sand	
	Pre-Vibration	Post vibration	Pre-Vibration	Post vibration
SPT_N	5	7	4	7
DCP Settlement (mm)	11	7	16	7
DMT Settlement (mm)	14	4	22	11
Allowable Bearing Capacity, Q_u (kPa)	328	400	192	220
DMT horizontal stress, K_D	2.7	3.9	0.8	1.1

4.3.11 **Settlement correlation in the chamber**

The average settlement in the chamber as predicted with the DMT and DCP device has been correlated with the DMT's K_D value. The data is displayed in Figure 4-15. There is no significant increase in the K_D value for Philippi sand after vibration; K_D values remain below 5. The West Coast sand responds well after vibration and the K_D value increase more significantly, resulting in lower settlement.

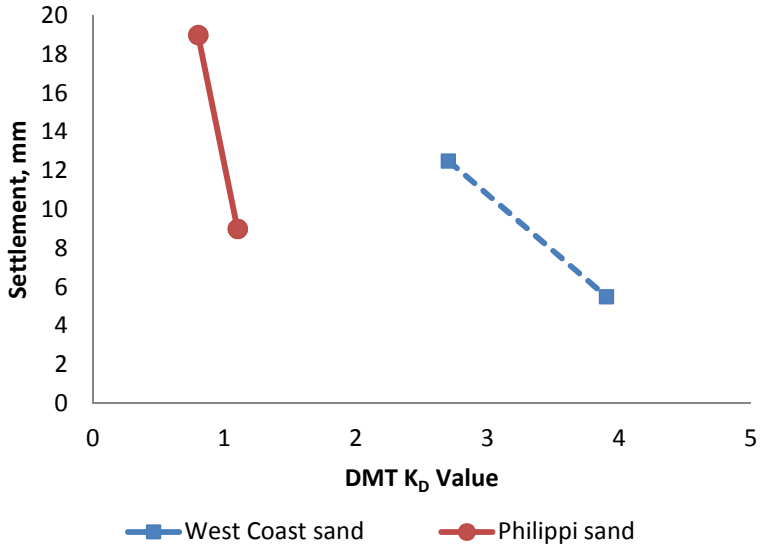

Figure 4-15 Settlement vs DMT K_D

4.3.12 **DMT stiffness readings in the chamber**

The readings for one set of DMT tests on the dry Philippi sand are shown in Table 4-21, including the results of the analytical results as deduced with the DMT E-Lab program. The lower half of the chamber yielded E-modulus values 60 Mpa and steadily increases with depth. The Philippi sand is not particularly resilient sand. This is borne out from comparative tests on the sand to check its stiffness using the CBR_{RL} reload test (the test procedure and detail not discussed in this study). The *E* value for this sand is low, calculated to be 64 MPa at optimum moisture content. This may resist pressure exerted by line loads on low cost housing foundations. The bearing capacity for homes with light masonry is in the order of 30-60 kPa. With a suitable safety factor, vertical loads must be curtailed to about 40 kPa. So the need to vibrate the soil with enough moisture is crucial to increase its stiffness and ultimately, bearing capacity.

Table 4-21 DMT readings on Philippi sand

Date	1/08/2008					
Diaphragm Calibration	Disc 50					
ΔA	0.05					
ΔB	0.4	Dry Philippi sand post-vibration				$E_{s,}$ Mpa (from DMT)
A-reading	*B-reading*	Depth	Bar Pressure	P_o	P_1	
0.2	2.6	280	5	0.15	2.2	56.9
0.15	2.9	340	6	0.09	2.5	66.9
0.15	2.7	405	8	0.1	2.3	61.1
0.2	2.7	585	13	0.15	2.3	59.7
0.2	3	615	15	0.13	2.6	68.6
0.25	3.1	650	18	0.18	2.7	70.0
0.25	3.5	685	22	0.16	3.1	81.6
0.25	3.7	710	30	0.15	3.3	87.4

Table 4-22 displays processed data for the West Coast sand such as the strength parameter, E_D (DMT-modulus), material Index I_D, and horizontal stress index, K_D. These strength parameters are important for settlement and bearing capacity calculations. Settlements are calculated by means of the one-dimensional formula (2.21), with $\Delta\sigma_v$ calculated according to Boussinesq (Jarquio et al, 1984) and M_{DMT},

is the constrained vertical modulus, estimated by the DMT. The latter may also be determined in an oedometer.

Table 4-22 DMT program results on West Coast sand

West Coast

23 Oct 2008 Neal.dat

CPUT

Neal PM

WC Sands

CPUT

Settlement vs Liquefaction

LEGEND

Z = Depth Below Ground Level

Po,P1,P2 = Corrected A,B,C readings

Id = Material Index

Ed = Dilatometer modulus

Ud = Pore Press. Index = (P2-Uo)/(Po-Uo)

Gamma = Bulk unit weight

Sigma' = Effective overb. stress

Uo = Pore pressure

INTERPRETED PARAMETERS

Phi = Safe floor value of Friction Angle

Ko = In situ earth press. coeff.

M = Constrained modulus (at Sigma')

Cu = Undrained shear strength

Ocr = Overconsolidation ratio

(OCR = "relative OCR"- generally realistic. If accurate independent OCR available, apply suitable OCR Factor)

SOUNDING PARAMETERS

DeltaA = 15 kPa

DeltaB = 40 kPa

GammaTop = 14.56 kN/m^3

FactorEd = 34.7

Zm = 0.0 kPa

Zabs = 0.0 m

Zw > Zfinal

Water Level below end of sounding

Reduction formulae according to Marchetti, ASCE Geot.Jnl.Mar. 1980, Vol.109, 299-321; Phi according to TC16 ISSMGE, 2001

Z (m)	A (kPa)	B (kPa)	C (kPa)	Po (kPa)	P1 (kPa)	P2 (kPa)	Gamma (kN/m^3)	Sigma' (kPa)	Uo (kPa)	Id	Kd	Ed (MPa)	Ud	Ko	Ocr	Phi (Deg)	M (MPa)	Cu (kPa)	West Coast DESCRIPTION
0.24	25	100		39	60		14.7	3	0	0.54	11.2	0.7		2.0	14.7		1.9	7	MUD
0.28	25	150		37	110		16.7	4	0	2.01	8.9	2.6				40	6.1		SILTY SAND
0.38	20	175		30	135		16.7	6	0	3.50	5.2	3.6				37	7.0		SAND
0.64	20	200		29	160		16.7	10	0	4.57	2.9	4.6				34	6.4		SAND

4.3.13 **Correlation of DCP and E_{PLT}**

The DCP_{DN} has been correlated to the expected modulus ,E_{PLT}, for the plate test in West Coast sand. Figure 4-16 suggests that a DCP_{DN} value of between 10 and 20 mm/blow would provide reasonable stiffness to light loads. Modulus values of 50-75 MPa can be expected. The DMT's method of predicting the modulus value, $E_{D,}$ is lower than the E_{PLT} trend predicted by Murad et al, (2004). The DCP method of modulus prediction cluster along the same trend that was produced by the aforementioned research for fine grained soils.

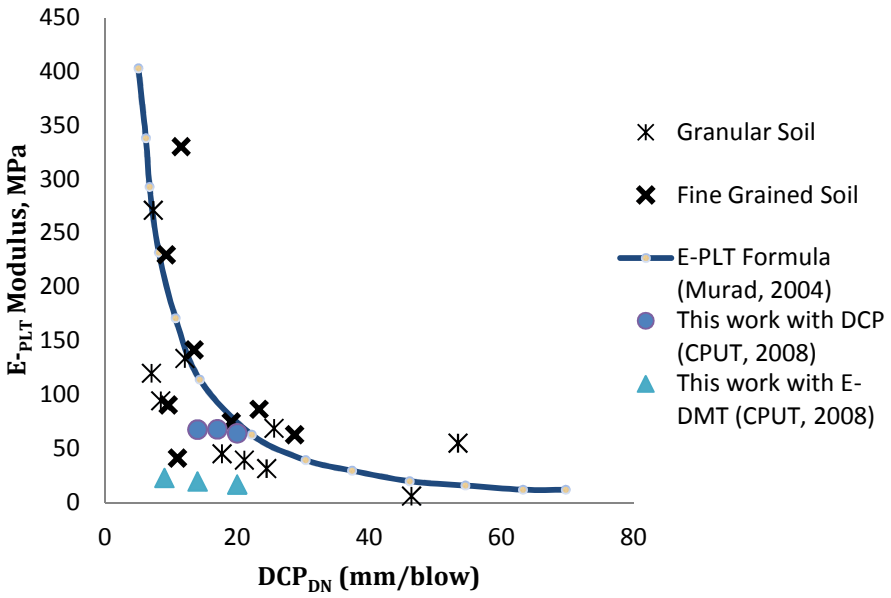

Figure 4-16 DCP_{DN} and E_D vs E_{PLT}

4.3.14 Correlation of % D_R and K_D values

The data shown in Figure 4-17 were determined on the West Coast sand samples only. The data points to a developing trend and confirms the previous research done by Monaco et al, (2005) and Tanaka and Tanaka (1998). The density measured in the chamber at the time of testing were D_R=4% (pre- vibration) to 62% (post-vibration). The relative densities were based on voids determined from samples extracted from the chamber. The testing of K_D stresses in the intermediate range and above will require further test work so that the trend can be better correlated with the aforementioned research work.

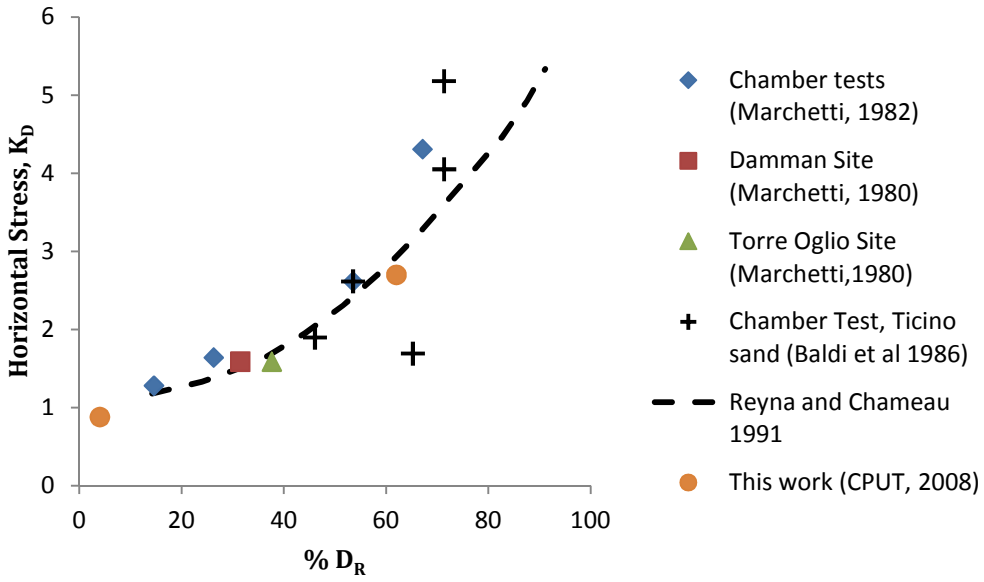

Figure 4-17 Trend analyses of % D_R vs K_D

4.3.15 **Recorded settlement in chamber sands**

The one dimensional elasticity formula can be used for settlement analyses in sand for large rafts (or the three dimensional elasticity formulas for small isolated footings). However, based on considerations by some authors, it is recommended to use the one dimensional formula in all cases (Burland, Broms & De Mello, 1977). The reasons for this are discussed further by Marchetti (1997). Figure 4-18 illustrates the first experimental research data that correlates how the expected settlement of compacted air dry sand reacts when exposed to loads; in this case the stiffness of the sand in the chamber has been measured with the DMT and the modulus has been plotted against the settlement. The Philippi sand is especially vulnerable when the E_D modulus is measured as low as 2 MPa. With modulus values this low, structures made of light brickwork cannot tolerate the resultant settlement built in similar sand. The West Coast sand, being easier to compact, show settlement values that appear in a narrow band and react in a non-significant manner under the loads applied. The settlement calculation assumed vertical loading to be in both cases 50 kPa and the Burland and Burbridge (1985) method was used. The differences in the settlement prediction between the two methods (DMT vs the inverted DCP_{DN} used in the Burland and Burbridge calculation) are less than 10 mm.

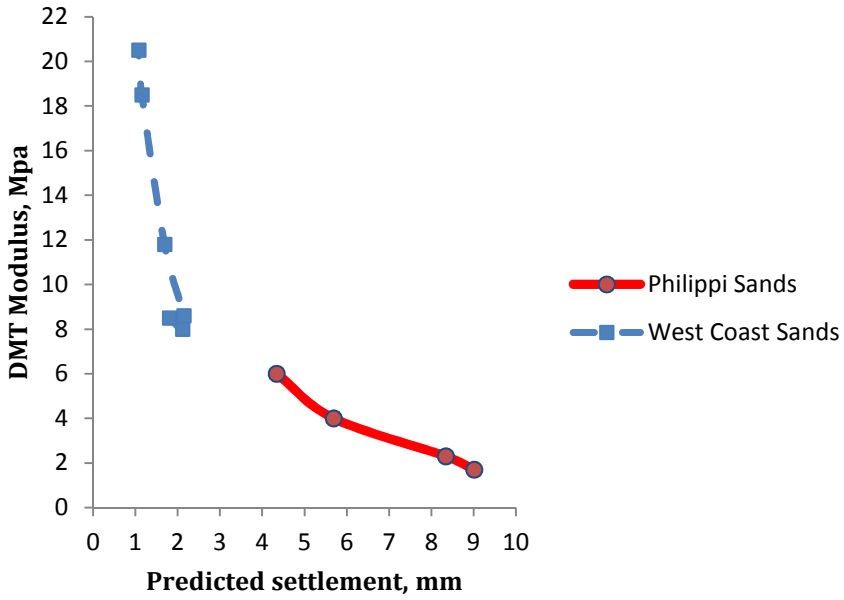

Figure 4-18 DMT-modulus vs settlement on research sand

4.4 Predicting liquefaction with the DMT

The CSR is calculated with use of the equation shown in (2.14). Using data supplied by the Council for Geoscience in Pretoria (Kijko & Graham, 1998), the Projected Ground Acceleration (PGA) value used for the Western Cape, was estimated to be 0.2 g_s. This places the Western Cape in a potentially hazardous zone according to Figure 2-42 in Chapter 2. (The earthquake of 1809 in the Milnerton area was reported to have resulted in the liquefaction of the local soils).

The suggested guidelines by Marchetti (2001) in evaluating the seismic zone against the recorded K_D value are displayed in Table 4-23. This will require that the sand from Philippi and the West Coast must be compacted to yield K_D values of above 1.7 to avoid possible liquefiable conditions.

Table 4-23 Seismicity values for K_D (Marchetti, 2001)

– Classification zone	– Suggested K_D value
– Non-seismic areas	– $K_D > 1.7$
– Low seismicity areas ($a_{max}/g = 0.15$)	– $K_D > 4.2$
– Medium seismicity areas ($a_{max}/g = 0.25$)	– $K_D > 5.0$
– High seismicity areas ($a_{max}/g = 0.35$)	– $K_D > 5.5$

The K_D values recorded in the calibration chamber for the Philippi sand yielded values as low as 0.9. To resist possible liquefaction the sand will need to be compacted sufficiently to yield a higher % D_R. It would appear that if vibratory compaction after saturation in Philippi sands does not significantly increase the horizontal stress. Residential homes with shallow foundations in this sand may require chemical stabilisation below the footings for added protection. The CSR has been estimated to be ± 0.12. This places the sand firmly in the liquefiable zone. Should a serious tremor occur, coupled with a high water table and K_D values of less than 5, liquefiable conditions may prevail (see plotted data in Figure 4-19). The West Coast dune sand falls within the same seismic category. This sand is less vulnerable and has a higher dry density with corresponding K_D values. The calibration chamber recorded K_D values of above 2.4 and should resist liquefaction if compacted adequately. Table 4-24 displays the data used for the assessment of the sands liquefiable resistance.

Table 4-24 K_D values for research dune sand

E_{DMT} (MPa)	σ' Philippi sand(kPa)	σ' West Coast sand (kPa)	CSR value Philippi-sand	CSR value West Coast sand	K_D West Coast sand	K_D Philippi sand
0.34	4.9	4.8	0.3	0.3	3.1	0.8
0.39	5.6	5.5	0.2	0.3	3.0	0.7
0.44	6.4	6.3	0.2	0.2	2.4	0.8
0.5	7.2	7.1	0.2	0.2	2.7	0.8
0.54	7.8	7.7	0.2	0.2	2.5	0.9
0.6	8.7	8.5	0.2	0.2	2.6	1.3
From reference chart (Seed & Idriss, 1982)		Ave	0.12	0.18	2.7	0.8

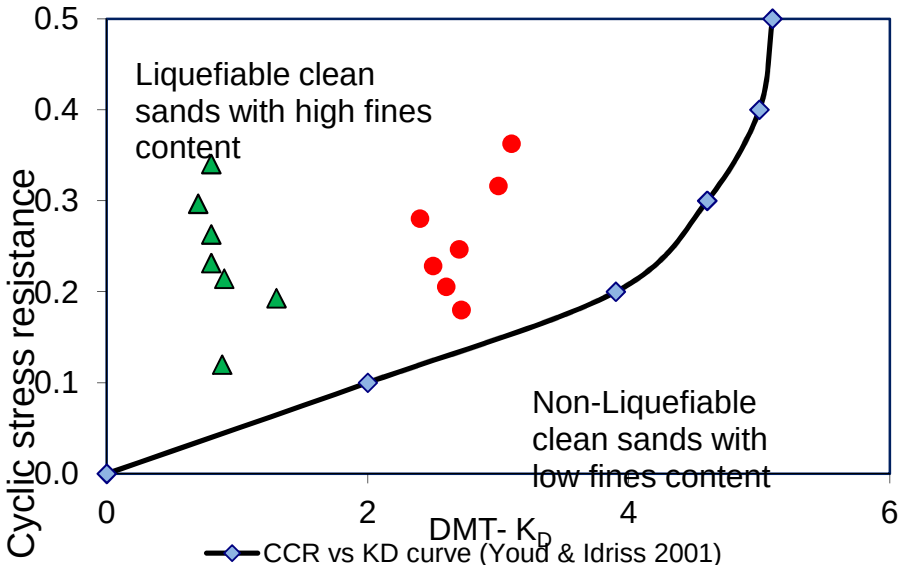

Figure 4-19 K_D vs CSR values for research dune sand

The highest chamber densification achieved in this research was D_R = 64 %. Similar densification for on-site conditions may result in lower horizontal stress. The DCP can be used in the trenches of footings to assess the level of compaction and thereby assess whether reasonable resistance to horizontal shear has been achieved.

4.5 Site inspection and findings

In this section of the study the findings in the field where homes have undergone structural damage are discussed. Images of significant damage were recorded.

4.5.1 Drainage problems

The drain covers were removed from storm water drains and many were found to be inadequately built. At one site, the drainage was particularly poor, with down pipes releasing water into the foundations itself. Figure 4-20 shows how poorly a storm water inspection drain is constructed that will allow storm water to drain directly back into the drainable sand layers below. The foundations at this site is founded on loose sand (D_R = 23%) with a high content of decomposed organic contamination. A high in-situ void ratio was calculated in the contaminated layers, allowing water to easily penetrate to below the founding levels. Figure 4-21 illustrates how this storm water downpipe discharges directly into the soil above a foundation.

Figure 4-20 Poor storm water drain construction

Figure 4-21 Poor down pipe design

Storm water down pipes was found to have the outlet directed at the foundations that were shallow in depth. Other outlets were discovered to have reverse invert levels which did not allow rain water to be led away from the property. Trial holes were dug (see Figure 4-22) to varying depths below the foundations to allow visual inspections to be made.

4.5.2 **Contamination in founding levels**

The upper sand layers are highly contaminated with organic debris including charcoaled twigs, branches and rotting leaves. Some small shale fragments from the Malmesbury Formation are also visible. A close up of all the fragments on a 0.6 mm sieve is shown in Figure 4-23.

Figure 4-22 Trial hole

Figure 4-23 Laboratory inspection of contamination

The contaminated layer thickness ranges from 1 to 1.35 m below the founding levels. This most likely represents an in-filled -dune hollow, possibly a borrow pit to extract fill sand for the roads in the vicinity, or may be a refuse pit, although no man-made refuse was found. The organic material may encourage the sand to develop collapse potential when saturated, which probably accounts for the excessive

settlement witnessed at this home. Figure 4-24 has been re-produced to illustrate previous research by Franklin (1973) on the variation of maximum dry unit weight with organic content.

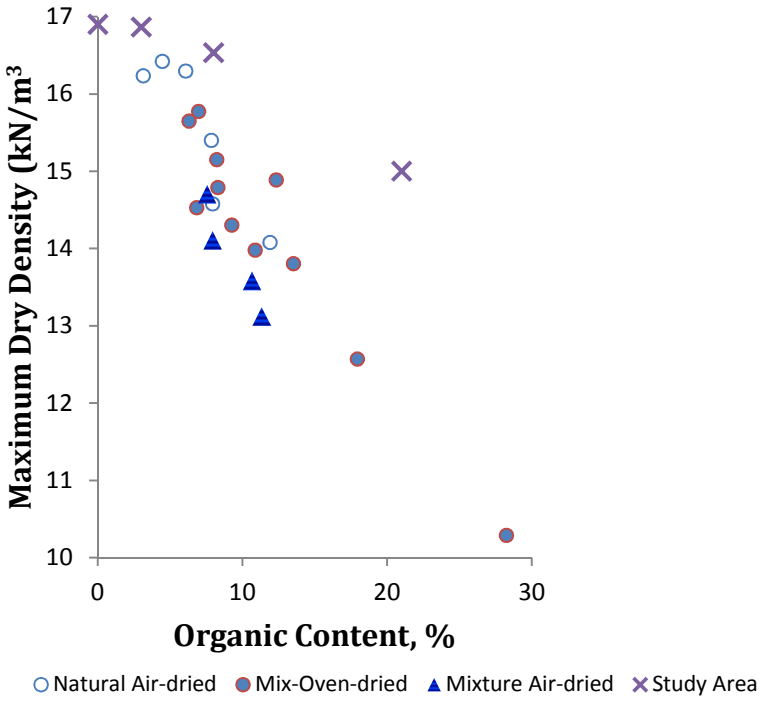

Figure 4-24 Unit weight vs % organic contamination (after Franklin et al, 1973)

There is a definite trend in the results for the contaminated drift sand from the study area in the Atlantic Beach Golf Estate (see Figure 4-24). The higher level of contamination has resulted in lower densities, thereby making the sand layer more compressible and vulnerable to settlement. Table 4-25 displays the results from an experiment in the chamber with 50% contaminated sand mixed with sand from the Blaauwberg study area.

4.5.3 **Settlement cracks**

Homes in the study area showing signs of settlement cracks all have foundations in the contaminated drift layers. The figures below provide evidence that the foundations are not placed deep enough and allowing excessive settlement to take place (Figure 4-25 to Figure 4-28). Sand from these areas were retrieved and remixed with 50% contaminated debris and organic matter. The sand mix was re-

compacted in the chamber with a light hand compactor under moist (5% mc) conditions. The relative density, R_D, was estimated with the DCP to be 18%, classifying the density in the chamber to be loose.

Table 4-25 DMT estimation for contaminated sand

Settlement calculations for 50/50 contamination			
ΔZ	σ'_v	M_{DMT}	S
0.2m	30.0 kPa	N/A	N/A
0.3m	38.5 kPa	0.2 MPa	5.8 mm
0.4m	42.5 kPa	0.1 MPa	17.0 mm
0.5m	45.5 kPa	0.4 MPa	5.8 mm
0.6m	47.5 kPa	3.4 MPa	0.88mm
		Total	Σ = 29.3 mm

The DMT has estimated the settlement in the contaminated sand-mixture to be 29 mm. The estimation of the settlement below homes where contamination (up to 23 % by mass) has been found on site, closely matches that of the DCP (see Table 3-13). The latter utilises the Terzaghi and Peck method (1967) and the inverted DCP_{DN} for the SPT_N value.

Figure 4-25 Shallow foundations

Figure 4-26 Light settlement cracks

Figure 4-27 Severe floor settlement

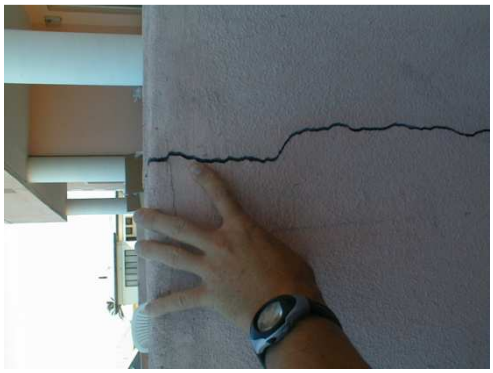

Figure 4-28 Moderate settlement cracks

If builders utilise the DCP device correctly and interpret the data precisely, then finding a suitable level to found upon should not be problematic. The above examples of structural damage could have been avoided and saved an unnecessary expense for the owners.

4.5.4 **Depth of founding levels**

From the DCP data (refer to Table 3-13) it becomes evident that the foundations for homes in the immediate area have been placed to shallow. The settlement within the first 1 m from NGL is above what the structure can tolerate and the foundation should have been placed deeper. This would mean more brickwork (using foundation bricks with a strength of >14 Mpa) up to the plinth level. The alternative is to provide support lower down, such as via the use micro-piles.

Chapter 5 Conclusions and recommendations

In this chapter the outcome of the objectives is discussed. The results from in-situ tests are interpreted and opinions are expressed. The laboratory results are used to validate the important strength parameters that are important in calculating settlement and bearing capacity in windblown sand. The in-situ soil test devices are also examined for its performance and relevance to the study. The objectives were as follows:

- To investigate problematic windblown (Aeolian) sands in a study area along the West Coast of the Cape Peninsula.
- To design and construct an open top calibration chamber to evaluate the characteristics of Aeolian sand.
- To investigate the possibility of liquefaction and correlate this to settlement in the chamber.
- To compare the DMT device to other in-situ test instruments such as the DCP.

5.1 The Calibration Chamber

An important objective for this study was to design, build and commission a calibration chamber that would be suitable for examining the properties of Aeolian sand (Figure 3-1). This has been achieved for the purposes of evaluating the performance of in-situ test equipment used on site. The chamber can be used to test other fine grained soils. The chamber can be vibrated with the attachment of its motors whether the soils are dry or moist. The airmount actuator allows relatively no load eccentricity from lateral motion and is stable during vibration. Relative densities have been achieved up to 62% and with further adaptation it is possible to achieve a higher $\%D_R$. The chamber diameter is wide enough to allow cone or blade penetration devices to be operated within.

5.2 Comparative work with in-situ devices

The DMT and DCP have been compared to each other in the chamber as far as the measurement of its parameters is concerned. Strength parameters such as bearing capacity and modulus have been correlated to other research work done with the plate bearing test (Murad, 2004).

5.2.1 **Bearing capacity and settlement**

The bearing capacity of the DMT has been calculated with the Marchetti reduction formula (2.11) while the DCP has been correlated with the Kessler and Paige-Green methods (2.7) and (2.8) respectively. The two DCP correlation methods are closely related and no significant differences were observed (see Table 4-12). When comparing the DMT results in Table 4-8 with the DCP results in Table 4-12, the DMT calculates the average bearing capacity at 74 kPa vs 78 kPa for the DCP. A difference of 5.4% exists between the two methods of bearing capacity calculation. The conclusion here is that the operator in the field can confidently trust the use of a DCP to predict bearing capacity in loose sands (*% D_R* <35%).

The predicted settlement between the DMT and DCP are closely related and no significant difference could be observed during the chamber tests. Reference is made to Figure 4-15. The settlement values were observed to be related to the change in K_D values as the chamber sand was densified from loose, D_R =35%, to medium dense, D_R =62% (see Figure 4-15). The conclusion here is that settlement in windblown sands will reflect a corresponding K_D value as far as an order of magnitude is concerned. For example, K_D values of 0.8 in Philippi sand can result in predicted settlement of 22 mm, which would be the maximum a masonry dwelling can tolerate. The DMT has proven that its method of settlement prediction correlates well with other established devices such as the DCP.

As stiffness (or modulus of elasticity) is a known parameter that controls settlement, a correlation was done between the DMT and DCP methods. The results for these two devices were compared to the work completed by Murad (2004) and can be seen in Figure 4-16 . The DCP values appear to follow the trend established by Murad at lower DCP_{DN} values, while the DMT cluster together and present even lower values. It may be that the DMT method for modulus prediction performs better at higher levels of horizontal stress and this should be assessed in another study.

5.2.2 **Correlation of predicted liquefaction and settlement**

The DMT has the unique ability to predict the stress history (horizontal stress) by means of the K_D value. The experiments conducted in this study in the chamber have shown that the K_D value increases with compaction and reduces the expectant settlement. The suggested minimum K_D values by Marchetti (2001) for areas subjected to medium seismic activity have been applied to the windblown sands in this study. On this basis, the Philippi sand has been found to be vulnerable. Low horizontal stress (below K_D = 5) indicate the possibility of liquefaction. The expected settlement for Philippi sand under “loose”

conditions can be above 22 mm, while less (below 10 mm) can be expected in the West Coast sand. The chamber will have to produce higher relative densities (>62%) to assess whether the DMT can measure K_D values above the minimum of 5.

The particle size distribution for the study sands were compared to previous research for potentially liquefiable sands (Sitharam, 2004). Although both sands in this research have a very low percentage of fines, the gradings do fall within the boundaries for liquefiable sands (see Figure 2-26). The average particle size distribution for the study sands have been overlaid on the graph produced by the aforementioned researcher and is displayed in Figure 4-7. Based on this assessment the West Coast sand appears to be less vulnerable than the Philippi and Atlantic Beach (contaminated) drift sand.

Contaminated sand has been found to exist in the upper drift zone. As an experiment the sand was mixed with organic matter and a mixture of 50/50 was placed inside the chamber. The DMT device was able to predict the expected settlement (29 mm) and classify the soil as silty –mud (I_D). The expected range of settlement on site with the DCP (using the Terzaghi and Peck procedure) was calculated to range between 11 and 28 mm (see Table 4-18). This table also classifies the area according to the NHBRC method for site zoning. Although the range of contamination varied on site, and is not the same level of contamination as the chamber experiment, the DMT was able to measure the lack of horizontal stress due to the "softness" of the material and predict the corresponding higher settlement (see Figure 4-24 and Table 4-25).

5.3 Investigating problematic Aeolian sands

Shifting sand on a construction site is always problematic during the season when the prevailing wind is active. In the Western Cape the South Easter (summer months) and North Wester (winter months) blows intensely, carrying more shifting sand onto site, thereby partially filling trenches prepared for footings. Trenches that are not kept clean by a vigilant construction team will lead to reduced width and thicknesses of the footings. An undersized footing can only result in premature cracking and the overall weakening of the structure. The softer pockets within the upper stratum of the sand deposits are accompanied by high levels of contamination. This contamination must be removed to as deep as 1.2 m and replaced with suitable filling sand of fine gravels.

Builders with limited experience can assess the firmness of the trench bottom with a "farm style" approach. The use of, for example, of a one meter probe made of 19 Ø mm ribbed rebar and a T-Piece

above, can be forced into the sand with the operators' body weight. Easy penetration (i.e., no excessive force required) will indicate soft spots that need attention, opposed to when immense force is required, thereby indicating reasonable firmness.

The average depth of the founding level in windblown sands along the Western Cape coast line is generally 500 mm below ground level. This depth however does not assure the builder of adequate bearing capacity. The upper zone of Aeolian sands (± 1.5 m) in the Atlantic Beach Golf Estate can contain as much as 21% of contaminated material, leading to voids and lower relative in-situ density. To investigate the situation, the DCP has been found to perform well in providing data that point to suitable founding levels. The correlation between the DCP_{DN} and the % D_R will provide useful information with regard to choosing a suitable founding level. The DCP should be able to penetrate these depths to assess the consistency of the soil and its predicted relative density.

5.3.1 **Assessing in-situ density with the DCP**

Figure 4-14 can be used as a guide for builders to assess the suitability of the sand deposit before and after trenching. The important aspect here to consider is that enough expert advice be gathered first before a decision is made to cast concrete. If no economic depth can be excavated for strip foundations then short-bored or micro piles should be considered to support the structure at a lower and firmer depth.

Sands classified as being very loose to medium dense should be improved by a suitable method of compaction. Overnight pre-wetting is suggested so that enough moisture is allowed to penetrate the sand. Compaction at ± 120 Hz (low frequency, high amplitude) should densify the sand to acceptable levels (Figure 4-8). DCP readings thereafter must verify the improvement before any casting of concrete is allowed. Suitable vibration (as was observed in the chamber) dramatically increases the bearing capacity. DCP_{DN} values in the footing trenches on site should not be more than 15 mm/blow to ensure adequate density.

5.3.2 **Comparison of in-situ methods**

The DMT could not be utilised on site which is unfortunate. The bearing capacity and settlement values calculated with the DMT reduction formula (2.11) and (2.21) respectively were found to be functional and well correlated with the DCP in the chamber tests.

On site the predicted settlement values were correlated between the DCP and Terzaghi & Peck methods. The trial holes AT.B1 – AT.B3 were contaminated with organic debris and yielded predicted DCP settlement of 11 - 20 mm. The Terzaghi & Peck method was equally comparative in its estimation, providing values of 6 - 24 mm (see Table 3-13).

The stress histories of windblown sand, measurable with the DMT, are unknown parameters in South Africa. This device should be incorporated into the geotechnical fraternity as far as trustworthy equipment is concerned. The device is easily adaptable to any conditions on site, is a useful piece of equipment in the laboratory and can predict the properties of varying soils with reasonable accuracy, from sandy silts to coarse fractions.

5.4 Recommendations

- The study area must be widened to include more land in windblown sand that may have similar geological properties. One particular area in mind is Atlantis, north of the Koeberg Power Plant, where low cost housing is planned. This study has uncovered that contaminated sand must be removed under shallow foundations to negate uncontrolled settlement. Micro-piling may be an economic alternative to support the foundations at a deeper level in cases where excessive differential settlement is predicted.

- Frozen samples of sand should be prepared for triaxial cyclic testing. These tests may be better suited for correlations between seismic loading and cyclic stress ratio. The DMT's K_D value could be correlated with this completion of such as study.

- A data base should be initiated that would become public domain. The geological hazards in areas marked with windblown sands should be classified for this purpose so that the public can become aware of the potential dangers before purchasing land for housing.

- The chamber must be deepened to allow testing up to 2.5 m. This will require sinking the chamber into the ground to allow adequate head cover. The chamber must be provided with state of the art adaptations for measuring more crucial data such as in-situ and boundary stress, pore water pressure, particle density and moisture content.

- The chamber tests can be better evaluated under a wider range of relative density, perhaps at D_R = 25, 45, 65, and 95%. Settlement predictions can be better evaluated in this way.

- The difficulties encountered with the original research methodology were the fact that no rigging device could be built or purchased that would have enabled test work with the DMT on-site. This aspect of the work will be addressed as an objective in a future study in contaminated Aeolian sand in the Western Cape. This rigging device will have to be equipped with shafts that can penetrate to at least 3.5 m deep, so that the contaminated drift and the firmer layers below can be examined. The calibration chamber however allowed the study to examine the behaviour of the sand samples at shallow depths during penetration with the DMT device.

References

AGIS NR Atlas. (2007) Natural Resiource Atlas for Soth Africa. ARC-Institute for Soil, Climate and Water. Pretoria, South Africa. [Online]. Available from http://www.agis.agric.za/agisweb/agis.html. [Accessed 15/12/2010]

Al-Khafaji & Andersland (1992). "*Geotechnical Engineering and Soil Testing*". International Edition. Saunder College Publishing, New York.

Amdurer. SS. (1956). *The Engineering Geology of the Cape Flats*. Ph.D Thesis, UCT, African Works Library. Unpublished

Andrus, R.D., Stokoe, K.H II, (2000). "*Liquefaction resistance of soils from shear-wave velocity*". Journal of Geotechnical and Geo-environmental Engineering, ASCE, 126(11):1015-1025

Anbazhagan, P. (2009). Department of Civil Engineering, Indian Institute of Science. [Online]. Available from: http://civil.iisc.ernet.in/ [Accessed 6/01/2010].

Australian Standards 1726 (1993). Geotechnical site investigations, 40 pp.

Bałachowski, L. (2006). "*Use of calibration chamber as a large triaxial apparatus Gdańsk University of Technology*", Narutowicza, Gdańsk 11/12, 80-952

Baldi, G., Bellotti, R, Ghionna, V, M. Jamiokowski, & Pasqualini, E. (1982). *"Design parameters for sands from CPT*". Proceedings from the Second European Symposium on Penetration Testing, Amsterdam, Holland.

Baldi G., Bellotti R., Ghionna V. N, Jamiolkowski M., Marchetti S & Pasqualini E. (1986). "*Flat dilatometer tests in calibration chambers*". Proceedings ASCE Conference In Situ 86, Blacksburg, VA, pp 431-446

Baligh, M.M. & Scott, R.F. (1975). "*Quasi Static Deep Penetration in Clays*". ASCE Journal GE, Vol. 101, No. GT11, 1119-1133

Bhandari, N. & Sharma, B. K. (2001). "*Importance of site amplification and interference of shear waves*". Abstracts of International Conference on Seismic Hazard with particular reference to Bhuj Earthquake of 26 January 2001, New Delhi, pp. 19–21

Bowles, J.E. (1996). "*Foundation Analysis and Design".* 5th Ed. McGraw-Hill, 1175 pp.

Briaud, J.L. & Miran, J. (1992). US DoT "*The Flat Dilatometer Test*". Department of Transportation - Fed. Highway Administration, Washington, D.C., Publication No. FHWA-SA-91-044, 102 pp

Broere, W. (2001). "*Tunnel Face Stability & New CPT Applications*". Phd Thesis Dissertation. Published and distributed by Delft University Press Science, TU Delft, Netherlands

Burland, J.B., Broms, B.B. & De Mello, V.F.B. (1977). "*Behaviour of foundations and structures*". Proceedings of the IX ICSMFE, Tokyo, Vol. 2, 495-546

Burland, J.B., & Burbidge, M.C. (1985). "*Settlement of foundations on sand and gravel"*. From the Proceedings of the Institution of Civil Engineers. Thomas Telford, London. Vol. 78 (Part 1), pp. 1325–1381.

BMSC Engineering Supplies, Web Page Information. (2008). [Online]. Available from: http://www.cbn.co.za/. [Accessed 19 April 2010]

Boussinesq, J. (1885). "*Theoretical essay on the balance of solid powder compared to that of bulk solids, and the loose earth pressure".* 2nd Ed. Brussels, 1885

Casagrande, A. (1936a). "*Characteristics of cohesionless soils affecting the stability of slopes and earth fills.*" Journul of the Boston Society qf Civil Engineers. January: reprinted in Contributions to Soil Mechunics 1925-1940, BSCE. pp. 25 J-276.

Coduto, P.D, (2001). *Foundation design, principles and practices*. Second Edition. Prentice Hall. Upper Saddle River, New Jersey

Current Science. (2004). "*Methods to evaluate liquefaction potential of soil*. (Extract from CURRENT SCIENCE, Journal Volume 87, No. 10, 25

Cole, D.I., (2005). Discussion on *"Aeolian and marine deposits of the Tabakbaai Quarry area, western Cape, South Africa*". South African Journal of Geology. 108: 578-579

Council for Geosceince, (2002). "*Probabilistic Peak Ground Acceleration Map for South Africa*". Courtesy of Seismology Unit.

Council for Geosceince, (2007). [Online]. Available from http://www.geoscience.org.za/ [Accessed 19 April 2010]

Cubrinovski, M. and Ishihara, K. (2002). *"Maximum and Minimum Void Ratio Characteristics of Sands"*, Soils and Foundations. Vol 42. N0 6, 65-78

Das, B.M. (2010). "*Principles of Geotechnical Engineering*". 7th Edition. Cengage Learning. Stamford, USA

Das, B.M. (2011). "*Principles of Soil Dynamics*". 2nd Edition. Cengage Learning. Stamford, USA.

De Cock, F., Van Impe, W.F. & Peiffer H. (1993). "*Atlas screw piles and tube screw piles in stiff tertiary clays"*. Proceeding from BAP II, Ghent, 359-367

Department of Environmental Quality. (1996). "*Measuring slopes under sand protection program*". [Online]. Available from http://www.michigan.gov/documents/deq/lwm-353-96-01_304423_7.pdf [Accessed 20 December 2010].

ELE International. (2010). Catalogue. [Online]. Available from http://www.ele.com/usa/index.php?option=com_docman&Itemid=110. [Accessed 18 Feb 2011].

Eurocode 7. (1997). "*Geotechnical design - Part 3: Design assisted by field testing*". Section 9: Flat dilatometer test (DMT).

Firestone, ASAM 011. Airstroke Selection Guide. [Online] Available from http://www.airsprings.com.au/ [Accessed 15 January 2010]

Franklin, A. F., Orozco, L. F., and Semrau, R. (1973). "*Compaction of Slightly Organic Soils*". Journal of the Soil Mechanics and Foundations Division, ASCE, Vol. 99. No SM7, 541-557.

Franki. (2010). Geotechnical Engineering Contractors - Micro Piles. [Online] Available from http://www.franki.co.za/content/index.cfm?navID=6&itemID=95 (1 of 5) [Accessed 4 December 2010]

Franceshini, G.,Compton,J., and Wigley,R. (2003). "*Sand Transport along the western Cape coast: gone with the wind?*" South African Journal of Science 99. Science in Action. pp. 317-318.

Gibbs, K.J. and Holtz, W.G. (1957). "*Research on determining the density of sands by spoon penetration testing*". Proceedings. IV ICSMFE, 1, 35-39.

Gravesen, S. (1960). "*Elastic Semi-Infinite Medium Bounded by a Rigid Wall with a Circular Hole".* Laboratoriet for Bygninsteknik, Danmarks Tekniske Højskole, Meddelelse No. 10, Copenhagen

Ghazavi, M., Hosseini, M. and Mollanouri, M. (2008). "*A Comparison between Angle of Repose and Friction Angle of Sand"*. 12th International Conference of International Association for Computer Methods and Advances in Geomechanics (IACMAG). Goa, India

Ghionna, V. & Jamiolkowski, M. (1991). "*A Critical Appraisal of Calibration Chamber Testing of Sands*". Proceedings from the 1st International Symposium on Calibration Chamber Testing, Potsdam, NY, p. 13-40

Goliger, A. Mahachi, J., and Niemann, HJ. (2008). "F*oundation erosion of houses due to action of wind"*. Division of Built Environment. Council for Scientific and Industrial Research. BBAA VI International Colloquium. Bluff Bodies Aerodynamics & Applications. Milano, Italy.

Hartnady, C.J.H.. Rogers, J. and Moore, J.(1989). "*Cape Peninsula excursion guide: Students excursion guide*". Geology Department, University of Cape Town (unpublished).

Harison, JA. (1986). *Correlation of CBR and Dynamic Cone Penetrometer strength measurement of soils.* Australian Road Research, 16(2), pp 130-136.

Hayes, J.A. (1990). "*The Marchetti Dilatometer and Compressibility*". Seminar on "In Situ Testing and Monitoring", Southern Onterio, Section of Canada. Geotechnical Society.

Head, K.H. (1981). "*Manual of soil laboratory testing*"; Volume 2: Permeability, shear strength and compressibility tests. Pentech Press, London, Plymouth, 683 pp.

Hill, R.S. and Theron, J.N., (1981). "*Silica sand of the Cape Flats*". Bulletin of the Geological Survey of South Africa, 69, 45 pp.

Holden, J. C. (1991). "*History of the first six CRB calibration chambers*". Proceedings from the First International Symposium on Calibration Chamber Testing, Potsdam, NY, U.S.A.

Hossain, M.S. & Khouri, B. (2005). "*Comparative Study of Different In-Situ Tests for Site Investigation*". Second International Conference on the Flat Dilatometer to be held in Washington DC, April 2-5, 2006.

Hsu, H & Huang, A.B. (1999). "*Calibration of Cone Penetration Test in Sand. Department of Civil Engineering*. National Chiao-Tung University, Hsinchu, Taiwan, R.O.C. Proceedings from the National Science Council. ROC(A) Vol. 23, No. 5, 1999. pp. 579-590

Hsu, H. (2008). "*A New Method for Preparing Calibration Chamber Specimens*". Article in Sea Technology. Copyright Compass Publications, Inc.

Jamiolkowski, M., Ladd, C.C., Germaine, J.T. & Lancellotta, R. (1985). "*New developments in field and laboratory testing of soils*". SOA Report, Proceedings from XI ICSMFE, San Francisco, Vol 1, 57-153

Jarquio, R., Jarquio, V. (1984). "*Vertical stress formulas for triangular loading". Journal of Geotechncial Engineering. Volume: 110*. Publisher, American Society of Civil Engineers.

Jendeby, L. (1992). "*Deep Compaction by Vibrowing*". Proceedings from Nordic Geotechnical Meeting NGM-92, Vol. 1, 19-24

Jung, H.S., Cho, C.G & *Chun, B.S., (2009). "The engineering properties of surface layer on very soft clay of the south coast in Korea".* Paper delivered to 2nd International Symposium on Cone Penetration testing. Huntington Beach, California, USA

Khafaji, A.L. and Andersland, O.B. (1992). "*Geotechnical Engineering and Soil Testing*". International Edition. Saunder College Publishing, New York.

Kessler Soils Engineering Products, Inc. (2009). DCP Manual viewed online. [Online]. Available from http://www.kesslerdcp.com/faqs.html. [Accessed on 12 December 2010].

Khozaghi, S. Choobbasti, A.J. (2005). "*Prediction of Liquefaction Potential in Soils Using Artificial Neural Networks*", [Online]. Available from: http://www.ejge.com/2007/Ppr0723/Ppr0723.pdf. [Accessed 12/02/2009]

Kijko, A. & Graham, G. (1998), "*Parametric Historic procedure for probabilistic seismic hazard assessment*". Part I: Assessment of maximum regional magnitude, m_{max}, Pure Appl. Geophys., 152, 413-442

Kleyn, E.G. (1975). "*Die gebruik van die Dinamiese Kegelpeilstaaf (DKP*)". Pretoria. Transvaal Provincial Administration. (Laboratory Report L2/74).

Kleyn, E.G., Van Heerden, M.J. (1983). *Using DCP Soundings to Optimize Pavement Rehabilitation*. Paper submitted for Annual Transportation Convention, Johannesburg. Report LS/83 Materials Branch, Transvaal Roads Department, Pretoria, South Africa.

Koester, J.P. (1993). "*Effects of Fines Type and Content on Liquefaction Potential of Low-to-medium Plasticity Fine-Grained Soils*". National Earthquake Conference, Central United States Earthquake Consortium, Memphis, Tennessee. 1, 67-75

Leonards, G.A. and Frost, J.D. (1988) "*Settlement of shallow foundations on granular soils".* Proceedings, ASCE, Journal Geotechnical. England, 114 (GT7), 79 1—809.

Lacasse, S. & Lunne, T. (1986). "*Dilatometer Tests in Sand*". Proceeding from ASCE Spec. Conf. on Use of In Situ Tests in Geotechnical Engineering. In Situ , Virginia Tech, Blacksburg.

Lunderstedt, D.K., (2007). "*Impact Assessment Report*". E3 Geotechnics Report. Nuclear 1 EIA and EMP. Published by Eskom Holdings Limited.

Lutenegger, A. J., (2006). "*Flat Dilatometer Method for Estimating Bearing Capacity of Shallow Foundations on Sand*", Proceedings of the 2nd International Conference on the Flat Dilatometer, pp.334-340.

Marchetti, S. & Crapps, D.K. (1981). "*Flat Dilatometer Manual*". Internal Report of G.P.E.

Marchetti, S. (1980). "*In Situ Tests by Flat Dilatometer*". ASCE Journal GED, Vol. 106, No. GT3, Mar., 299-321

Marchetti, S. (1982). "*Detection of liquefiable sand layers by means of quasi-static penetration tests*". Proceedings from 2nd European Symposium on Penetration Testing, Amsterdam, 689-695

Marchetti, S. (1997). "*The Flat Dilatometer: Design Applications*". Proceedings from the 3rd International Geotechnical Engineering Conference, Keynote lecture, Cairo University, Jan., 421-448

Marchetti S. (1999). "*On the calibration of the DMT membrane*". L'Aquila University, Italy. Internal technical note, pp 9

Marchetti, S., Monaco, P., Totani, G. & Calabrese, M. (2001). "*The flat dilatometer test (DMT) in soil investigations*". A report by the ISSMGE Committee TC 16. Proceedings, International Conference on In-Situ Measurement of Soil Properties & Case Histories, Bali, Indonesia, 95-131

Meyerhof, G.G. (1959). "*Compaction of sands and bearing capacity of cohesionless soils*." Journal of Soil Mechanics and Foundation Division. ASCE,85. NO. SM6.pp1-29

Mayne, P. W. & F. H. Kulhawy. (1991). "*Calibration chamber database and boundary effects correction for CPT data*". Proceedings from the 1st International Symposium on Calibration Chamber Testing, Potsdam, NY, U.S.A.

Mohammandi, S.D., Nikoudel, M.R., Rahimi, H. and Khamehchiyan, M. (2007). *"Application of the Dynamic Cone Penetrometer (DCP) for determination of the engineering parameters of sandy soils".* Engineering Geology, 101 (3-4), pp 195-203

Monaco P., Marchetti, S., Totani, G & Calabrese, M. (2005). "*Sand liquefiability assessment by Flat Dilatometer Test (DMT)*". Paper delivered to University of L'Aquila, Italy, Local Conference, Osaka.

Monaco, P. and Marchetti, S. (2007) "*Evaluating Liquefaction Potential by Seismic Dilatometer (S_{DMT}) accounting for Aging*" Proceedings. 4th International Conference on Earthquakes. Geotechique Engineering. Thessaloniki.

Mn Road (2002). Department of Transportation Office of Minnesota Road Research. *User Guide to the Dynamic Cone Penetrometer*.[viewed http://www.mnroad.dot.state.mn/us] pdf copy

Mountain, M.I., van der Merwe, W.J. and Rosenthal, G.N. (1989). "Engineering geology of Cape Town in Contributions to engineering geology". Volume 1. A publication by the South African Institute of Engineering Geologists in collaboration with the Geological Survey of South Africa. 15-17; 21 pp

Murad, Y. Abu-Farsakh, Alshibli, K., Nazzal, M., & Ekrem Seyman. (2004). "*Assessment of in-situ test technology for construction control of base courses and embankments*". Faculty of Engineering and Architecture, Department of Civil and Environmental Engineering, American University of Beirut. pp 107

NBRI. (1984). :*A Technical Guide to Good House Construction"*. Published by the Association of Building Societies, Johannesburg.

Paige-Greem, P., Du PLessis, L. (2009). "*The Use And Interpretation Of The Dynamic Cone Penetrometer (DCP) Test"*. Version 2. CSIR Built Environment. Pretoria

Pournaghiaza, M., Russell, A.R., Khalili, N. (2011). "*Development of a new calibration chamber for conducting cone penetration tests in unsaturated soils".* Canadian Geotechnical Journal. Nr 48 (2): 314–321. Published by NRC Research Press

Parker Hannifin Corporation. 2010. [Online]. Available from: http://www.parker.com/
[Accessed 01/02/2010]

Raymond, G.P. (1997). "*Unified Soil Classification System*". Geotechnical, Engineering. American Society for Testing Materials (ASTM) via the two Standards ASTM-D2457 and ASTM-D2488

Reyna, F. & Chameau, J.L, (1991). "*Dilatometer Based Liquefaction Potential of Sites in the Imperial Valley*". Proceedings from the 2nd International Conference on Recent Advances in Geotechnical Earthquake Engineering and Soil Dynamics, St. Louis, USA.

Rosenthal, G. (2002). Seminar. "*Introduction to use of the DCP for Foundations"*. Paper read at SAICE workshop. Stellenbosch Business School.

Rogers, J. (1980). "*First report on the Cenozoic sediments between Cape Town and Elands Bay"*. Report, Geological Survey of South Africa, 1980-0249, 109 pp.

Sadek, S & Saleh, M, (2004). "*The effect of carbonaceous fines on the cyclic resistance of poorly graded sands*". Geotechnical Geological Engineering (2007) 25:257–264. Published online: 27 October 2006_ Springer Science + Business Media B.V. 2006

Salgado, R. (1993). "*Analysis of Penetration Resistance in Sands*". Ph.D. Dissertation. Department of Civil Engineering, University of California at Berkeley, Berkeley, CA, U.S.A.

Sampson,L.R. (1984). "*Investigation of the correlation between CBR and DCP"*. Pretoria: National Institute for Transport and Road Research, CSIR. (Technical Note TS/33/84).

Schmertmann, J.H. (1986). ASTM Subcommittee D 18.02.10. "*Suggested Method for Performing the Flat Dilatometer Test*". ASTM Geotechnical Testing Journal, Vol. 9, No. 2, Atlanta, Vol. 2: 883-888

Schmertmann, J. (2006) *Informal discussion with Mr Schmertmann on 3 April, Baltimore*. Held at Second International Conference on the Flat Dilatometer. Washington DC, April 2-5, 2006

Schmertmann, J.H, (1988). *Report No. FHWA-PA-87-022+84-24 to Pennsylvania DoT*, Office of Research and Special Studies, Harrisburg, PA, in 4 volumes.

Schmertmann, J.H., Baker, W., Gupta, R. & Kessler, K. (1986). "*CPT/DMT Quality Control of Ground Modification at a Power Plant*". Proceedings from Special Conference .Blacksburg. ASCE Geotechnical Spectrum. Publication No. 6, 985-1001.

Shamrani, M. A. (2004). "*Innovative Scheme for Evaluation of Soil Induced Stresses Using a Customized Two-Point Gauss Formula*". Journal of King Saud University, Engineering Sciences, Volume 17, No. 2.143-169 pp

Seed, H.B & I. M. Idriss. (1982)."*Ground motions and soil liquefaction during earthquakes"*. Earthquake Engineering Research Institute, Berkeley, CA, 134 pp

Seed, H.B & Idriss, I.M. (1971). "*Simplified Procedure for Evaluating Soil Liquefaction Potential*". Journal of Soil Mechanics. ASCE vol. 97, no. SM9, 1249-1273

Sitharam, T, GovindaRaju, L, Ramana, GV, & Hanumantha, C. (2004). "*Dynamic properties and liquefaction potential of soils*". Current science, Vol. 87, No. 10, 25.

South African Bureau of Standards, (1976). "*Standard specifications for sand for plaster and mortar*". SABS, 17 pp

Stapelberg, D.J. (2005*). "The Engineering Geology of the Melkbosstrand Area".* Explanation of the 1:50 000-Scale Map Sheet 3318 CB Melkbosstrand, Western Cape. Council for Geoscience, South Africa

Stott, T. (2011). "*Koeberg on the Edge*."Quote from newspaper article. Tabletalk. [Dated 23 March 2011]

Tanaka, H. & Tanaka, M. (1998). "*Characterization of Sandy Soils using CPT and DMT"*. Soils and Foundations, 38(3), 55-65

Terzaghi, K, Peck, R.B. (1967*). Soil Mechanics in Engineering Practice*, Second Edition: John Wiley & Sons, New York, p 729

Theron, J.N., Gresse, P.G., Siegfried, H.P, and Rogers, J. (1992). "*The Geology of the Cape Town Area*". Explanation of Sheet 3318 (1:250000), Geological Survey of South Africa

TMH1. (1986). Technical Methods for Highways. "Determining the grain size distribution of soil". TMH 1:A1(a) Chapter 1. Issued by the South African National Accreditation System.

TMH6 DRAFT METHOD ST6. (1984). "*Measurement of the In Situ Strength of soils by the Dynamic Cone Penetrometer (DCP)*".Special Methods for Testing Roads. Technical Methods for Highways (TMH), ISBN 07988 2289 9, Pages 19 to 24

Transport Research Laboratory. (1993). "*A guide to the structural design of bitumen-surfaced roads in tropical and sub-tropical countries*". Crowthorne: TRL. (Overseas Road Note 31).

Totani, G., Calabrese, M. & Monaco, P. (1998). "*In situ determination of C_h by flat dilatometer (DMT)*". Proceedings from 1st International Conference on Site Characterization ISC

Troncoso, J.H. & Verdugo (1985). "*Silt Content and Dynamic Behaviour of Tailings Sands.*" Proceedings from ICSMFE, San Francisco, Vol. 3, pp. 131—1314

US Geological Survey, (2008). "*What was that on the Richter scale*?" [Online]. Available from: http://hvo.wr.usgs.gov/ [Accessed 25/02/ 2008]

Yamamuro, J.A. & Lade, P.V. (1998). "*Steady-state concepts and static liquefaction of silty sands*". Journal of Geotechnical and Geo-environmental engineering, 124(9): 868-877

Youd, T.L. & Idriss, I.M. (2001). "*Liquefaction Resistance of Soils*". Summary Report from the 1996 NCEER and 1998 NCEER/NSF Workshops on Evaluation of Liquefaction Resistance of Soils. Journal GGE ASCE, 127(4), 297-313.

Visser, H.N. (1970). "*Die geologie van Blad 3318CB (Melkbosstrand)*": Field report of the Geological Survey of South Africa (unpublished,).

Zhou, Y.C. Xu, B.H., Yu, A.B., and Zulli, P. (2002). "*An experimental and numerical study of the angle of repose of coarse spheres".* Powder Technology 125, 45–54.

Zhou, Y.C., Chen, Y. Han, K. (2005). "Correlation of liquefaction resistance with shear wave velocity based on laboratory study using bender element". Journal of Zhejiang University SCIENCE. ISSN 1009-3095

APPENDICES

Appendix A. **Miscellaneous data**

The contents of this chapter include data not deemed necessary to include in the main body of the study. Some of the data are linked to other important calculations, i.e. moisture content needed for voids. Design data for calibration chamber are also found here. Images of structural damage referred to in the main text are shown here.

Table A.1 Marchettis' DMT reduction formula (Marchetti, 2001)

SYMBOL	DESCRIPTION	BASIC DMT REDUCTION FORMULAE	
p_0	Corrected First Reading	$p_0 = 1.05\ (A - Z_M + \Delta A) - 0.05\ (B - Z_M - \Delta B)$	Z_M = Gage reading when vented to atm. If ΔA & ΔB are measured with the same gage used for current readings A & B, set $Z_M = 0$ (Z_M is compensated)
p_1	Corrected Second Reading	$p_1 = B - Z_M - \Delta B$	
I_D	Material Index	$I_D = (p_1 - p_0) / (p_0 - u_0)$	u_0 = pre-insertion pore pressure
K_D	Horizontal Stress Index	$K_D = (p_0 - u_0) / \sigma'_{v0}$	σ'_{v0} = pre-insertion overburden stress
E_D	Dilatometer Modulus	$E_D = 34.7\ (p_1 - p_0)$	E_D is NOT a Young's modulus E. E_D should be used only AFTER combining it with K_D (Stress History). First obtain $M_{DMT} = R_M E_D$, then e.g. $E \approx 0.8\ M_{DMT}$
K_0	Coeff. Earth Pressure in Situ	$K_{0,DMT} = (K_D / 1.5)^{0.47} - 0.6$	for $I_D < 1.2$
OCR	Overconsolidation Ratio	$OCR_{DMT} = (0.5\ K_D)^{1.56}$	for $I_D < 1.2$
c_u	Undrained Shear Strength	$c_{u,DMT} = 0.22\ \sigma'_{v0}\ (0.5\ K_D)^{1.25}$	for $I_D < 1.2$
Φ	Friction Angle	$\Phi_{safe,DMT} = 28° + 14.6° \log K_D - 2.1° \log^2 K_D$	for $I_D > 1.8$
c_h	Coefficient of Consolidation	$c_{h,DMTA} \approx 7\ cm^2 / t_{flex}$	t_{flex} from A-log t DMT-A decay curve
k_h	Coefficient of Permeability	$k_h = c_h\ \gamma_w / M_h$ ($M_h \approx K_0\ M_{DMT}$)	
γ	Unit Weight and Description	(see chart in Fig. 16)	
M	Vertical Drained Constrained Modulus	$M_{DMT} = R_M E_D$ if $I_D \le 0.6$ $R_M = 0.14 + 2.36 \log K_D$ if $I_D \ge 3$ $R_M = 0.5 + 2 \log K_D$ if $0.6 < I_D < 3$ $R_M = R_{M,0} + (2.5 - R_{M,0}) \log K_D$ with $R_{M,0} = 0.14 + 0.15\ (I_D - 0.6)$ if $K_D > 10$ $R_M = 0.32 + 2.18 \log K_D$ if $R_M < 0.85$ set $R_M = 0.85$	
u_0	Equilibrium Pore Pressure	$u_0 = p_2 = C - Z_M + \Delta A$	In free-draining soils

Table A.2 Accelerometer vibration frequencies on Philippi sand

Assistance from Dr Jonkers (University of Cape Town) was received in measuring these frequencies and providing the data. An accelerometer was used to measure the frequencies inside and outside the chamber wall.

SLM & RTA Summary						
Translated:	01-Aug-08	17:56:14				
File Translated:	C:\Ac Projects\Schools\Cape Technikon\D1.slmdl					
Model Number:	824					
Serial Number:	A0790					
Firmware Rev:	4.23					
Software Version:	3.12					
Name:	A. Jongens					
Descr1:	Jongens Keet Associates					
Descr2:	+27 (0)21 7945643					
Setup:	SLM&RTA.ssa					
Setup Descr:	SLM & Real-Time Analyzer					
Location:						
Note 1:						
Note 2:						
Overall Any Data						
Start Time:	01-Aug-08	11:24:49				
Elapsed Time:	00:05.1					
	A Weight	C Weight	Flat			
Leq:	56.4 dBA	70.6 dBC	71.2 dBF			
SEL:	63.5 dBA	77.7 dBC	78.3 dBF			
Peak:	69.3 dBA	80.8 dBC	81.4 dBF			
	2008/08/01 11:24	2008/08/01 11:24	2008/08/01 11:24			
Lmax (slow):	61.0 dBA	74.4 dBC	71.8 dBF			
	2008/08/01 11:24	2008/08/01 11:24	2008/08/01 11:24			
Lmin (slow):	54.3 dBA	70.0 dBC	70.4 dBF			
	2008/08/01 11:24	2008/08/01 11:24	2008/08/01 11:24			
Lmax (fast):	57.7 dBA	71.4 dBC	71.9 dBF			
	2008/08/01 11:24	2008/08/01 11:24	2008/08/01 11:24			
Lmin (fast):	54.0 dBA	69.9 dBC	70.0 dBF			
	2008/08/01 11:24	2008/08/01 11:24	2008/08/01 11:24			
Lmax (impulse):	58.2 dBA	71.7 dBC	72.2 dBF			
	2008/08/01 11:24	2008/08/01 11:24	2008/08/01 11:24			
Lmin (impulse):	54.3 dBA	70.0 dBC	70.4 dBF			
	2008/08/01 11:24	2008/08/01 11:24	2008/08/01 11:24			
Spectra						
Start Time:	01-Aug-08	11:24:49	Run Time:	00:05.1		
Freq Hz	Leq 1/3 Oct	Leq 1/1 Oct	Max 1/3 Oct	Max 1/1 Oct	Min 1/3 Oct	Min 1/1 Oct
12.5	1.9		3.9		-6.9	
16	5	8.9	6.2	8.8	0.9	2.9
20	4.8		-0.4		-2.9	
25	7.3		8.3		-1.2	
31.5	10	66.3	12.1	65.5	4.7	65.3
40	66.3		65.5		65.3	
50	64.7		64.5		64.5	
63	17.4	65.4	18.3	65.7	12.8	64.5
80	57.2		59.6		43.1	
100	55.9		59.1		31.2	
125	63.4	65.7	64.7	67.2	61.2	63.3
160	60.7		61.6		59.1	
200	61		62.8		57.5	
250	58.1	63.1	59.4	64.7	56	60.3
315	51.1		52.3		50.2	
400	47.6		49		43.9	
500	40.8	48.6	42	50.2	38.9	45.2
630	35.6		39.2		29.3	
800	34		36.7		25.2	
1000	23	34.6	26.5	37.3	19.5	26.9
1250	22.1		24.8		18.4	
1600	19.3		20.1		17.9	
2000	20.2	32.1	20	32.3	19.1	30.8
2500	31.6		31.7		30.3	
3150	38.4		38.4		36.8	
4000	34.6	42	34.7	42.2	33.4	40.6
5000	37.8		38.3		36.6	
6300	38.7		37.3		37	
8000	39.4	44	40.3	44.1	38.6	43
10000	39.6		39.9		38.8	
12500	42.5		42.7		41.5	
16000	43.1	47.2	43.3	47.6	42	46.1
20000	41.5		42.4		40.4	

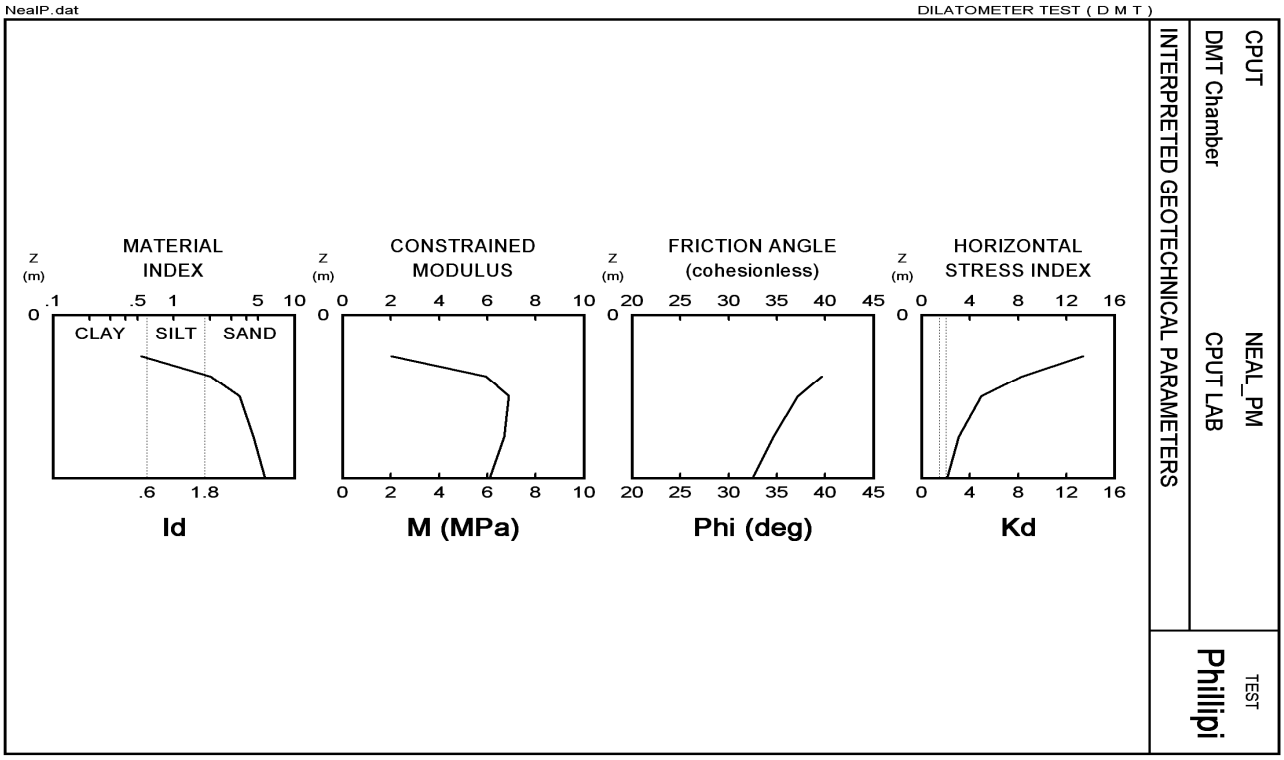

Figure A.1 DMT graphic for strength parameters (CPUT chamber, 2008)

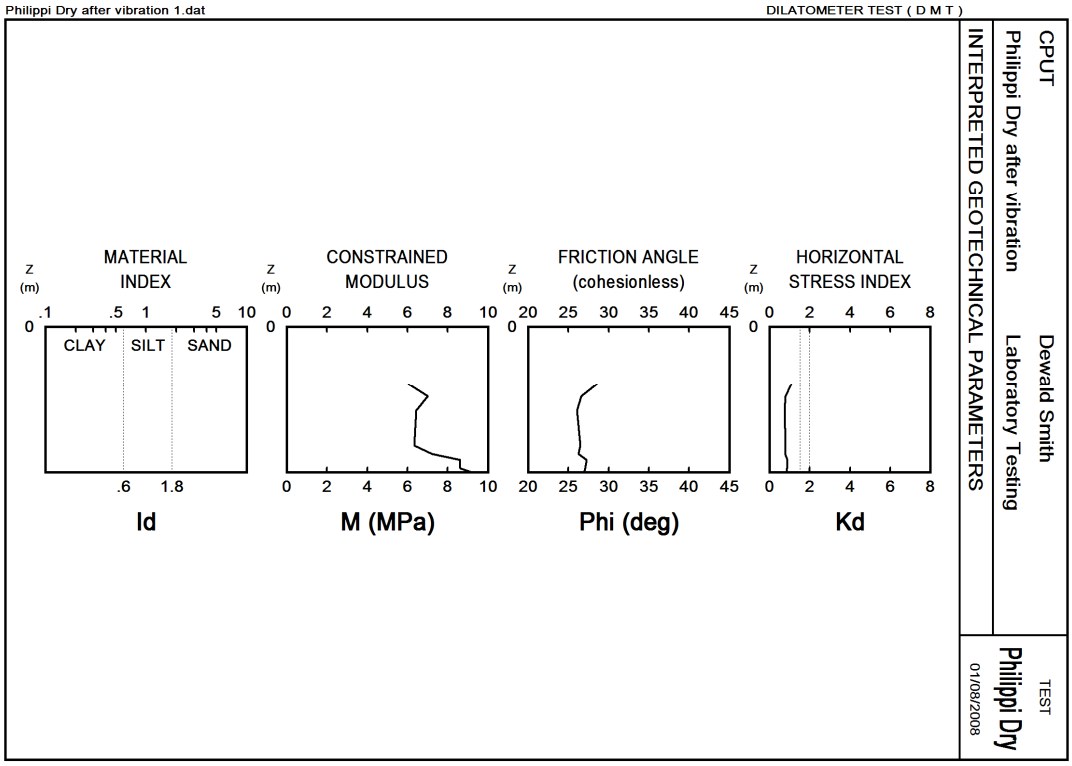

Figure A.2 DMT parameters for non-vibrated Philippi sand (CPUT chamber, 2008)

Table A.3 Software calculations for bearing capacity and settlement_pre-vibration (WC)

The software provides two settlement estimates, namely Burland and Burbrige (1985) and Bowles (1986). The SPT_N values have been estimated with the inverted DCP_{DN}.

```
CORRECT BEARING CAPACITY    04-08-2008
Run No:  1    Page  1
    Project Name:West Coast pre-vibr
Reference Number:
        Engineer:

BEARING CAPACITY AND SETTLEMENT DATA

SETTINGS                        Units          SI
                      Units of Load            kiloNewtons per square meter
Influence Value (x Footing Width)              2 times
                       Footing Type            Strip

LOADING
                         Total Load            50.
          Inclination of Load (deg)             0
                  Eccentricity (m)              .

SOIL 1
                      Density (kN/m^3)          14.6
                 Footing Depth (m)              0.8

SOIL 2
                      Density (kN/m^3)          14.6
               Friction Angle (deg)             39
                    Cohesion (kN/m^2)           0
                       Width (m)                0.8
               Effective Width (m)              .8
                        Length (m)              8.
             Groundwater Depth (m)              1
           Ave N-Value (bl/305mm)               5
FACTORS                          Nc            67.85
                                 Fcs           .
                                 Fcd           .
                                 Fci           .
                                  Nq           55.94
                                 Fqs           1.
                                 Fqd           1.22
                                 Fqi           1.
                                  Ng           77.31
                                 Fgs           1.
                                 Fgd           1.
                                 Fgi           1.
RESULTS
              Cohesion Term (kN/m^2)            .
            Surcharge Term (kN/m^2)             798.8
                Wedge Term (kN/m^2)             185.5
             Large Footing Correction           1.
 Ultimate Bearing Capacity (kN/m^2)             984.4
          Required Factor of Safety              3
Allowable Bearing Capacity (kN/m^2)             328.1
   Actual Bearing Pressure (kN/m^2)             50.
            Actual Factor of Safety             19.7
SETTLEMENT             (Bowles) (mm)            7.64
          (Burland & Burbidge) (mm)             11.43
```

Table A.4 Software calculations for bearing capacity and settlement_post vibration (WC)

```
CORRECT BEARING CAPACITY    09-08-2008
Run No:  2    Page  1
    Project Name: West Coast_post vibr.
Reference Number:
        Engineer:

BEARING CAPACITY AND SETTLEMENT DATA

SETTINGS                        Units          SI
                    Units of Load          kiloNewtons per square meter
Influence Value (x Footing Width)          2 times
                     Footing Type          Strip

LOADING
                       Total Load          50.
        Inclination of Load (deg)           0
                Eccentricity (m)           .

SOIL 1
                    Density (kN/m^3)       16.9
               Footing Depth (m)           0.8

SOIL 2
                    Density (kN/m^3)       16.9
             Friction Angle (deg)          39
                  Cohesion (kN/m^2)         0
                       Width (m)            0.8
             Effective Width (m)           .8
                     Length (m)            8.
          Groundwater Depth (m)            1
         Ave N-Value (bl/305mm)             7
FACTORS                          Nc        67.85
                                 Fcs       .
                                 Fcd       .
                                 Fci       .
                                  Nq       55.94
                                 Fqs       1.
                                 Fqd       1.22
                                 Fqi       1.
                                  Ng       77.31
                                 Fgs       1.
                                 Fgd       1.
                                 Fgi       1.
RESULTS
             Cohesion Term (kN/m^2)        .
            Surcharge Term (kN/m^2)        924.7
               Wedge Term (kN/m^2)         274.5
           Large Footing Correction        1.
 Ultimate Bearing Capacity (kN/m^2)        1199.1
         Required Factor of Safety          3
Allowable Bearing Capacity (kN/m^2)        399.7
   Actual Bearing Pressure (kN/m^2)        50.
            Actual Factor of Safety        24.
SETTLEMENT              (Bowles) (mm)      5.19
          (Burland & Burbidge) (mm)        7.13
```

Table A.5 Software calculations for bearing capacity and settlement_pre vibration (PH)

```
CORRECT BEARING CAPACITY    01-08-2008
Run No:  6    Page  1
    Project Name: Philippi sand pre-vibr.
Reference Number:
        Engineer:

BEARING CAPACITY AND SETTLEMENT DATA

SETTINGS                        Units          SI
                        Units of Load          kiloNewtons per square meter
Influence Value (x Footing Width)              2 times
                         Footing Type          Strip

LOADING
                          Total Load           50.
        Inclination of Load (deg)               0
                Eccentricity (m)                .

SOIL 1
                       Density (kN/m^3)        14.6
                Footing Depth (m)              0.8

SOIL 2
                       Density (kN/m^3)        14.6
             Friction Angle (deg)              35
                   Cohesion (kN/m^2)            0
                       Width (m)               0.8
             Effective Width (m)               .8
                      Length (m)               8.
           Groundwater Depth (m)               1
          Ave N-Value (bl/305mm)               4
FACTORS                          Nc            46.11
                                 Fcs           .
                                 Fcd           .
                                 Fci           .
                                 Nq            33.29
                                 Fqs           1.
                                 Fqd           1.25
                                 Fqi           1.
                                 Ng            37.14
                                 Fgs           1.
                                 Fgd           1.
                                 Fgi           1.
RESULTS
              Cohesion Term (kN/m^2)           .
            Surcharge Term (kN/m^2)            487.8
                Wedge Term (kN/m^2)            89.1
           Large Footing Correction            1.
 Ultimate Bearing Capacity (kN/m^2)            577.
          Required Factor of Safety             3
Allowable Bearing Capacity (kN/m^2)            192.3
   Actual Bearing Pressure (kN/m^2)            50.
            Actual Factor of Safety            11.5
SETTLEMENT              (Bowles) (mm)          9.55
          (Burland & Burbidge) (mm)            15.62
```

Table A.6 Software calculations for bearing capacity and settlement_post vibration (PH)

```
CORRECT BEARING CAPACITY    01-08-2008
Run No:  9    Page  1
    Project Name: Philippi sand _post vibr.
Reference Number:
        Engineer:

BEARING CAPACITY AND SETTLEMENT DATA

SETTINGS                      Units          SI
                    Units of Load          kiloNewtons per square meter
Influence Value (x Footing Width)          2 times
                     Footing Type          Strip

LOADING
                       Total Load          50.
        Inclination of Load (deg)           0
                Eccentricity (m)            .

SOIL 1
                    Density (kN/m^3)        16.2
               Footing Depth (m)            0.8

SOIL 2
                    Density (kN/m^3)        16.2
             Friction Angle (deg)           35
                  Cohesion (kN/m^2)          0
                      Width (m)             0.8
             Effective Width (m)            .8
                    Length (m)              8.
          Groundwater Depth (m)             1
         Ave N-Value (bl/305mm)             7
FACTORS                        Nc           46.11
                               Fcs          .
                               Fcd          .
                               Fci          .
                                Nq          33.29
                               Fqs          1.
                               Fqd          1.25
                               Fqi          1.
                                Ng          37.14
                               Fgs          1.
                               Fgd          1.
                               Fgi          1.
RESULTS
            Cohesion Term (kN/m^2)          .
          Surcharge Term (kN/m^2)           541.3
              Wedge Term (kN/m^2)           118.9
           Large Footing Correction         1.
 Ultimate Bearing Capacity (kN/m^2)         660.1
         Required Factor of Safety           3
Allowable Bearing Capacity (kN/m^2)         220.
   Actual Bearing Pressure (kN/m^2)         50.
            Actual Factor of Safety         13.2
SETTLEMENT             (Bowles) (mm)        5.27
          (Burland & Burbidge) (mm)         7.13
```

Table A.7 DCP data for West Coast sand in the chamber

West Coast sand					
Test hole 1		Test hole 2		Test hole 3	
Depth (mm)	mm/blow	Depth (mm)	mm/blow	Depth (mm)	mm/blow
10		40		30	
85	75	125	85	100	70
140	55	195	70	155	55
200	60	250	55	210	55
250	50	305	55	255	45
300	50	353	48	300	45
355	55	402	49	350	50
410	55	450	48	400	50
455	45	488	38	450	50
505	50	530	42	500	50
570	65	574	44	550	50
625	55	615	41	600	50
660	35	640	25	645	45
700	40	675	30	670	25
735	35	705	30	705	35
760	25	735	30	740	35
785	25	755	20	770	30
		780	25		
Average Depth per blow		Average Depth per blow		Average Depth per blow	
48,21 mm/blow		42 mm/blow		45,71 mm/blow	

Figure A.3 DMT graphics for properties on moist West Coast Sand

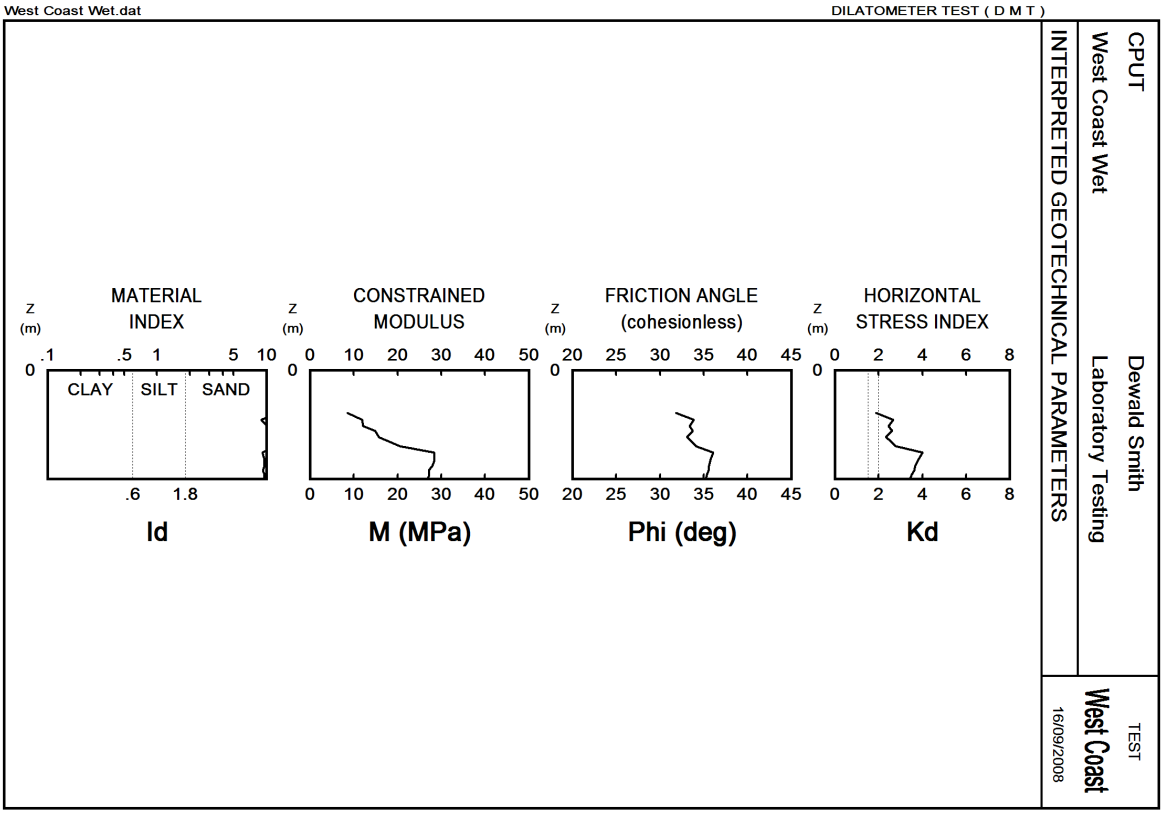

Table A.8 Full DMT graphics for parameters on dry Philippi sand (CPUT Chamber, 2008)

Philippi Dry

01/08/2008Philippi Dry after vibration 1.dat

CPUT

Dewald Smith

Philippi Dry after vibration

Laboratory Testing

Test Hole 1

LEGEND
Z = Depth Below Ground Level
Po,P1,P2 = Corrected A,B,C readings
Id = Material Index
Ed = Dilatometer modulus
Ud = Pore Press. Index = (P2-Uo)/(Po-Uo)
Gamma = Bulk unit weight
Sigma' = Effective overb. stress
Uo = Pore pressure

INTERPRETED PARAMETERS
Phi = Safe floor value of Friction Angle
Ko = In situ earth press. coeff.
M = Constrained modulus (at Sigma')
Cu = Undrained shear strength
Ocr = Overconsolidation ratio (OCR = "relative OCR"- generally realistic. If accurate independent OCR available, apply suitable OCR Factor)

SOUNDING PARAMETERS
DeltaA = 5 kPa
DeltaB = 40 kPa
GammaTop = 50.0 kN/m^3
FactorEd = 34.7
Zm = 0.0 kPa
Zabs = 0.0 m
Zw > Zfinal

Water Level below end of sounding
Reduction formulae according to Marchetti, ASCE Geot.Jnl.Mar. 1980, Vol.109, 299-321; Phi according to TC16 ISSMGE, 2001

Z (m)	A (kPa)	B (kPa)	C (kPa)	Po (kPa)	P1 (kPa)	P2 (kPa)	Gamma (kN/m^3)	Sigma' (kPa)	Uo (kPa)	Id	Kd	Ed (MPa)	Ud	Ko	Ocr	Phi (Deg)	M (MPa)	Cu (kPa)	Philippi Dry DESCRIPTION
0.28	20	260		15	220		16.7	14	0	13.43	1.1	7.1				29	6.0		SAND
0.34	15	290		12	250		16.7	15	0	19.83	0.8	8.3				27	7.0		SAND
0.41	15	270		12	230		16.7	16	0	18.17	0.7	7.6				26	6.4		SAND
0.58	20	270		15	230		16.7	19	0	14.33	0.8	7.5				26	6.3		SAND
0.62	20	300		15	260		16.7	20	0	16.33	0.8	8.5				26	7.2		SAND
0.65	25	350		18	310		16.7	20	0	16.22	0.9	10.1				27	8.6		SAND
0.69	25	350		18	310		16.7	21	0	16.22	0.9	10.1				27	8.6		SAND
0.71	25	370		18	330		16.7	21	0	17.33	0.9	10.8				27	9.2		SAND

Appendix B. **Calibration Chamber Design**

The content here is related to the design detail for the calibration chamber.

Table B.1 Airmount isolator criteria.

AIRMOUNT® ISOLATORS

Style Number	Design Height	Load (at Design Height) at 100 PSIG (pounds)	Natural Frequency (@ 80 PSIG) f_n(cpm)	% of Isolation at Forced Frequency	
				400 CPM %	800 CPM %
SHAPED SLEEVE					
1M1A-0	2.5	570	220		91.8
1M1A-1	3.0	593	162	90.0	95.5
2M1A	DO NOT USE 2M1A AS AN AIRMOUNT ISOLATOR				
2M2A	2.0	198	232		90.8
SINGLE CONVOLUTION					
16	3.0	1120	237		90.3
16ST	3.0	1000	240	87.0	97.0
131	3.5	1510	181	74.4	94.6
110	4.5	1790	162	80.2	95.7
116	4.5	2360	163	80.2	95.7
116-1	5.5	2530	139	86.3	96.9
115	4.5	3010	166	79.1	95.5
19	5.0	5680	156	82.1	96.0
19-.75	5.5	5260	156	82.0	96.0
113	5.0	8800	150	83.6	96.4
113-1	5.5	10,200	133	87.7	97.2
153-2	6.0	12,385	121	89.9	97.7
119**	5.0	14,520	138	86.5	96.9
121**	5.0	18,450	142	85.5	96.7
126**	5.0	28,290	133	87.5	97.1
138-1.5	6.0	41,620	124	89.3	97.5
148-1	5.5	85,200	118	90.5	97.8
DOUBLE CONVOLUTION					
25	5.5	1180	154	82.5	96.1
255-1.5	6.0	1524	129	87.6	97.2
224	6.5	1940	126	89.0	97.5
26	8.0	2140	111	91.6	98.0
20	8.5	2720	116	90.7	97.8
20-2	10.0	3238	97	93.7	98.5
22	9.5	5400	106	92.4	98.2
22-1.5	10.5	5310	106	92.4	98.2
21	9.5	8330	105	92.6	98.3
21-2	10.5	9210	95	94.1	98.6
233-2	11.25	9917	89	95.0	98.8
28**	9.5	12,120	101	93.2	98.4
203**	9.5	18,890	97	93.7	98.5
29**	9.5	25,350	92	94.4	98.7
200	9.5	34,620	93	94.2	98.6
215	10.5	40,980	86	95.1	98.8
248-2	11.0	79,730	83	95.5	98.9

Table B.2 Vibratory Motor specifications

This table displays the vibratory motor specifications. The choice of the motor type is dependant on the centrifugal force required. The suppliers offered the VV05N2-380 V model operating at 50 Hz.

TECHNICAL FEATURES 2 POLES - 3000 RPM 50Hz / 3600 RPM 60 Hz														
CODE	TYPE	SIZE	CENTRIFUGAL FORCE				STATIC MOMENT		WEIGHT		IMPUT POWER		MAX CURRENT	
			Kgf		kN		Kgmm		Kg		kW		A	
			50Hz	60Hz	50Hz	60Hz	50Hz	60Hz	50Hz	60Hz	50Hz	60Hz	50Hz 380V	60Hz 460V
V2001	VV03N/2	BA	120	110	1,18	1,08	12	7,5	5,8	5,6	0,17	0,17	0,33	0,29
V2002	VV05N/2	BA	205	190	2,01	1,87	20	13	6,3	5,9	0,17	0,17	0,33	0,29
V2003	VV10N/2	CA	320	310	3,14	3,04	32	21	9,7	9,2	0,25	0,26	0,57	0,48
V2004	VV15N/2	DA	520	490	5,10	4,81	52	34	14,8	13,8	0,43	0,47	0,76	0,71
V2005	VV25N/2	EA	800	770	7,85	7,56	80	53	21	20	0,61	0,65	1,0	0,95
V2012	VV35N/2 (**)	GA	1150	1100	11,3	10,8	144	76	24	23	0,95	1,1	1,6	1,6
V2006	VV38N/2	IB	1600	1500	15,7	14,7	159	104	43	41,5	1,9	1,9	3,2	2,8
V2007	VV40N/2	IB	2350	2250	23,1	22,1	234	155	53	51,5	2,1	2,1	3,4	2,9
V2008	VV45N/2	MB	3500	3150	34,3	30,9	348	217	96	91	3,8	3,8	6,2	5,4
V2009	VV55N/2	MB	4000	3800	39,2	37,3	398	262	98	93	3,8	3,8	6,2	5,4
V2010	VV60N/2	MB	5200	5200	51,1	51,1	517	359	110	108	4,7	4,7	4,6	6,5

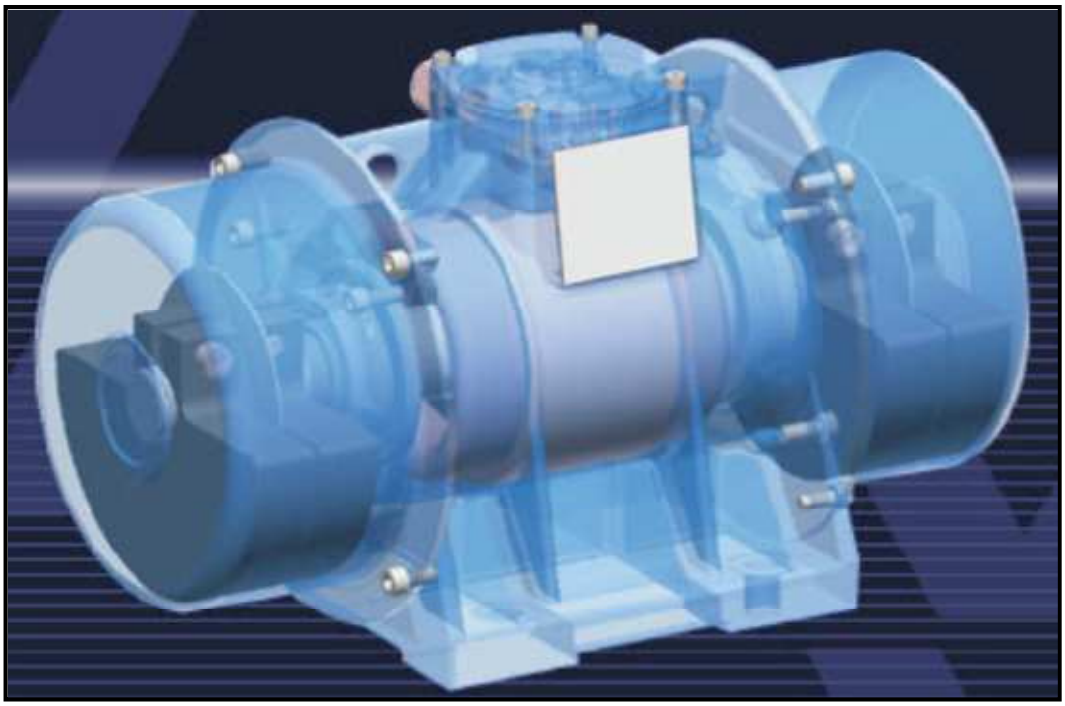

Figure B.1 Airmount position under the chamber. The tyre is inflated to 2 bars.

Figure B.2 Geofabric lining

The chamber base was lined with geo-fabric above the saturation pipes. The gravel was sieved G5 gravel. All fractions passing the 4.75 mm was discarded, so that clogging during drainage was kept to a minimum.

Table B.3 Senso Gauge specifications

The table here displays the specifications of the Senso-gauge, supplied by Hyflo and manufactured by Parker. (CPUT Chamber, 2009)

Input dimensions		Low pressure		
Measuring range	bar	-1 to 4	-1 to 10	-1 to 16
Overload pressure	bar	10	20	40
Burst pressure	bar	12	25	50
Measuring element		ceramic		
Switching cycles		> 100 mio.		
Tightening Torque	35 Nm			
Medium Temperature		25 °C to +85 °C		
Weight		± 300 grams		
Output dimensions				
Accuracy		0.5% FS typical		±1% FS max
Temperature drift		±0.02 % FS/°K typical		±0.03 % FS/°K max
Long-term stability		± 0.2 % FS/a		
Repeatability		± 0.25% FS		
Display accuracy		±0.5% FS typical ± 1 digit ±1% FS max ± 1 digit		
Response speed				
Switch output		<10ms		
Analogue output		<10 ms		

Figure B.3 CAD design for DMT shaft coupling

Figure B.4 CAD design for DMT shaft coupling

Figure B.5 CAD design for DMT shaft assembly

Figure B.6 CAD design for DMT shaft screw assembly

Figure B.7 CAD design for DMT shaft mid-section assembly

Measurements taken with a calliper for the purposes of determining the angle of repose for the study sands.

Figure B.8 Height measurement for angle of repose

Figure B.9 Width measurement for angle of repose

The standard density funnel for in-place sand replacement was used for pluviating sand during maximum and minimum void (e) determinations. The height above the mould was set to 100 mm.

Figure B.10 Apparatus for sand pluviation

Table B.4 Raw data for void calculations

This table presents the raw data used for calculating all applicable voids and % relative density, D_R

Sample Nr		Big Bay.D1 N GPS S33.47.06.4 E 18.27.06.6						
Mould Specifications		Sample 1	Sample 2	Sample 3	Sample 4	Sample 5	Sample 6	
Height w/spacer, mm	78		G_s					
Diameter, mm	101	2.65						
Weight w/spacer, g	2581							
Volume, m^3	0.000624924							
		Voids, max						Ave
Mould + dry loose sand		3497	3498	3498	3500	3500	3502	
Mass dry loose sand		916	917	917	919	919	921	
Minimum density, kg/m^3		1465.8	1467.4	1467.4	1470.6	1470.6	1473.8	1469.2
voids, e max		0.808	0.806	0.806	0.802	0.802	0.798	0.804
		Voids, min						
Mould + dry comp. sand		3650	3643	3655	3657	3640	3658	
Mass dry comp. sand		1069	1062	1074	1076	1059	1077	
Maximum density		1710.6	1699.4	1718.6	1721.8	1694.6	1723.4	1711.4
voids, e min		0.549	0.559	0.542	0.539	0.564	0.538	0.548
In-situ wet density		1726	1735	1729	1723	1716	1722	1723
In-situ moisture content		3.61	3.2	3.6	3.7	3.2	3.4	3.3
In-situ dry density		1665.9	1681.2	1668.9	1661.5	1662.8	1665.4	1668.0
In-situ voids, e		0.591	0.576	0.588	0.595	0.594	0.591	0.589
% D_R		83.9%	93.2%	82.6%	78.8%	87.4%	79.4%	84.2%

Table B.5 DCP raw data

3 LANDS END, AT ANTIC BEACH (Aeolian wind blown dune sands, UCSC classification = SW-SP)

TEST 1	Depth BGL	PR-mm/blow	CBR [3]	Q_u (kPa) [2]	TEST 2	Depth BGL	PR-mm/blow	CBR	C (kPa)	TEST 3	Depth BGL	PR-mm/blow	CBR	Q (kPa)	TEST 4	Depth	PR-mm/blow	CBR	Q (kPa)	TEST 5	Depth	PR-mm/blow	CBR	Q (kPa)	TEST 6	Depth	PR-mm/blow	CBR	Q (kPa)
0.0	50.0				0.0	1280.0				0.0	470.0				0.0	85.0				0.0	115.0				0.0	280.0			
3.0	145.0	31.7	6.1	86.8	3.0	1290.0	3.3	75.8	462.9	3.0	580.0	35.7	5.2	77.8	2.0	275.0	95.0	1.8	38.3	2.0	315.0	100.0	1.7	36.9	2.0	410.0	65.0	2.7	50.8
3.0	265.0	40.0	4.7	72.9	3.0	1310.0	6.7	34.9	276.4	3.0	695.0	38.3	4.9	75.3	2.0	350.0	37.5	5.0	76.5	2.0	400.0	42.5	4.4	69.7	2.0	450.0	20.0	10.2	122.1
3.0	490.0	75.0	2.3	45.7	3.0	1320.0	3.3	75.8	462.9	3.0	795.0	33.3	5.3	83.5	2.0	420.0	35.0	5.4	80.5	2.0	470.0	35.0	5.4	80.5	2.0	485.0	17.5	11.8	134.9
3.0	595.0	35.0	5.4	80.5	3.0	1335.0	5.0	48.1	342.4	3.0	875.0	26.7	7.1	98.6	2.0	460.0	20.0	10.2	122.1	2.0	530.0	30.0	6.5	90.3	2.0	520.0	17.5	11.8	134.9
3.0	675.0	26.7	7.4	98.6	3.0	1345.0	3.3	75.8	462.9	3.0	955.0	26.7	7.1	98.6	2.0	490.0	15.0	14.1	151.2	2.0	580.0	25.0	7.9	103.4	2.0	545.0	12.5	17.3	173.2
3.0	740.0	21.7	9.3	115.1	3.0	1350.0	1.7	164.8	775.1	3.0	1050.0	31.7	6.1	86.8	2.0	530.0	20.0	10.2	122.1	2.0	640.0	30.0	6.5	90.3	2.0	570.0	12.5	17.3	173.2
3.0	815.0	25.0	7.9	103.4	3.0	1370.0	6.7	34.9	276.4	3.0	1150.0	33.3	5.3	83.5	2.0	570.0	20.0	10.2	122.1	2.0	690.0	25.0	7.9	103.4	2.0	600.0	15.0	14.1	151.2
3.0	895.0	26.7	7.4	98.6	3.0	1380.0	3.3	75.8	462.9	3.0	1235.0	28.3	6.7	94.3	2.0	600.0	15.0	14.1	151.2	2.0	750.0	30.0	6.5	90.3	2.0	625.0	12.5	17.3	173.2
3.0	980.0	28.3	6.9	94.3	3.0	1390.0	3.3	75.8	462.9	3.0	1330.0	31.7	6.1	86.8	2.0	630.0	15.0	14.1	151.2	2.0	815.0	32.5	5.9	85.1	2.0	655.0	15.0	14.1	151.2
3.0	1060.0	26.7	7.4	98.6	3.0	1405.0	5.0	48.1	342.4	3.0	1395.0	21.7	9.3	115.1	2.0	655.0	12.5	17.3	173.2	2.0	880.0	32.5	5.9	85.1	2.0	685.0	15.0	14.1	151.2
3.0	1135.0	25.0	7.9	103.4	3.0	1425.0	6.7	34.9	276.4	3.0	1445.0	16.7	12.5	139.9	2.0	680.0	12.5	17.3	173.2	2.0	950.0	35.0	5.4	80.5	2.0	720.0	17.5	11.8	134.9
3.0	1230.0	31.7	6.1	86.8	3.0	1440.0	5.0	48.1	342.4	3.0	1475.0	10.0	22.2	204.5	2.0	700.0	10.0	22.2	204.5	2.0	1010.0	30.0	6.5	90.3	2.0	760.0	20.0	10.2	122.1
3.0	1340.0	36.7	5.2	77.8	3.0	1470.0	10.0	22.2	204.5	3.0	1505.0	10.0	22.2	204.5	2.0	720.0	10.0	22.2	204.5	2.0	1065.0	27.5	7.1	96.4	2.0	800.0	20.0	10.2	122.1
3.0	1420.0	26.7	7.4	98.6	3.0	1515.0	15.0	14.1	151.2	3.0	1535.0	10.0	22.2	204.5	2.0	740.0	10.0	22.2	204.5						2.0	840.0	20.0	10.2	122.1
3.0	1480.0	20.0	10.2	122.1	3.0	1550.0	11.7	18.6	182.3	3.0	1565.0	10.0	22.2	204.5	2.0	760.0	10.0	22.2	204.5						2.0	900.0	30.0	6.5	90.3
3.0	1530.0	16.7	12.5	139.9	3.0	1570.0	6.7	34.9	276.4	3.0	1600.0	11.7	18.5	182.3	2.0	785.0	12.5	17.3	173.2						2.0	990.0	45.0	4.1	66.8
3.0	1575.0	15.0	14.1	151.2	3.0	1600.0	10.0	22.2	204.5	2.0	1620.0	10.0	22.2	204.5	2.0	800.0	7.5	30.6	253.3						2.0	1060.0	35.0	5.4	80.5
3.0	1615.0	13.3	16.0	165.1	3.0	1620.0	6.7	34.9	276.4	2.0	1645.0	12.5	17.3	173.2	2.0	820.0	10.0	22.2	204.5										
3.0	1650.0	11.7	18.6	182.3	3.0	1640.0	6.7	34.9	276.4	2.0	1670.0	12.5	17.3	173.2	2.0	840.0	10.0	22.2	204.5										
3.0	1685.0	11.7	18.6	182.3	3.0	1665.0	8.3	27.2	234.2	2.0	1690.0	10.0	22.2	204.5	2.0	855.0	7.5	30.6	253.3										
3.0	1720.0	11.7	18.6	182.3	3.0	1680.0	5.0	48.1	342.4	2.0	1715.0	12.5	17.3	173.2	2.0	870.0	7.5	30.6	253.3										
3.0	1750.0	10.0	22.2	204.5	3.0	1690.0	3.3	75.8	462.9	2.0	1730.0	7.5	30.5	253.3	2.0	885.0	7.5	30.6	253.3										
3.0	1780.0	13.0	16.5	168.2	3.0	1700.0	3.3	75.8	462.9	2.0	1745.0	7.5	30.5	253.3	2.0	900.0	7.5	30.6	253.3										
3.0	1810.0	7.0	33.0	266.6	3.0	1710.0	3.3	75.8	462.9	2.0	1755.0	5.0	48.1	342.4	2.0	920.0	10.0	22.2	204.5										
3.0	1840.0	10.0	22.2	204.5	3.0	1715.0	1.7	164.8	775.1	2.0	1770.0	7.5	30.5	253.3	2.0														
3.0	1875.0	11.7	18.6	182.3	3.0	1730.0	5.0	48.1	342.4	2.0	1785.0	7.5	30.5	253.3	2.0														
3.0	1910.0	11.7	18.6	182.3	3.0	1745.0	5.0	48.1	342.4	2.0	1795.0	5.0	48.1	342.4	2.0														
3.0	1945.0	11.7	18.6	182.3	3.0	1750.0	1.7	164.8	775.1	2.0	1815.0	10.0	22.2	204.5	2.0														
										2.0	1840.0	12.5	17.3	173.2	2.0														
	no resistance		Ave Q_u	134.9		no resistance		Ave Q	582.3	2.0	1855.0	7.5	30.5	253.3	2.0														
			s/deviation	21.6				s/deviation	131.8	2.0	1870.0	7.5	30.5	253.3	2.0														
	PR Ave	22.6	Settlement	19.0		PR Ave	5.5	Settlement	9.7	2.0	1890.0	10.0	22.2	204.5	2.0														
	SPT N	13.5	E_s [5]	39919		SPT N	54.5	E_s [6]	39395117.5622	2.0	1910.0	10.0	22.2	204.5	2.0														
			Densification	Medium Dense				Densification	Dense	2.0					2.0														
			Compaction	90-95%				Compaction	95-98%	2.0					2.0														
											PR Ave	16.1	Ave Q	180.6		PR Ave	17.4	Ave Q	176.4		Ave PR	36.5	Ave Q	84.8		Ave PR	22.9	Ave Q	126.8
											SPT N	18.9	s/deviation	73.8				s/deviation	60.5				s/deviation	17.1				s/deviation	36.6
											% RD	43.5	Settlement	24.0				Settlement	12.0				Settlement	12.0				Settlement	6.0
													E_s [4]	77169				E_s [4]	65180				E_s [4]	15604.0				E_s [4]	38653.8
													Densification	Medium Dense				Densification	Medium Dense				Densification	Loose				Densification	Medium Dense
													Compaction	90-95%				Compaction	90-95%				Compaction	85-90%				Compaction	90-95%

Notes

1 CL soils CBR < 10: CBR = 1 / (0.017019*PR)^2

CH soils: CBR = 1/ (0.002871*PR)

For analysis of shallow foundations an estimate of bearing capacity can be made from the following equations adapted from the Portland Cement Association (PCA) showing the relationship between bearing capacity and CBR.

2 $Q_u = (3.794 * CBR^{0.661}) * 6.89$ (kPa)

3 CBR = 292 / $PR^{1.12}$ (% in-situ)

4 Settlement Calculations (mm)

Calculates settlement of a footing placed on a cohesionless material (sand) using the Schmertmann method (Schmertmann, 1970, Schmertmann et al, 1978). Only the lower 1 m considered below actual foundation

5 Differential Settlements

Consult NHBRC Guidelines Manual 1 & 2, 1999

Site classification based on 50% expected differential settlement of total consolidation

CPT, $Q_c = 7.56 * Ln(N_{DCP}) - 9.28$

N_{DCP} DCP blows/450 mm

6 Es = soil elasticity, based on Plate test comparitive research by Murad (Murad, et al, 2004: Peh, 1990)

=(5142.61/($PR^{1.57}$-14.8)) -3.49 Mpa

Figure B.11 Study Area (Melkbos Strand)

Appendix C. **Structural damage caused by settlement in windblown sand**

The images here were recorded and supplied by the local regulatory body, the NHBRC, designated by Government to control the quality of building standards.

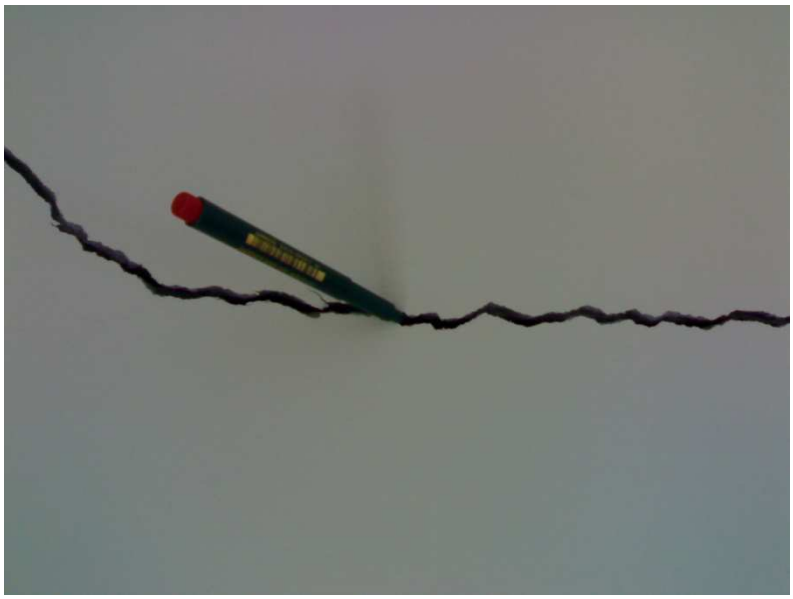

Figure C.1 NHBRC images of severe horizontal settlement cracks

Figure C.2 NHBRC images of severe vertical settlement cracks